Fiber Fracture in Continuous-Fiber Reinforced Composite Materials

During Cyclic Loading

by

Ahmad Razvan

Dissertation submitted to the Faculty of the

Virginia Polytechnic Institute and State University

in partial fulfillment of the requirements for the degree of

Doctor of Philosophy

in

Engineering Mechanics

APPROVED:

K.L. Reifsnider, Chairperson

E.G. Henneke II

J.C. Duke

E.R. Johnson

C.W. Smith

April 27, 1992

Blacksburg, Virginia

Fiber Fracture in Continuous-Fiber Reinforced Composite Materials

During Cyclic Loading

by

Ahmad Razvan

K.L. Reifsnider, Chairperson

Engineering Mechanics

(ABSTRACT)

The final tensile fracture of any composite structure is primarily due to the failure of its constituents, namely fibers and matrix in the present case. To date, no experimental data exists, to the author's knowledge, to define the behavior of constitutive fibers of a composite structure throughout its life span. The prime candidate for a fiber—based investigation is unidirectional zero—degree composite coupons. But unidirectional coupons do not demonstrate any significant loss of stiffness during fatigue cycling compared to other lay-ups. Even if stiffness degradation was significant, due to the nature of damage in this material system it would be impossible, practically, to monitor that change using conventional techniques (e.g. an extensometer) because the damage and failure process destroys the integrity of the contact between those devices and the material, under cyclic conditions.

This investigation presents the findings of a fiber-based investigation of unidirectional composite material systems. In particular, a unidirectional graphite/epoxy system was studied, and the influence of applied load level on fiber fractures, and their influence on damage growth documented. A damage monitoring technique (patent pending) was developed to accurately record the state of damage in this material system without the usage of extensometers or strain gages. Following this method, two new damage norms were introduced, namely, "percent phase damage" and "percent gain damage". Fiber fracture, strength degradation, and the life of unidirectional specimens were investigated and recorded as a function of various load levels.

Fiber fracture, in general, showed no definitive growth pattern during fatigue cycling. It appears that the majority of the broken fibers that occur over nearly 90% of the life are due to the initial applied load cycle. This is one of the key findings of this investigation. "Proof testing" which is a common practice in industry for "verifying" the integrity of a structure, could very well be causing significant subsequent reductions in life. With these findings as a base, it is now possible to postulate the first well—founded mechanistic model of fiber—dominated fatigue degradation under tensile loading.

Dedication

For the difficult times I have caused through my distance, and for their continued support and encouragement as I pursued my 23 years of studies, I dedicate this dissertation to my parents Iraj and Shahrbanou Razvan, my brother Ali, and my fiancee for keeping up with all my moods throughout the completion of this manuscript.

Acknowledgements

The author would like to sincerely thank the following people for their contribution and help throughout the completion of this work.

- Dr. Kenneth L. Reifsnider, for not serving as a "chairman" or an "advisor", but being a friend. The author's indebtness to him is beyond any acknowledgement.

- Special appreciation is due to Dr. Stinchcomb, Dr. Duke, Dr. Henneke, and Dr. Kriz for their *great insight* that helped shape many of the investigative directions detailed herein.

- Dr. E. Johnson, and Professor C.W. Smith for serving on the author's graduate committee.

- Bob Davis, Archie Montgomery, and Bill Shaver for cutting the specimens, and their assistance in the machine shop.

- George Lough for keeping all the test frames up and running.

- Barbara Wengert, Sheila Collins, and Melba Morrozof for all their help and support, their help was invaluable.

- To Jack Lesko, Steven Lee, Kin Liao, Robert Swain, C. Haldeman, and the rest of the Material Response Group students for their friendship, and the great working environment they all create by their humor.

- Mehran Elahi, the author's office mate and friend, for making the Dynamic Signal Analysis and "MR-PHASE 4000" possible. The author's graduation would not have been possible without his assistance.

- Mrs. Forouzandeh Farnoush, the author's "*future*" mother in law, for her overt support in all of the author's endeavors.

- Mr. and Mrs. Manouchehr Razvan, the author's uncle and aunt, for being a constant source of encouragement.

- To the author's parents Iraj and Shahrbanou, brother, Ali, his friend and fiancee, Sharrareh, for all their encouragement, help, and love throughout the time of graduate study to whom I dedicate this manuscript.

Table of Contents

List of Tables

List of Illustrations

CHAPTER I

INTRODUCTION

High performance structures that must be tailored to sustain severe and complex loading while maintaining reliable and safe performance over a period of time are prime candidates for the application of continuous—fiber reinforced laminated composite materials. Primary structures in aircraft and other vehicles are examples of such applications. It is generally not possible to reproduce all of the engineering environments in which such components must serve in the test laboratory. It is particularly difficult to establish the nature of long—term response from laboratory tests that cannot be conducted over the required service life of the component in general.

Many engineering applications involve applied loads that vary in time. The behavior of materials under these conditions is generally characterized by applying cyclic loading in a "fatigue" test. Various cyclic tensile and compressive amplitudes are generally applied, and the number of cycles required to fail the material under those conditions is recorded. In some cases, tests may be terminated and residual strength determined after some period of cyclic loading. The data from such tests are usually characterized by empirical means and generalized by implication or extrapolation to a variety of service conditions for

which the materials were not specifically tested in the laboratory, as required for various anticipated design situations.

The most common variable in such generalization is the cyclic load level. In homogeneous materials, such as common metals, where fatigue degradation is often dominated by self—similar crack propagation, the effect of cyclic load amplitude variation on the micro-mechanism of fatigue damage development has been widely investigated and characterized in many cases [1-12]. Damage accumulation in continuous fiber reinforced laminated composite materials has also been widely documented [13-24]; however, a fundamental understanding of the relationship of damage mechanisms and failure modes that control the short—term behavior of composite laminates at high cyclic load levels to the mechanisms that control the long—term fatigue behavior at low cyclic amplitudes has not been established.

In order to investigate the effect of load levels on damage growth evolution in these laminated materials, the damage growth mechanisms need to be identified and separated. The mechanisms and microstructural details of fatigue—induced failure in polymer composite laminates have been the subject of numerous studies. Some of the more frequently cited failure features include fiber fracture, fiber pullout, fiber/matrix splitting, and matrix damage described as hackles, serrations, lacerations, and chevrons. Most of these studies concentrated on microscopic examinations of the fractured surfaces rather than on the individual plies of the laminate. To date, no ply—level fiber—based failure mechanism based on microstructural evidence has been proposed for long—term fatigue behavior, and the role of fiber failure (or even its "general character") has not been established.

The influence of load level on the mechanism of damage growth and evolution can only be determined if a ply level approach is taken. It is only then that the influence of fiber fracture, delamination, fiber matrix interaction and their influence on the global response of the laminate can be observed. A detailed analysis using such an approach has been

made by Razvan et al. [13]. It was shown that the fundamental nature of fiber fracture and delamination pattern development is dependent upon cyclic load level. Fiber fractures tend to form localized patterns under high cyclic loads, and more widely dispersed patterns at low load levels. The load level is also found to influence the development of matrix damage, primarily the extent to which delamination and matrix damage grows during cyclic loading. Delamination (under fully reversed loading) is much more dominant at lower load levels, while matrix cracking is more extensive at higher load levels. These results are consistent with the argument that delamination is a growth phenomenon. In general, it is suggested that load level has opposite effects on certain damage modes. Elevated cyclic stress levels tend to accelerate and emphasize initiation—dominated damage modes such as localized fiber fracture and matrix cracking, but suppress growth—dominated modes such as delamination compared to low—level excitation. While it is certainly true that high load levels will cause more rapid growth of growth—dominated damage, the extent of such damage is limited by the fact that smaller amounts of growth can occur before fracture occurs at such high load levels. Also, since (in the "real world") high and low load levels tend to occur independently of the cyclic rate of loading, the effect of loading rate (which is higher at high loads for a fixed frequency) is also important to the load—level influence.

Because of these facts, several engineering consequences are expected. Remaining strength at a percent of life will, in general, depend on cyclic load level and the consequent damage development patterns. "Equal damage" concepts are likely to be difficult to define since the consequence of any damage development will depend on the subsequent level of cyclic loading. Nondestructive test techniques which are insensitive to differences in fiber fracture patterns are not likely to be good "predictions" of remaining strength after damage. And the "best" laminate for low—level cyclic loading may not be the "best" laminate for high—load level cyclic loading. Finally, any successful model of remaining strength should account for load—level variations in damage development. Therefore, in

order to fully understand damage, each individual factor involved in defining "damage" should be characterized. From the above arguments, it is evident that delamination and fiber fracture are two of the most important modes in damage evolution in fibrous composite materials. Delamination has been the subject of numerous studies; on the other hand, the influence of fiber fracture has not received the attention it deserves. Generally the final fracture of any continuous—fiber composite part (regardless of geometry, stacking sequence, and material property) involves fracture of fibers. The evolution of fiber fracture throughout life is still a mystery. The influence of fiber fracture on the response of laminates can only be investigated by isolating them from the influence of other damage modes such as delamination. Unidirectional, zero degree, specimens are prime candidates for such a study, and were used for most of the present study.

Even though the history of modeling uni—directional composite materials dates as far back as 1967 when Hedgepeth [25] presented his analysis, there is still no definite model that can predict the fiber—controlled remaining life of a structural component. Hedgepeth's original approach shared the assumption common to shear—lag analyses, that no additional damage other than the initial notch is considered. This work was extended by Hedgepeth and Van Dyke for the case of specific broken filaments [26] and longitudinal splitting in the matrix [27]. Goree and Gross [28] extended Hedgepeth's solution to include an arbitrary number of broken fibers as well as longitudinal yielding and splitting of the matrix. They extended the latter solution to account for longitudinal matrix damage, in addition to transverse matrix and fiber damage in the vicinity of the flaw [29]. The understanding of the splitting mechanism is of paramount importance, due to its complexity and effect on the final fracture of the laminate. Splittings are known to mitigate the effect of discontinuities, and therefore to reduce the likelihood of a rapid fracture through the plane of the discontinuity. Characterization and understanding of the nature of such splittings has been the subject of numerous studies [30-33]. Mar demonstrated the lessening of the strain concentration as the growth of the splits physically separates the laminates into load

carrying and non—load carrying strips [31]. Garg [32] argues that once the split initiates, the propagation occurs only due to shear. Wolla [33] extends this argument to two modes of longitudinal matrix splittings being responsible for the final fracture of the laminate. He notes that after split initiation, a region of slow, stable split growth occurs. This is followed by a distinct transition into a rapid split growth region. Wolla explains the discrepancies between actual and predicted results to be likely caused by interference with the fracture path and irregular damage such as fiber breaks and crossover of matrix splits. He also argues the shortcoming of the classical shear—lag model in predicting the complete longitudinal split growth in a brittle matrix composite. Dharan [34] divides this fatigue response into three distinct life ranges. In the first region, (<200 reversals), a small dependence of the fatigue life on cycling is observed where the behavior is dependent upon the fiber mean strength and strength distribution. In the second region (200 to 10^6 reversals), the logarithm of the applied stress decreases almost linearly with the logarithm of the number of cycles. Fatigue failure in this region occurs by the growth of matrix microcracks, which leads to preferential fiber failure, and is followed by interfacial shear failure. In the third region (>10^6 reversals), the applied stress is below the microcrack initiation stress and no failure is expected. Reedy, [35] by comparison with 3—D finite element analysis, demonstrated some benefits in the usage of shear lag analysis. He notes the importance of the shear lag model for composites with 1) a relatively stiff matrix that can carry substantial load (e.g. boron/aluminum) and 2) a highly anisotropic fiber which has a shear modulus not much greater than that of the matrix in which it is embedded (e.g. Kevlor 49/ epoxy). Brittle matrix composites have been modeled using different approaches [36].

The time dependency of the final fracture behavior has almost been ignored in all of the previously discussed models. Laminated composites are known to have altered responses under long—time static or cyclic loading [37]. This time dependency is related to the strength reduction of the matrix (or of the fiber—matrix interface surface) at a higher rate

with increasing numbers of cycles than that of the strength in the direction of the fibers [38]. Fatigue failure modes and the sequence of damage accumulation is highly dependent on the stress level. Lorenzo has reported fiber—controlled failure in low—cycle specimens and matrix crack failures in high—cycle specimens [39]. He also concludes that fiber break and matrix cracking are the dominant mechanisms during fatigue in unidirectional laminates. This is in contrast to transverse matrix cracking, dispersed longitudinal cracking, localized longitudinal cracking, delaminations along transverse cracks, and local delaminations at the intersection of longitudinal and transverse cracks in cross ply laminates [15]. In these laminates, in many cases most of the fiber failures and damage localization occurs in the last 10% of the life of the laminate [18]. While elsewhere [14] it has been argued that most of the fiber fracture occurs during the early stages of life due to the initial high load levels. It has been shown by the author [13,40] that this behavior is affected by the stacking sequence and the material system.

Understanding the initiation, growth, and final fracture of the composite laminate has helped in the development of various fracture models for predicting such events as: first ply failure [41], residual strength [42], damage evolution using a homogenization method and the thermodynamic theory of generalized standard materials [43], stiffness degradation and remaining life [16], ultimate strength [44], the effect of interfacial shear strength on the ultimate strength [45], dynamic response [46], and incremental failure accumulation using finite element analysis [47]. Various statistical models have also been proposed [48-53] using Weibull distribution concepts with the hope of predicting the state of fiber fracture, and the remaining life of the composite laminate. Failure models which have fiber fracture densities and behavior incorporated in their schemes lack experimental backup. There are very few reported experimental results on fiber fracture density [54] and its influence (or lack of influence) on the final fracture of the laminate. This is primarily due to the difficulty associated with monitoring damage in unidirectional laminates [55-56].

Due to the statistical nature of the fatigue damage evolution mechanism in unidirectional material systems, thorough analysis of such events as residual strength degradation and fiber fracture has not been possible [56-57]. Severe surface matrix splitting results in debonding of extensometer tabs from the surface of the specimen. If extensometers can not be used, monitoring stiffness change—using classical methods—as a measure of damage is not possible. Therefore, a new experimental technique other than life estimation based on the median life or on stiffness degradation should be used for analyzing damage evolution and growth mechanisms throughout life.

Several investigators have utilized dynamic stress—strain signals in order to characterize fatigue damage development by measuring phase and stiffness where the phase values are obtained either from direct measurement at the zero—crossing points of signals, or by constructing a hysterisis loop [58]. This procedure still requires use of an extensometer or an attached strain gage to measure strain. Using an experimental procedure similar to that of So [59], Elahi et al. [60] proposed a new technique for measuring dynamic stiffness of fatigue cycled specimens. He utilized the load and stroke signals from a servo hydraulic test machine to measure quantities such as phase lag and gain, for measuring damping and compliance, respectively.

In an effort to determine the state of damage in unidirectional laminates using non-contact methods, the approach of Elahi et al. [60] was undertaken. Detailed analysis of the dynamic response of composite laminates demonstrated the possibility of incorporating such an approach for damage growth analysis and determination of the stage of damage within the laminate. Application of such an approach made it possible to estimate the degree of damage in unidirectional laminates at any given time in life of the specimen with reasonable accuracy. Knowing the damage state, fiber fracture behavior throughout life was investigated. The remainder of this dissertation is devoted to the investigation of the characteristics and behavior of fiber fracture and its influence on strength degradation and remaining life of the unidirectional graphite/epoxy composite laminates.

CHAPTER II

EXPERIMENTAL PROCEDURE

A detailed study of the damage evolution and life of unidirectional laminates was performed. Specially designed laminates were fatigued and examined for fiber fracture, remaining strength and life through out the fatigue life of the specimen.

Specimen Geometry: Eight-ply unidirectional panels were made of Hexcel's graphite/epoxy prepreg (AS6/F584) with a layer of release cloth (non-Teflon coated) embedded at the middle ply (Figure 1). This layer made it possible to deply the specimen at the mid—plane for fiber fracture analysis at various stages of life. Glass epoxy tabs with 30° tapering were used to reduce the stress concentration as well as fiber fracture in the gripped section due to gripping the specimens. This is represented by Figure 2 A&B for unidirectional satin weave Celion 3000/PMR-15 specimens. High fiber fracture density at the gripped section is the result of extremely high grip pressure needed to avoid specimen/grip slippage. Such grip effects was reduced by tabbing the specimens at the grip sections. Tabs and the tab-section surfaces of the panels were lightly sand-blasted for cleaning as well as to increase the mechanical friction between the two adjoining surfaces.

American Cyanamid's FM-300K adhesion film was used for binding the tabs to the panels. The tabs were bonded to the panels at 0.5 MPa (75 psi) for 1 hour after being preheated for 30 minutes at 175°C (350°F) in an autoclave. The test specimens shown in Figure 1 were cut at 0° from the laminated panels after cure of the grip tabs [56].

Residual Strength Measurement: Residual tensile strength of the specimens was obtained by stopping the fatigue cycling at various stages of life (or damage) and quasi—statically loading the specimens to failure at a loading rate of 880 N/s (200 lbf/s). To avoid failure of the specimens at the gripped section, a minimal grip pressure of 5.52 MPa (800 psi) was used. This grip pressure was high enough to avoid specimen/grip slippage and yet low enough to avoid premature failure of the specimen due to the grip effect.

Ultimate Tensile Strength Measurement: Following the same loading rate as in the residual strength measurement, eight specimens were tested for ultimate tensile strength. Of the eight specimens loaded quasi-statically to failure, four were laminated without any release cloth and four were laminated with a layer of release cloth, at the mid—plane, as described earlier. The four specimens without any release cloth had ultimate tensile strengths of 339,591, 344,081, 377,961, and 340,000 psi. The specimens with the release cloth had ultimate tensile strengths of 347,500 psi, 340,000, 353,333, 360,000 psi. An average ultimate tensile strength of 350,408 psi was used throughout this investigation.

Deply Technique: The specimens were deplied using Freeman's deplying technique [8] in a modified tube furnace with argon purging to avoid oxidation of fibers at elevated temperatures. A pyrolysis time of 15 minutes at 600° C (1112° F) was found to be sufficient. Pyrolysis time was judged by the ease of deplying and the amount of remaining matrix. This was of extreme importance, because in fiber fracture analysis the amount of fiber fracture due to deplying had to be minimized, while at the same time enough matrix had to be kept to ensure that the relative position of fibers within the ply remained intact.

Fiber Fracture Count: Fatigue tested and deplied specimens were examined for fiber fracture using a Joel JCM 35 scanning electron microscope. The central 1 in. gage section of the specimens was examined for fiber fracture. Fractured fibers were counted in the form of singlets (Figure 3), doublets (Figure 4), triplets (Figure 5), and finally clusters of more than three broken fibers.

2.1.1.1 Damage Evolution Monitoring Based on the Classical Median Life Approach.

Specimens were fatigue cycled (R = 0.1) at 60%, 65%, 70%, 75%, and 80% σ_u and the S—N diagram for this material system was obtained. Representative samples were taken at early, middle life, and impending failure based on the median life of each representative group (10%, 50%, and 95% life according to the S—N data) for residual strength and fiber fracture measurements.

Damage evolution monitoring based on the median life technique was later proved to be inadequate due the large scatter in life data in this material system. As was discussed in Chapter I, the method of Elahi et. al [60] was adapted to the present study. Dynamic mechanical analysis proved to be a viable method for damage evolution monitoring. Application of this technique made it possible to examine fatigued specimens based on a uniform damage term regardless of the life of specimen as noted by the cycles to failure.

2.1.1.2 Damage Evolution Monitoring Based on the Dynamic Mechanical Approach.

Dynamic analysis of fatigued structures can be easily modelled using a discrete parameter model as illustrated in Figure 6. The idealized elements are called mass, spring, damper,

and excitation. Energy is stored by the system in the mass and the spring in the form of kinetic and potential energy, respectively. Energy enters the system through excitation and is dissipated through damping.

The relationship among the constituents of the system (mass, stiffness, and damping) is given by equation 1.1.

$$m\ddot{x} + c\dot{x} + kx = f(t) \qquad [1.1]$$

Equation 1.1 is referred to as the equation of motion for the single degree of freedom (SDOF) system depicted in Figure 6. The constant coefficients *m, c,* and *k* represent the system parameters as illustrated in Figure 6. The natural frequency and damping factor of the system is calculated using the definitions in equation 1.2.

$$\omega_n^2 = \frac{k}{m}, \quad 2\zeta\omega_n = \frac{c}{m} \quad \text{or} \quad \zeta = \frac{c}{\sqrt{2km}} \qquad [1.2]$$

The natural frequency, ω_n is in units of radians per second (*rad/s*). The typical units displayed on a digital signal analyzer, however, are in Hertz (Hz). The damping factor (ζ) can also be represented as a percent of critical damping—the damping level at which the system experiences no oscillations. Although there are three damping cases, only the underdamped case ($\zeta<1$) is generally important for structural dynamics applications.

When there is no excitation, the roots of the equation are as shown in equation 1.3.

$$s_{1,2} = -\sigma + j\omega_d \quad \text{where} \quad \sigma\text{—DAMPING RATE}, \quad \omega_d\text{—DAMPED NATURAL FREQUENCY} \qquad [1.3]$$

Each root has two parts: the real part or decay rate, which defines damping in the system and the imaginary part, or oscillatory rate, which defines the damped natural frequency, ω_d. This free vibration response is illustrated in Figure 7.

When excitation is applied, the equation of motion [1.1] leads to the frequency response of the system. The frequency response is a complex quantity and contains both real and imaginary parts (rectangular coordinates). It can be presented in polar coordinates as magnitude and phase, as well. Because it is a complex quantity, the frequency response function cannot be fully displayed on a single two dimensional plot. One method of presenting data is to plot the polar coordinates, magnitude and phase versus frequency as illustrated in Figure 8. At resonance, $\omega = \omega_n$, the magnitude is a maximum and is limited only by the amount of damping in the system. The phase ranges from 0° to 180° and the response lags the input by 90° at resonance [61-62].

Even though application of frequency response analysis is predominantly in electrical network analysis, the various forms of frequency response function based on the type of response variable are also defined from a mechanical engineering viewpoint. They are somewhat intuitive and do not necessarily correspond to electrical analogies. These forms are summarized in Table 1. Using the frequency response of a dynamic signal analyzer, phase lag and compliance between the load and stroke signal could be determined. The frequency response measurement, often called the "transfer function", is the ratio of a system's output to its input, and yields compliance (X/F) as a function of frequency. Frequency response is calculated as the ratio of the cross spectrum to the load signal's power spectrum as shown in equation 1.4.

$$H(f) = \frac{G_{sl}}{G_{ll}} \quad \text{where:} \quad G_{sl} \text{ is the cross spectrum}, \quad G_{ll} \text{ is the load signal's power spectrum} \qquad [1.4]$$

The cross spectrum of the load/stroke signals is calculated by multiplying the complex conjugate of the load spectrum by the stroke spectrum as given by equation 1.5.

$$G_{sl} = (F_s)(F_l^{\Pi}) \quad \text{where:} \quad F_s \text{ is the load spectrum's complex conjugate}, \quad F_l^{\Pi} \text{ is the stroke signal's linear spectrum} \qquad [1.5]$$

The power spectrum measurement shows the load signal in the frequency domain. It is computed by multiplying the FFT of the signal by its complex conjugate (Eqn. 1.6).

$$G_{ll} = (F_l)(F_l^{\Pi}) \quad \text{where:} \quad F_l \text{ is the load signal's linear spectrum}, \quad F_l^{\Pi} \text{ is its complex conjugate} \qquad [1.6]$$

It is evident from the above formulation that the dynamic compliance of any mechanical structure or system could be determined using the displacement from any applied forcing function [63-64].

From a practical stand point, the applied force function could be a sinusoidal waveform load signal and the displacement could be the stroke signal from a servo hydraulic load frame, or the strain signal off the extensometer's amplifier. If this is true, the possibility of omitting the usage of an extensometer is worth exploring. Dynamic stiffness determination by non—contact methods could bring about opportunities for investigation of fiber fracture analysis which have not been possible to date. Damage evolution and property degradation in unidirectional composite laminates could be monitored and stage of life could be estimated. Life estimation based on the median life need not be used, hence the costly statistical analysis which requires large sample sizes could be avoided.

2.1.1.3 Dynamic Mechanical Analysis as a Tool For Monitoring Damage State in Uni-directional Composite laminates.

Using the specimen configuration of Figure 1, S—N data were obtained and dynamic response measurement recorded. Dynamic data acquisition was performed using an HP 9000/PC-315 computer in—line with an HP 5208 data acquisition control unit as well as an HP 3562A dynamic signal analyzer (Figure 9). A software routine was developed for real

time dynamic response monitoring.[1] Phase lag and gain response of the load/stroke signals from the MTS servo—hydraulic load frame were plotted in conjunction with the load and stroke data. To avoid disk storage overflow, data were sampled according to their relative change with respect to the previous events.

Working in a frequency domain, all the measurements were made at the system's excitation frequency in a linear resolution mode. First, by using the cross spectrum function, the fundamental frequency was determined and the marked (Figure 10A-B). Then the phase lag and gain measurements were made at this frequency using a frequency response measurement function (Figure 11A-B).

Dynamic response for the unidirectional laminates demonstrated a general characteristic behavior. Modelling this behavior made it possible to identify the stage of damage in the material. Two new damage terms were identified and, as will be explained in Chapter III, "percent phase damage" and "percent gain damage" illustrated good correlation with the residual strength, and fiber fracture density as well as the remaining life measurements. Specimens were fatigue cycled and tests stopped at predetermined values of percent phase and gain damage. Two sets of specimens were fatigued and stopped for residual strength and fiber fracture density analysis at various degrees of damage as depicted by the new damage norms.

---

1 "Dynamic Measurement Scheme for Characterization of Material Property Evolution", Patent pending, Reifsnider, K.L., Razvan, A., Elahi, M..

CHAPTER III

RESULTS & DISCUSSION

As discussed earlier, unidirectional laminates demonstrate a large scatter in their life data. Initially the median life data were used to determine the stage of life for this material system. After several trials, this method was abandoned, and the dynamic mechanical approach was used instead [55, 56]. In the present Chapter, results obtained from the first phase of study are discussed and then the final technique is treated and discussed at length [57, 60, 65, 66].

3.1.1.1 Damage Evolution Monitoring Based on the Classical Median Life Approach.

The S—N diagram for the material system illustrated in Figure 1 was obtained and, based on the stabilization of the Weibull shape parameter (Figure 12), further testing was terminated. Using such an approach, a sample size of 30, 39, 49, 43, and 42 for 60%, 65%, 70%, 75%, and 80% σ_u, respectively, was found to be sufficient (Figure 12). The S—N diagram for this material system is illustrated in Figure 13 and tabulated in Table 2 — Table 7.

The unidirectional laminates showed very little change in stiffness throughout their life. Damage monitoring becomes even more complicated at approximately 50% of life when severe surface matrix splitting causes separation of the extensometer from the specimen surfaces (Figure 14). The separation of the extensometer leaves no other choice than to base the life of specimens on the average or median life from the S—N diagram. Based on the S—N data for this material system, the median life of samples at each load level could be determined. Due to the wide variation in cycles to failure (life), this approximation is very rough indeed. For example, only half of the samples that were fatigued at a load level of 75% failed at between 1,668 and 38,728 cycles; these numbers represent, respectively, the first and third quartiles of the cycles to failure. The median life for these samples is 2,979 cycles. By fatigue cycling a sample for 1,000 cycles, one may conclude, based on the median life, that this sample is at one—third of its potential life. There is a one—fourth chance, however, that the life would have been greater than 38,728 cycles; if this is in fact the case, then this sample is at less than one—fortieth of its potential life! Similarly, if it happens to be a sample with an actual life of less that 1,668 cycles, which occurs one—fourth of the time, then this sample has less than half of its life left. Therefore, the variability of survival times is too great to make fixed stopping times a reliable method of uniformly estimating the damage state of a given specimen for the purpose of predicting life or for the purpose of measuring remaining strength (or any other variable) as a function of fractions of life. This had a pivotal effect on the present effort.

Residual strength degradation as a function of life based on the median life demonstrates the unreliability of such an approach (Figure 15). Various specimens were stopped at various stages of life at 70% σ_u, according to the median life, and the residual strength of the specimens was determined. The random behavior of fiber fracture and residual strength proves the inconsistency of this approach for approximating the stage of life.

The development of a new experimental technique or approach is paramount to achieving an understanding of the response of unidirectional composite laminates. If the stage of life

could be approximated with a certain degree of repeatability, then further analysis of strength degradation and fiber fracture would be possible, but in the absence of such a scheme, no technique could offer a consistent method for estimating and predicting life. Such a scheme is proposed below.

3.1.1.2 Damage Evolution Monitoring Based on the Dynamic Mechanical Approach.

Phase lag and gain response of unidirectional specimens, regardless of their respective lives, demonstrated a characteristic behavior. As is evident from Figure 16 — Figure 17, three distinct regions are produced throughout the life of specimens, resembling that of compliance change of cross ply laminates, as explained in Chapter II. Taking advantage of this characteristic behavior, after several more tests, it was noticed that the relative change between the initial phase lag and gain values with respect to their final values before specimen fracture, on the average, remains constant. In the case of 65% σ_u, 108% and 18% change for phase lag and gain were found, respectively. The percent change calculations were based on equation 3.1.

$$\%\ Change = \frac{I - F}{I} \times 100 \quad \text{where} \quad \begin{array}{l} I = \text{Initial value} \\ F = \text{Final value} \end{array} \qquad [3.1]$$

Using this characteristic relative change, new specimens were tested, and, based on their initial phase lag and gain, their final phase lag and gain were approximated using equation 3.2.

$$F = I \times \left(1 - \frac{\%\ \text{change}}{100}\right) \qquad [3.2]$$

The approximate final value was then used to estimate the stage of life for the new specimens using equation 3.3.

$$\% \text{ damage} = 100 - \left[\frac{F - C}{F - I} \times 100 \right] \quad \text{where} \quad F = \text{Final value}, \; I = \text{Initial value}, \; C = \text{Current value} \qquad [3.3]$$

Equation 3.3 is normalized relative to the initially obtained value to represent damage on a relative scale of 0% for no damage and 100% for expected failure. Depending on the term used, the percent damage term was named "percent phase damage" or "percent gain damage". Based on this approach, "MR—PHASE 4000" software was developed, and these new damage norms were monitored in real time (Figure 16 — Figure 17). Various specimens were fatigue cycled and stopped based on the percent phase and gain damage. These specimens were later loaded quasi—statically to failure for residual strength measurements. A similar technique was followed and specimens were collected for fiber fracture analysis. Table 8 and Figure 18 — Figure 19 illustrate the residual strength degradation as a function of these new damage norms for 65% σ_u.

This characteristic behavior was not observed for 70% σ_u fatigue tested specimens. At 70% σ_u, the initial load levels are so high that excessive matrix damage initiated from the first few cycles. Damage in unidirectional laminates under high load levels is predominantly in the form of matrix splitting [55-56]. In the presence of matrix splits, damage becomes predominantly concentrated in the region of the split. This is clearly demonstrated in Figure 20 where fiber fractures are concentrated at the matrix split while the neighboring areas are free from any fiber fractures. Due to the splitting—dominated damage, using the same approach as the one used for 65% σ_u, revealed no characteristic behavior. Further analysis of the test data showed inconsistency between the initial phase lag and gain from specimen to specimen. This is in line with the previous argument that the failure

of unidirectional specimens at high load levels is dominated by matrix splitting. If the initial values could not be used as an initial state, the previous approach could not be applied.

At 50% σ_u, after 3000 cycles, no change of phase lag and gain was observed (Figure 21 — Figure 22). Therefore, the final value of phase lag and gain at 50% σ_u for each specimen was used as an initial condition for that specimen. In other words, specimens were fatigue cycled at 50% σ_u for 3000 cycles after which the test was stopped and loading was changed to 70% σ_u. Following such an approach, a consistent initial state was obtained, and the previous percent change approach was once again found to be characteristic. Phase lag and gain percent changes of 229% and 20% were recorded respectively. Residual strength and fiber fracture measurement were then performed and results illustrated good correlation with the 65% σ_u case. The results are tabulated in Table 9 and Figure 23 — Figure 24. Figure 25 — Figure 26 illustrate the load level dependency of residual strength in this material system. In the case of unidirectional materials, the load level dependency has never been quantified before, and is a significant step towards understanding their response is demonstrated in these figures. As is evident, there is a threshold in life beyond which specimens fatigued at 70% σ_u have lower strength, for the same percentage of remaining life, than the specimens tested at 65% σ_u. Until the middle stages of life, 65% σ_u specimens demonstrate a lower residual strength than the specimens fatigued at 70% σ_u, after which the strength at 70% σ_u falls below the specimens tested at 65% σ_u. However, this difference is not large, compared to the spread of data.

Fiber fracture data for both load levels demonstrate the spread and scatter in the data for such measurements (Table 10 — Table 11). The data are not as convincing as it is argued in such theoretical models as Batdorf [48-50] for quasi-static loading. Whether arguments such as Batdorf's are valid or not, cannot be deduced from the present data. Some key issues could be addressed with the available information and they are as follows:

1. At 65% σ_u:

a. The number of singlets appears to increase as a function of % gain damage and stay constant relative to the % phase damage. Even though the observed increase in the singlet formation (in the case of % gain damage), relative to the spread in the data is not convincing, mathematically the increase resembles that of an exponential function (Figure 27 — Figure 28).

b. Doublets and triplets appear to remain constant relative to both % phase and % gain damage (Figure 29 — Figure 32).

c. The total fiber fracture, or the sum of all the broken fibers (singlets, doublets, and triplets), also seems to follow the arguments presented in 1-a & 1-b (Figure 33 — Figure 34).

2. At 70% σ_u:

a. The number of singlets relative to % gain and % phase damage appears to stay constant (Figure 35 — Figure 36). As is evident from Figure 37 — Figure 40, doublet and triplet formations do not show any pronounced dependence on the new damage norms as well. This lack of dependence is further illustrated in the total fiber fracture data presented in Figure 41 — Figure 42.

From an experimental standpoint, a specimen fails when all its constitutive fibers are fractured at least once. The details of this process are obscured by the limitations in the experimental procedure and the way the data are presented. Experimentally the following short comings and limitations are known to exist:

1. For the phase lag and gain to be calculated by the dynamic signal analyzer, the specimen has to undergo at least 300 cycles. So, the initial state of the fiber fracture is based on 300 cycles and not 1 or 2 cycles.

2. Based on case 1, it is evident that the closest a datum point could be collected to the end of life is also about 300 cycles.

3. Even if the data are collected at the very beginning of life, the specimen could not be deplied at the mid—plane since the specimen has not delaminated at that early stage of life, a requirement for deplying purposes[2].

With all these short comings, the data reveal some important characteristics of the nature of fiber fracture. From the residual strength data of Figure 18 — Figure 19 and Figure 23 — Figure 24, the validity of the two new damage norms is evident. If these two norms are valid damage parameters, then why the fiber fracture data not show any relationship such as the relationship shown by the residual strength data needs to be determined. The answer could lie on the absence of data in both extremes of the spectrum of life, namely, the beginning and end. Therefore, it is suggested that the data represent only the middle stage of damage relative to fiber fracture. If this argument is true, then the number of fiber fractures does not increase substantially after the initial cycle, and Graphite fibers do not fatigue under the given loading conditions. This is, once again, in support of the argument presented by Reifsnider [19] that the majority of fibers should break due to the initial load levels.

To fully understand the nature of such an argument, twenty four specimens were quasi—statically loaded to 80%, 85%, 90%, 91%, 92%, 93%, 94%, and finally 95% σ_u (three specimens at each load level). After the quasi—static load, each specimen was then fatigued at 65% σ_u till 50% phase or gain damage was recorded. Following the previously discussed procedure, each specimen was deplied and examined for fiber fracture. Another group of specimens, after being quasi-statically loaded to the above load levels, were fatigue cycled to failure. Following this stage, life and fiber fracture variation due to initial

---

[2] The reader is referred to Chapter II, and is reminded of the presence of a release cloth at the mid section of the laminate.

high load levels should be indicative of such influence, if any, on the damage state of this material. Results are given in next section.

3.1.1.3 Influence of Initial High Static Loading on the State of Fiber Fracture.

As discussed in the last section, several specimens were quasi—statically loaded to 80%, 85%, 90%, 91%, 92%, 93%, 94%, and 95% σ_u. A few specimens failed at high load levels of 94% and 95% σ_u, but the ones which survived were fatigued at 65% σ_u. The latter specimens were divided into two groups; one group was stopped after approximately 50% phase damage, and then deplied for fiber fracture counts. Specimens in the second group were fatigued to failure and the S—N plot at 65% σ_u was obtained. Results are tabulated in Table 12 and Table 13. Figure 44 through Figure 47 also demonstrate the singlet, doublet, triplet, quad-plet, and finally the total number of fractured fiber formations in these specimens. Figure 43 illustrates the S—N diagram for this material system due to the described loading history. Singlet fiber fracture counts revealed an exponentially increasing growth pattern with increasing static load levels prior to the fatigue cycling at 65% σ_u (Figure 44). Doublet, triplet and total fiber fracture counts revealed no significant pattern and appear to stay constant within the data scatter (Figure 45 — Figure 47).

The S—N diagram of Figure 43 illustrates the influence of initial high load levels on the fatigue life of the specimens at 65% σ_u. As discussed in earlier sections, singlet formations demonstrated no further initiation after the first few cycles of life until the last few cycles before specimen failure (Figure 27 and Figure 28). Due to such evidence, we conclude that the behavior demonstrated in Figure 43 is primarily due to the initial high load levels and not to the fatigue cycling at 65% σ_u.

Fatigue Cycling and High Load Levels and The Influence on Fiber Fracture Spacing.: Assuming a uniform density of fiber fractures throughout the cross section of the specimen, one can hypothesize a hexagonal distribution for the fiber fractures as illustrated in Figure 48. The area of each of the unit cells (hexagons) is defined as equation 3.4.

$$A_{uc} = \frac{3\sqrt{3}}{2}\left(\frac{d_{ff}}{2}\right)^2 \quad \text{where} \quad A_{uc} = \text{Area of the unit cell (Hexagon)}, \; d_{ff} = \text{distance between broken fibers} \qquad [3.4]$$

The total surface area of the specimen is, hence, given by equation 3.5.

$$A_t = N_{ff} \times A_{uc} \quad \text{where} \quad N_{ff} = \text{Number of broken fibers}, \; A_t = \text{Total surface area} \qquad [3.5]$$

The total surface area of each specimen was measured prior to every test, and the fiber fractures were also counted as part of the study. Having both the total area and the number of fiber fractures, one can easily calculate the distance between broken fibers in the plane of observation (d_{ff}) as a function of N_{ff} (Equation 3.6).

$$d_{ff} = \left[\left(\frac{8\sqrt{3}}{9}\right)\frac{A_t}{N_{ff}}\right]^{\frac{1}{2}} \qquad [3.6]$$

Knowing N_{ff} at each load level, d_{ff} could be expressed as a function of initial applied static load level (% σ_u). According to Figure 49, specimens loaded to higher initial load levels have smaller fiber fracture spacings than the specimens loaded to lower initial load levels. Using least square fits of Figure 49 and Figure 43, namely equations 3.7 and 3.8,

$$d_{ff} = 0.84\, e^{-0.03\,(\%\sigma_u)} \qquad [3.7]$$

$$L = 1.41 \times 10^6 \times e^{-0.078\,(\%\sigma_u)} \qquad [3.8]$$

where L = Life at 65% ultimate tensile strength

$\%\sigma_u$ = Percent of the ultimate tensile strength used in static loading

one can easily solve for $\%\sigma_u$ in equation 3.8 and substitute it into equation 3.7 to obtain a relationship between fiber fracture spacing and life at 65% σ_u.

$$d_{ff} = 0.84 \left[\frac{L}{1.41 \times 10^6} \right]^{0.38} \qquad [3.9]$$

Equation 3.9 is derived if an exponential fit is assumed for equation 3.8. Considering the scatter in data, a linear fit could also be used in Figure 43. Using a linear fit for the data in Figure 43 results in equation 3.10. (Figure 50)

$$L = 1{,}097{,}804 - [5460 \times (\%\sigma_u)] \qquad [3.10]$$

Solving for % σ_u in equation 3.10 and substituting it in equation 3.7 results in equation 3.11.

$$d_{ff} = 0.84 \, e^{0.03\left(\frac{L - 1{,}097{,}804}{5460}\right)} \qquad [3.11]$$

Equations 3.9 and 3.11 are illustrated in Figure 51. Discarding, the outlyer data point, as marked on Figure 50 and Figure 51 and expanding the scale reveals the sensitivity of such an analysis to the kind of fit used for the data. The dashed trend line in Figure 52 is hypothetically illustrative of fiber fracture spacing and its influence on life of specimens. The specimens with a greater fiber fracture spacing live longer than similar specimens with smaller fiber fracture spacing. In fact, one could postulate a simple proportionality between the fiber fracture spacing and the number of cycles to failure. If one considers a typical Paris— type growth law [67], of the form of equation 3.12

$$\frac{da}{dn} = \alpha \, G^{\beta} \qquad [3.12]$$

where G is the strain energy release rate and α and β are material constants for matrix crack growth at the local level (between fiber breaks), and if G is constant during that growth (which may be a reasonable assumption under locally strain—controlled conditions

[68], then equation 3.12 suggests that the number of cycles to failure is directly proportional to the distance between fiber fractures.

CHAPTER IV

CONCLUSION

The finai tensile fracture of any composite structure is primarily due to the failure of its constituents, namely fibers and matrix in the present case. Numerous investigations have concentrated on the interaction between these constituents and how they control or influence the final failure of the structure. Mathematical models have also been proposed to predict the remaining life and strength of these structures based on a predefined or measured damage states. Even though a majority of these predictive methodologies consider the engineering properties of both the fiber and matrix, and take into account the fiber-matrix interaction as well as the matrix damage state, they rarely consider the specific influence of fibers, and especially the fractured fibers in such studies.

To date, no experimental data exists, to the author's knowledge, to define the behavior of constitutive fibers of a composite structure throughout the life span of that structure. This is mainly due to the difficulty associated with conducting such experimental analysis. The prime candidate for a fiber—based investigation is unidirectional zero—degree composite coupons. But unidirectional coupons do not demonstrate any significant loss of stiffness during fatigue cycling compared to other lay-ups (e.g. quasi-isotropic or orthotropic). Even

if stiffness degradation was significant, due to the nature of damage in this material system it would be impossible, practically, to monitor that change using conventional techniques (e.g. an extensometer or strain gages) because the damage and failure process destroys the integrity of the contact between those devices and the material, under cyclic conditions [57]. It is also very difficult to derive the nature of fiber fracture in the interior of a specimen. In fact, no nondestructive method for detecting individual fiber fractures, their location, and the local conditions around such a break is known. Furthermore, taking composites apart, systematically, to determine those details is remarkably difficult, and time consuming. Knowing all the difficulties associated with unidirectional composite studies, it is not hard to imagine why such a data set is not yet created.

Through extensive research on this subject, the current manuscript presents the findings of a fiber-based investigation of unidirectional composite material systems. In particular, a unidirectional graphite/epoxy system was studied, and the influence of applied load level on fiber fractures, and their influence on damage growth documented. The affect of fiber fracture on the damage state of composites varies from one material system to another. Common logic dictates that "virgin" structures should have few broken fibers, while "failed" structures should have all their constitutive fibers broken at least once. What happens in between these two states is a question poorly addressed in the literature. Depending on the material system, it is shown by the author that delamination and fiber fracture often have related roles in the final failure of specimens [13,40]. Quasi-isotropic laminates, for example, demonstrated delamination preceding fiber fracture, while in orthotropic specimens fiber fracture precedes delamination. Load level was also proven to influence the damage initiation and growth mechanisms [15]. This is especially important when accelerated laboratory—generated data are to be used in the actual design of structures. High load levels (typical of "short" laboratory tests) demonstrate initiation—dominated failure, while low load levels (typical of "long" service life) cause failure due to growth—dominated mechanisms.

If fiber fracture is to be investigated, one has to be able to separate their influence from other damage mechanisms (e.g. delamination). As discussed earlier, unidirectional specimens are prime candidates for such an investigation. In order for such a study to be unbiased and accurate, a special specimen configuration was designed [56]. Testing machines had to be more accurately aligned [55], and, to make quantitative damage monitoring possible, a new approach had to investigated [57, 60, 65, 66]. A damage monitoring technique (patent pending) was developed to accurately record the state of damage in this material system without the usage of extensometers or strain gages. Following this method, two new damage norms were introduced, namely, "percent phase damage" and "percent gain damage". Fiber fracture, strength degradation, and the life of unidirectional specimens were investigated and recorded as a function of various load levels, using these norms to establish "comparable" specimens during cyclic loading, i.e., cyclic loading was interrupted to record data based on these norms.

Fiber fracture, in general, showed no definitive growth pattern during fatigue cycling. It appears that the majority of the broken fibers that occur over nearly 90% of the life are due to the initial applied load cycle. Fiber fracture could be mapped during the life of the specimen as a three—stage growth phenomenon. In the first few cycles, a majority of the weak fibers break and fiber fracture initiation is "halted" while other damage mechanisms come into play. A Second stage is characterized by almost no further fiber fracture until the very last few cycles prior to failure when the rest of the fibers break. Further study of this initiation mechanism revealed a direct relationship between the fiber fracture state and the applied load level. Subjecting the specimens to quasi-static loading at high load levels (80, 85, 90, 91, 92, 93, 94, and 95% σ_u) prior to fatigue cycling at a fixed lower load level (65% σ_u) demonstrated higher fiber fracture densities at higher pre—load levels, regardless of the fatigue cycles at lower load levels. This is one of the key findings of this investigation. "Proof testing" which is a common practice in industry for "verifying" the integrity of a structure, could very well be causing significant subsequent reductions in life.

In summary, this investigation has provided the following salient new findings:

1. During cyclic loading of unidirectional fiber—dominated composite coupons, the evolution of fiber fracture has at least three distinct phases, an early stage (a few percent of life) in which fibers fail in a manner fully dominated by load level, a secondary stage (typically 80% of the life) when very few additional fibers break, and a third stage in which matrix (and interface) damage alters local stress states and links up fiber fracture process to an extent that a catastrophic fiber fracture process is initiated. These three stages present three distinct opportunities to influence the fatigue response of such composites, a fact not previously identified.

2. Using an experimental damage norm that is sensitive to fiber fracture, it was conclusively shown that remaining strength of a fiber—dominated coupon in tension is proportional to fiber fracture density. Since deriving fiber fracture density and determining remaining strength both require destruction of a specimen, this had previously not been established (although widely assumed).

3. Loading to a high level of stress quasi—statically (as one would do in proof testing) before cyclically loading such coupons can greatly reduce fatigue life, if the static load level is high enough to cause significant fiber fracture(of the order of 90% of static strength) in the present case. Moreover, it was found that this reduction in life correlates with the experimentally determined distance between fiber fractures as a function of load level. Based on typical representations of crack growth rates, this strongly suggests that life after stage I fiber fracture is controlled by crack growth in the matrix material.

With these findings as a base, it is now possible to postulate the first well—founded mechanistic model of fiber—dominated fatigue degradation under tensile loading. Although beyond the scope of this document, it is clear that with a knowledge of the cyclic

load level to define stage I fiber fracture and, therefore, stage II crack growth lengths, and subsequent (correct) modeling of stage II crack growth, fatigue life can be mechanistically modeled in these materials, the first time such an approach has been suggested or possible. As a continuing effort, interaction terms between fiber and matrix as well interface between the two could also be incorporated in the model. It is hoped that this dissertation is a first (essential) step in that direction.

Bibliography

1. Rolfe, S.T., and Barsom, J.M., *Fracture and Fatigue Control in Structures; Applications of Fracture Mechanics,* Prentice Hall, N.J., 1977.

2. *Fatigue Under Complex Loading*, R.M. Wetzel, Ed., The Society of Automotive Engineers, Inc., Warrendale, PA, 1975.

3. *Fatigue Mechanisms*, STP 675, J.T. Fong, Ed., American Society for Testing and Materials, Philadelphia, 1980.

4. *Damage in Composite Materials*, STP 775, K.L. Reifsnider, Ed., American Society for Testing and Materials, Philadelphia, 1980.

5. Hahn, H.T., "Fatigue Behavior and Life Prediction of Composite Laminates," *Composite Materilas: Testing and Design (Fifth Conference)*, STP 674, S.W. Tsai, Ed., American Society for Testing and Materials, Philadelphia, 1979, pp. 383-417.

6. Reifsnider, K.L., Schulte, K., and Duke, J.C., "Long—Term Fatigue Behavior of Composite Materials," *Long—Term Behavior of Composites, ASTM STP 813,* T.K. O'Brian, Ed., American Society for Testing and Materials, Philadelphia, 1983, pp. 136-159.

7. Jamison, R.D., "Advanced Fatigue Damage Development in Graphite Epoxy Laminates," Ph.D. dissertation, College of Engineering, Virginia Polytechnic Institute and State University, Blacksburg, VA, Aug. 1982.

8. S.M. Freeman, Characterization of Lamina and Interlaminar Damage in Graphite/Epoxy Composites by the Deply Technique. *Composite Materials: Testing and Design (Sixth Conference), ASTM STP 787,* I.M. Daniel, Ed., American Society for testing and Materials, pp. 50-62 (1982)

9. W.D. Bascom, D.J. Boll, D.L. Huston, B. Fuller and P.J. Phillips, Fractographic Analysis of Interlaminar Fracture, *Toughened composites, ASTM STP 937,* Norman J. Johnston, Ed., American Society for Testing and Materials, Philadelphia, pp. 131-149 (1987).

10. P.S. Theocaris and C.A. Stassinakis, Crack Propagation in Fibrous Composite Materials Studied by SEM, *J. Composite Materials* 15, pp. 133-141 (1981).

11. R.A. Kline and F.H. Chang, Composite Failure Surface Analysis, *J. Composite Materials*, 14, pp. 315-324 (1980).

12. W.M. Jordan and W.L. Bradley, Micromechanisms of Fracture in Toughened Graphite-Epoxy laminates, *Toughened Composites, ASTM STP 937*, N. J. Johnston, Ed., American Society for Testing and Materials, Philadelphia, pp. 95-114 (1987).

13. Razvan, A., Bakis, C.E., Reifsnider, K.L., "Influence of Load Factors on Damage Growth Mechanisms of Notched Composite Materials", Composite Materials: Testing and Design (Ninth Volume), ASTM-STP 1059, S.P. Garbo, Ed., American Society for Testing and Materials, Philadelphia, 1990, pp. 371-389.

14. Bakis, C. E., Stinchcomb, W. W., "Response of Thick, Notched Laminates Subjected to Tension-Compression Cyclic Loads,", *Composite Materials: Fatigue and Fracture, ASTM STP 907*, H. T. Hahn, Ed., American Society for Testing and Materials, Philadelphia, 1986, pp. 314-334.

15. Razvan, A., Bakis, C. E., Wagnecz, L., Reifsnider, K. L., "Influence of Cyclic Load Amplitude on Damage Accumulation and Fracture of Composite Materials," *Journal of Composites Technology & Research, Vol. 10, No. 1, Spring 1988, pp. 3-10.*

16. Charewicz, A. and Daniel, I. M., "Damage Mechanisms and Accumulation in Graphite/Epoxy Laminates,", *Composite Materials: Fatigue and Fracture, ASTM STP 907*, H. T. Hahn, Ed., American Society for Testing and Materials, Philadelphia, 1986, pp. 274-297.

17. Whitworth, H. A., "Modeling Stiffness Reduction of Graphite/Epoxy Composite Laminates", *Journal of Composite Materials*, Vol. 21, April 1987, pp. 362-372.

18. Highsmith, A. L. and Reifsnider, K. L., "Internal Load Distribution Effects During Fatigue Loading of Composite Laminates", *Composite Materials: Fatigue and Fracture, ASTM STP 907*, H. T. Hahn, Ed., American Society for Testing and Materials, Philadelphia, 1986, pp. 233-251.

19. Reifsnider, K. L., and Stinchcomb, W. W., "A Critical- Element Model of the Residual Strength and Life of Fatigue-Loaded Composite Coupons," *Composite Materials: Fatigue and Fracture, ASTM STP 907*, H. T. Hahn, Ed., American Society for Testing and Materials, Philadelphia, 1986, pp. 298-313.

20. Irvine, T. B., and Ginty, C. A., "Progressive Fracture of Fiber Composites", *Journal of Composite Materials*, Vol. 20, March 1986, pp. 166-184.

21. Jamison, R. D. and Reifsnider, K. L., "Assessment of Microdamage Development During Tensile Loading of Graphite/Epoxy Laminates", *Final Report DAAG29-82-K-0190*, U. S. Army Research Office, POB 12211, Research Triangle Park, NC 27709, (Virginia Polytechnic Institute and State University, Blacksburg, VA 24061-4899).

22. Bakis, C. E., "A Test Method to Measure the Response of Composite Materials Under Reversed Cyclic Loads", Presented at the ASTM second symposium on

Test Methods and Design Allowables for Fiber Composites, 3-4 Nov. 1986, Phoenix, AZ.

23. Rummel, W.D., Tedrow, T., Brinkerhoff, H.D., "Enhanced X-ray Stereoscopic NDE of Composite Materials," AFWAL-TR-80-3053, Final Report, June 1980, FDL, AFSC, Air Force Wright Aeronautical Laboratories, WPAFB, OH.

24. Sendeckyj, G.P., Maddux, G.E., and Porter, E., "Damage Documentation in Composites by Stereo Radiography," *Damage in Composite Materials, ASTM STP 775,* K.L. Reifsnider, Ed., American Society for Testing and Materials, 1982, pp. 16-26.

25. Hedgepeth, J.M., "Stress Concentrations for Filamentary Structures", NASA TN D-882, 1961.

26. Hedgepeth, J.M., "Local Stress Concentrations in Imperfect Filamentary Composite Materials", Journal of Composite Materials , Vol. 1, 1967, pp. 294-309.

27. Van Dyke, P., Hedgepeth, J.M., "Stress Concentrations from Single Filament Failures in Composite Materials", Textile Res.,39, 1969, pp. 613-626.

28. Goree, J.G., Gross, R.S., "Analysis of a Unidirectional Composite Containing Broken Fibers and Matrix Damage", Engineering Fracture Mechanics, Vol.13, 1979, pp. 563-578.

29. Dharani, L.R., Jones, W.F., Goree, J.G., "Mathematical Modeling of Damage in Unidirectional composites", Engineering Fracture, 17, 6, 1983, pp. 555-573.

30. Gregory, M.A., Herakovich, C.T., "Predicting Crack Growth Direction in Unidirectional Composites", Journal of Composite Materials, 20, 1986, pp. 67-85.

31. Mar, J.W., Lin, K.Y., "Characterization of Splitting Process in Graphite/Epoxy Composites", Journal Composite Materials, 13, 1979, pp. 278-287.

32. Garg, A.C., "0° Split Initiation in Fiber Reinforced Composites", Engineering Fracture Mechanics, Vol. 24, No. 2, 1986, pp. 255-261.

33. Wolla, J.M., Goree, J.G., "Experimental Evaluation of Longitudinal Splitting in Unidirectional Composites", Journal of composite Materials, 21, 1987, pp. 49-67.

34. Dharan, C.K., "Fatigue Failure Mechanisms in a Unidirectionally Reinforced Composite Material", Fatigue of Composite Materials , ASTM STP 569, American Society for Testing and Materials, 1975, pp. 171-188.

35. Reedy, E.D., "Fiber Stresses in a Cracked Monolayer: Comparison of Shear-Lag and 3-D Finite Element Predictions", Journal of Composite Materials, 18, 1984, pp. 595-607.

36. Ermolenko, E.F., "A Model of Failure of a Unidirectional Fiber Plastic With a Brittle Matrix", Mech. Comp. Mat, 21, 2, 1985, pp. 162-170.

37. Tsykalo, V.A., "Simulation of Damage Accumulation and Crack Formation Processes in Unidirectional Composites", Mech. Comp. Mat., 21, 2, 1985, pp. 183-188.

38. Rabotnov, Y.N., et.al., "Cyclic Strength of Unidirectional Carbon-Reinforced Plastics in Tensile Loading at an Angle in Relation to the Reinforcement Direction", Mech. Comp. Mat., 21, 2, 1985, pp. 158-162.

39. Lorenzo, L., Hahn, H.T., "Fatigue Failure Mechanisms in Unidirectional Composites", Composite Materials: Fatigue and Fracture, ASTM STP 907, American Society for Testing and Materials, Philadelphia, 1986, pp. 210-232.

40. A. Razvan, C.E. Bakis, K.L. Reifsnider, "S.E.M. Investigation of Fiber Fracture in Composite Laminates", Materials Characterization—An International Journal, Vol. 24, No. 2, 1990, pp. 179-190.

41. Dvorak, G.J., Laws, N., "Analysis of First Ply Failure in Composite Laminates", Engineering Fracture Mechanics , 25, 5/6, 1986, pp. 763-770.

42. Rotem, A., "Fatigue and Residual Strength of Composite Laminates", Engineering Fracture Mechanics , 25, 5/6, 1986, pp. 819-827.

43. Lene, F., "Damage Constitutive Relations for Composite Materials", Engineering Fracture Mechanics , 25, 5/6, 1986, pp. 713-728.

44. Chang, F.K., Chang, K.Y., "A Progressive Damage Model for Laminated composites Containing Stress Concentrations", Journal of Composite Materials, 21, 1987, pp. 834-855.

45. Shih, G.C., Ebert, L.J., "Theoretical Modelling of the Effect of the Interfacial Shear Strength on the Longitudinal Tensile Strength of Unidirectional Composites", Journal of composite Materials, 21, 1987, pp. 207-224.

46. Murakami, H., Hegemier, G.A., "A Mixture Model for Unidirectionally Fiber-Reinforced Composites", Journal of Applied Mechanics, 53, 1986, pp. 765-773.

47. Ochoa, O.O., Engblom, J.J., "Analysis of Progressive Failure in Composites", Composites Science and Technology , 28, 1987, pp. 87-102.

48. Batdorf, S.B., "Tensile Strength of Unidirectionally Reinforced Composites -I", Journal of Reinforced Plastics and Composites, 1, 1982, pp. 153-164.

49. Batdorf, S.B., Ghaffarian, R., "Tensile Strength of Unidirectionally Reinforced Composites -II", Journal of Reinforced Plastics and Composites , 1, 1982, pp. 165-176.

50. Batdorf, S.B., Ghaffarian, R., "Size Effect and Strength Variability of Unidirectional Composites", International Journal of Fracture , 26, 1984, pp. 113-122.

51. Hwang, W., Han, K.S., "Statistical Study of Strength and Fatigue Life of Composite Materials", Composites , 18, 1, 1987, pp. 47-53.

52. Gutans, J., Tamuzs, V., "Strength Probability of Unidirectional Hybrid Composites", Theoretical and Applied Fracture Mechanics , 7, 1987, pp. 193-200.

53. Phani, K.K., "The Strength-Length Relationship for Carbon Fibers", Composite Science and Technology , 30, 1987, pp. 59-71.

54. Jamison, R.D., "Fiber Fracture in Composite Laminates", International Conference on Composite Materials-VI , 3, 1987, pp. 185-199.

55. Razvan, A., Simonds, R.A., Reifsnider, K.L., Stinchcomb, W.W., "Effects of Load Train alignment on the Fatigue Failure Characteristics of Unidirectional

Graphite/Epoxy Composite Materials," *Journal of Reinforced Plastics and Composites*, Vol. 11, No. 3, March 1992, pp.310-323.

56. Razvan, A., Reifsnider, K.L., "Fiber Fracture and Strength Degradation in Uni-Directional Graphite/Epoxy Composite Materials," *Theoretical and Applied Fracture Mechanics*, Vol. 16, No. 1., 1991, pp. 81-89.

57. Razvan, A., Elahi, M., Reifsnider, K.L., Gaylord, C., "Damage Evolution Monitoring in Unidirectional Graphite/Epoxy Composite Materials," *Proceedings of the 1991 Spring Conference of the Society for Experimental Mechanics*, June 10-13,1991, Milwaukee, Wisconsin.

58. Lifshitz, J.M., "Deformational Behavior of Unidirectional Graphite/Epoxy Composite Under Comporessive Fatigue," *J. of Composite Technology & Research*, Vol. 11, No. 3, Fall 1989, pp. 99-105.

59. So, C.K., Lai, T.C., and Tse, P.C., "The Measurement of Material Damping by Free—Vibration Technique with Periodic Excitation", *Experimental Technique*, Vol. 7, Sep. 1988, pp. 413-433.

60. Elahi, M., Razvan, A., Reifsnider, K.L., "Characterization of Composite Materials Dynamic Response Using Load/Stroke Frequency Response Measurement," *Composite Materials: Fatigue and Fracture*, ASTM STP 1156, (in press).

61. "The Fundumental of Signal Analysis", *Application Note 243*, Hewlett Packard Co., 1989.

62. "The Fundumental of Modal Testing", *Application note 243-3*, Hewlett Packard Co. 1989.

63. *HP 3562-A Operating Manual, Dynamic Signal Analyzer*, Hewlett Packard Co., March 1990.

64. *Computational Methods In Structural Dynamics*, Meirovitch, L., Sijthoff & Noordhoff, 1980.

65. Razvan, A., Elahi, M., Reifsnider, K.L., "Fiber Fracture and Strength Degradation Analysis in Unidirectional Graphite/Epoxy Materials via Dynamic Mechanical Testing," *Composite Materials: Fatigue and Fracture*, ASTM STP, (accepted for publication).

66. Elahi, M., Razvan, A., Reifsnider, K.L., "Influence of Fiber—Matrix Interface on Dynamic Response of CFRP," *Composite Materials: Fatigue and Fracture*, ASTM STP, (accepted for publication).

67. Paris, P.C., Erdogan, F., "A Critical Analysis of Crack Propagation Laws," *Journal of Basic Engr.*, Vol. 85, 1963, p 528.

68. O'Brian, T.K., "Towards a Damage Tolerance Philosophy for Composite Materials and Structures," *Composite Materials: Testing and Design (Ninth Volume)*, ASTM STP 1059, S.P. Garbo, Ed., American Society for Testing and Materials, Philadelphia, 1990. pp. 7-33.

Appendix A

Tables

Table 1. Different Forms of Frequency Response.

Definition	Response	Variable
Compliance	$\frac{X}{F}$	$\frac{DISPLACEMENT}{FORCE}$
Mobility	$\frac{V}{F}$	$\frac{VELOCITY}{FORCE}$
Inertance	$\frac{A}{F}$	$\frac{ACCELARATION}{FORCE}$

Table 2. S—N data for 8—ply graphite/epoxy laminate at 60% ultimate strength.

Specimen #	$N_{failure}$	Average (Median)	Weibul Parameters	
			α	β
SN3-1	2,403,240			
SN3-3	7,881,920			
SN3-6	4,135,601			
SN3-7	7,565,160			
SN3-8	9,906,804			
SN3-9	11,992,505			
SN3-11	3,987,324			
SN3-12	6,604,190			
SN3-13	7,204,820			
SN3-14	8,395,891			
SN3-15	10,097,693			
SN3-16	8,330,743			
SN3-18	4,626,800			
SN3-19	2,339,410			
SN3-20	5,055,522			
SN3-21	12,860,280			
SN3-23	6,815,911			
SN3-24	16,653,502			
SN3-25	1,256,378			
SN3-27	5,912,666			
SN3-28	1,280,142			
SN3-29	5,987,634			
SN3-30	2,068,569			
SN3-32	14,542,559			
SN3-33	2,758,260			
SN3-34	4,376,978			
SN3-35	4,537,064			
SN3-37	5,115,977			
SN3-38	5,178,283			
SN3-39	6,308,511	6,900,333		
SN3-40	16,704,605	(6,710,050)	1.73	7,754,593

Table 3. S—N data for 8—ply graphite/epoxy laminate at 65% ultimate strength.

Specimen #	$N_{failure}$	Average (Median)	Weibul Parameters	
			α	β
SN5-1	5,131,668			
SN5-2	2,207,925			
SN5-3	432,983			
SN5-4	2,213,055			
SN5-5	2,703,331			
SN5-6	2,945,936			
SN5-8	2,645,112			
SN5-9	2,358,805			
SN5-10	7,887,005			
SN5-11	2,944,780			
SN5-12	6,517,765			
SN5-13	3,149,355			
SN5-14	1,865,949			
SN5-16	459,689			
SN5-17	2,401,376			
SN5-18	1,787,059			
SN5-19	371,484			
SN5-20	1,035,588			
SN5-21	3,250,402			
SN5-22	164,257			
SN5-23	167,040			
SN5-25	2,141,080			
SN5-26	2,657,951			
SN5-27	1,015,979			
SN5-28	4,896,031			
SN5-29	2,473,120			
SN5-30	1,293,098			
SN5-32	1,638,624			
SN5-33	251,049			
SN5-36	494,623			
SN5-37	1,369,172			
SN5-39	2,816,096			
SN5-43	757,645			
SN5-44	2,653,670			
SN5-46	1,817,623			
SN5-47	128,808			
SN5-48	609,889			
SN5-49	3,988,324	2,321,463		
SN5-50	6,893,718	(2,207,925)	1.23	2,478,860

Table 4. S—N data for 8—ply graphite/epoxy laminate at 70% ultimate strength.

Specimen #	$N_{failure}$	Average (Median)	Weibul Parameters	
			α	β
SN1-1	1,700			
SN1-2	136,150			
SN1-3	831,520			
SN1-4	399,380			
SN1-5	2,582,960			
SN1-6	36,170			
SN1-7	179,030			
SN1-8	682,410			
SN1-9	922,550			
SN1-10	520,340			
SN1-11	700,660			
SN1-12	1,070,179			
SN1-13	46,830			
SN1-15	32,060			
SN1-16	1,577			
SN1-17	169,432			
SN1-18	56,892			
SN1-19	33,289			
SN1-20	1,030			
SN1-21	5,264			
SN1-22	200,209			
SN1-23	264,019			
SN1-24	1,662			
SN1-25	7,622			
SN1-26	85,097			
SN1-27	489,724			
SN1-28	15,215			
SN1-29	64,059			
SN1-30	5,648			
SN1-31	20,672			
SN1-32	51,254			
SN1-33	57,846			
SN1-34	769,191			
SN1-35	15,401			
SN1-36	442,736			
SN1-37	4,623			
SN1-38	42,165			
SN1-39	1,649			
SN1-40	68,836			
SN1-41	454,380			

Table 5. S—N data for 8—ply graphite/epoxy laminate at 70% ultimate strength-(continued from Table 4).

Specimen #	$N_{failure}$	Average (Median)	Weibul Parameters	
			α	β
RSM-7M	1,171			
RSM-3L	8,855			
RSM-4L	7,377			
RSM-6L	255,327			
RSM-7L	465,517			
RSM-8L	296,660			
RS-70-E1	3,400			
RS-70-E2	1,128	260,663		
RS-70-M1	174,873	(57,369)	0.53	147,909

Table 6. S–N data for 8–ply graphite/epoxy laminate at 75% ultimate strength.

Specimen #	$N_{failure}$	Average (Median)	Weibul Parameters	
			α	β
SN4-1	4,708			
SN4-2	9,218			
SN4-3	6,462			
SN4-4	81,228			
SN4-5	357,206			
SN4-6	736,455			
SN4-7	38,728			
SN4-8	280,001			
SN4-9	193,849			
SN4-10	3,395			
SN4-11	6,767			
SN4-12	138,066			
SN4-13	176,902			
SN4-14	1,668			
SN4-16	986			
SN4-18	3,980			
SN4-19	1,352			
SN4-20	1,983			
SN4-21	1,138			
SN4-22	1,819			
SN4-23	1,961			
SN4-24	2,979			
SN4-25	734			
SN4-26	2,251			
SN4-27	2,397			
SN4-28	2,413			
SN4-29	4,035			
SN4-30	1,969			
SN4-31	66,341			
SN4-32	2,395			
SN4-33	2,619			
SN4-34	1,465			
SN4-35	5,798			
SN4-36	1,196			
SN4-37	2,820			
SN4-38	55,563			
SN4-39	8,311			
SN4-40	141,859			
SN4-41	1,079			
SN4-42	6,350			
SN4-43	557			
SN4-44	1,615	54,980		
SN4-45	6,511	(2,979)	0.47	19,466

Table 7. S—N data for 8—ply graphite/epoxy laminate at 80% ultimate strength.

Specimen #	$N_{failure}$	Average (Median)	Weibul Parameters	
			α	β
SN2-1	250			
SN2-2	380			
SN2-4	300			
SN2-5	830			
SN2-6	490			
SN2-7	320			
SN2-8	610			
SN2-9	1,730			
SN2-10	1,187			
SN2-11	936			
SN2-12	931			
SN2-13	2,049			
SN2-14	715			
SN2-15	1,440			
SN2-16	1,520			
SN2-17	3,289			
SN2-18	2,715			
SN2-19	1,500			
SN2-20	1,259			
SN2-21	742			
SN2-22	564			
SN2-23	1,227			
SN2-24	414			
SN2-25	692			
SN2-26	240			
SN2-27	643			
SN2-28	954			
SN2-29	1,017			
SN2-30	622			
SN2-31	299			
SN2-32	1,038			
SN2-33	282			
SN2-35	453			
SN2-36	892			
SN2-37	452			
SN2-38	1,069			
SN2-39	504			
SN2-40	779			
SN2-41	637			
SN2-42	258			
SN2-43	632	884		
SN2-44	266	(703)	1.52	990

Table 8. Residual strength data at 65% ultimate strength relative to % phase and % gain damage

SPECIMEN #	N	DAMAGE		$\sigma_{res.}$ (PSI)
		% GAIN	% PHASE	
RS-65-M6	1,794	4.47	5.9	384,000
RS-65-E12	909	6.13	5.48	361,650
RS-65-E10	854	4.40	16.48	338,850
RS-65-E11	1,260	20.76	11.64	343,350
RS-65-E7	3,573	18.96	11.86	337,000
RS-65-M8	42,382	20.98	20.09	353,000
RS-65-E9	71,623	19.42	43.43	362,250
RS-65-E5	18,245	62.13	51.10	276,000
RS-65-M9	23,926	23.16	51.59	324,850
RS-65-E8	33,087	90.22	62.27	304,905
RS-65-M10	250,784	36.64	63.19	368,500
RS-65-M7	775,342	42.29	69.94	333,000
RS-65-L3	120,764	50.18	82.16	325,250
RS-65-E6	885,848	83.16	83.88	307,000

Table 9. Residual strength data at 70% ultimate strength relative to % phase and % gain damage

SPECIMEN #	N	DAMAGE		$\sigma_{res.}$ (PSI)
		% GAIN	% PHASE	
RS-70-E3	786	29.94	79.47	360,500
RS-70-E5	6,001	16.45	94.82	350,000
RS-70-M2	1,174	33.19	97.21	306,190
RS-70-M3	2,438	27.75	72.62	345,500
RS-70-M5	4,999	11.93	79.90	367,500
RS-70-L1	3,522	51.40	112.88	294,286
RS-70-L2	37,002	14.58	77.10	345,000

Table 10. Fiber Fracture data for 65% UTS Based on % Phase and % Gain Damage.

Specimen I.D.	N	DAMAGE		Fiber Fracture Counts			
		% Phase	% Gain	Singlet	Doublet	Triplet	Quad-plet
FF-65-E2	787	9.50	1.32	80	33	18	1
FF-65-E3	4761	210.46	5.88	32	22	3	0
FF-65-E4	1244	10.71	0.74	81	45	16	1
FF-65-E5	1814	15.47	2.83	72	56	8	0
FF-65-M1	5849	65.87	7.47	106	76	12	2
FF-65-M2	98103	63.47	13.96	68	54	7	0
FF-65-M3	151002	49.33	15.80	34	23	4	1
FF-65-L1	125644	200.16	45.29	130	87	17	3
FF-65-L2	584653	88.67	13.50	94	51	18	1
FF-65-L3	156001	70.71	14.98	49	41	4	0
FF-65-L4	85002	80.06	80.66	127	113	7	0
FF_65_L5	46288	30.65	14.98	443	390	23	1
FF-65-L6	140008	73.22	60.09	84	76	4	0
FF-65-L7	999998	82.02	49.92	567	528	19	1

Table 11. Fiber Fracture data for 70% UTS Based on % Phase and % Gain Damage.

Specimen I.D.	N	DAMAGE		Fiber Fracture Counts			
		% Phase	% Gain	Singlet	Doublet	Triplet	Quad-plet
FF_70_E1	483	53.44	51.89	268	195	27	5
FF_70_E2	773	50.97	26.41	291	241	22	2
FF_70_E3	773	73.19	55.85	57	44	5	1
FF_70_E4	467	63.56	54.62	206	178	14	0
FF_70_M3	2438	71.17	28.37	354	275	32	5
FF_70_M6	1375	115.18	91.67	161	145	5	2
FF_70_M7	2142	94.66	60.73	80	66	7	0
FF_70_L9	59492	105.15	5.47	97	78	8	1
FF_70_L1	3522	106.16	76.91	109	78	11	3

Table 12. Statically loaded and fatigue cycled at 65% UTS specimens fiber fracture data.

			DAMAGE		Fiber Fracture Counts			
$\%\sigma_u$ (static)	Specimen I.D.	N @ 65% σ_u	% Phase	% Gain	Singlet	Doublet	Triplet	Quad-plet
93	L93654	500000	40.50	74.53	210	8	1	0
93	FF93653	180338	49.33	23.12	469	22	1	0
92	L92652	500000	31.52	81.93	233	21	1	0
90	L90652	500000	58.97	39.15	163	36	2	0
90	FF90655	65688	50.10	21.35	522	91	21	8
90	FF90654	97326	50.92	18.09	353	35	0	0
85	FF85652	17155	52.40	38.51	137	18	0	0
80	FF80653	676483	45.29	57.42	168	9	0	0
80	FF80652	494145	60.10	47.61	201	18	3	0
65	FF-65-L2	584653	88.67	13.50	51	18	1	1
65	FF-65-M2	98103	63.47	13.96	54	7	0	0
65	FF-65-L3	156001	70.71	14.98	41	4	0	0

Table 13. S—N data for specimens fatigued at 65% UTS after being loaded quasi-statically to higher load levels.

Specimen I.D.	Static load % UTS	DAMAGE % Phase	DAMAGE % Gain	$N_{failure}$
FF94651	94	133.23	103.58	2970
L95651	95	138.78	71.08	2745
L94651	94	79.04	82.09	302424
L93653	93	77.17	81.77	105122
L93651	93	-----	-----	788301
L92651	92	60.34	107.95	460510
L90651	90	69.06	89.99	3051022
FF80654	80	85.68	116.87	186315
RS_65_L1	65	-----	-----	696196
RS_65_M2	65	-----	-----	680767

Appendix B

Figures

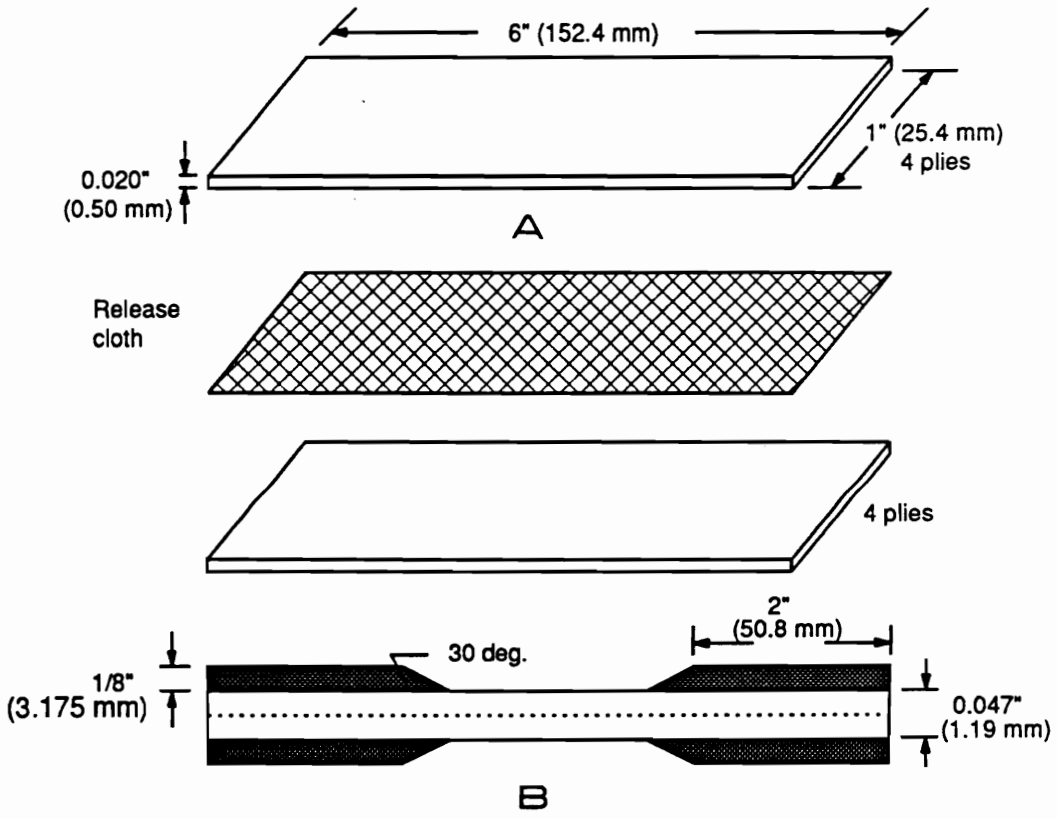

Figure 1. Test specimen dimensions in inches (mm.): (A) Laminate assembly, (B) Test specimen with bonded tabs. (Load applied horizontally)

Figure 2. Example of gripped affected zone: (A) gripped and (B) gage section.

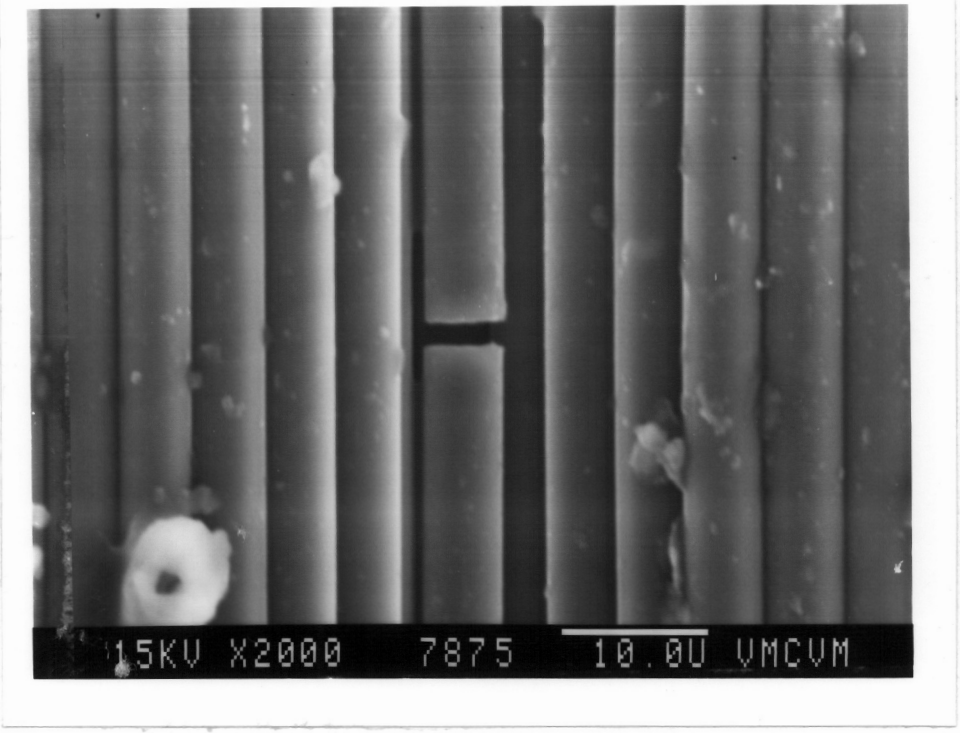

Figure 3. Example of a singlet fiber fracture.

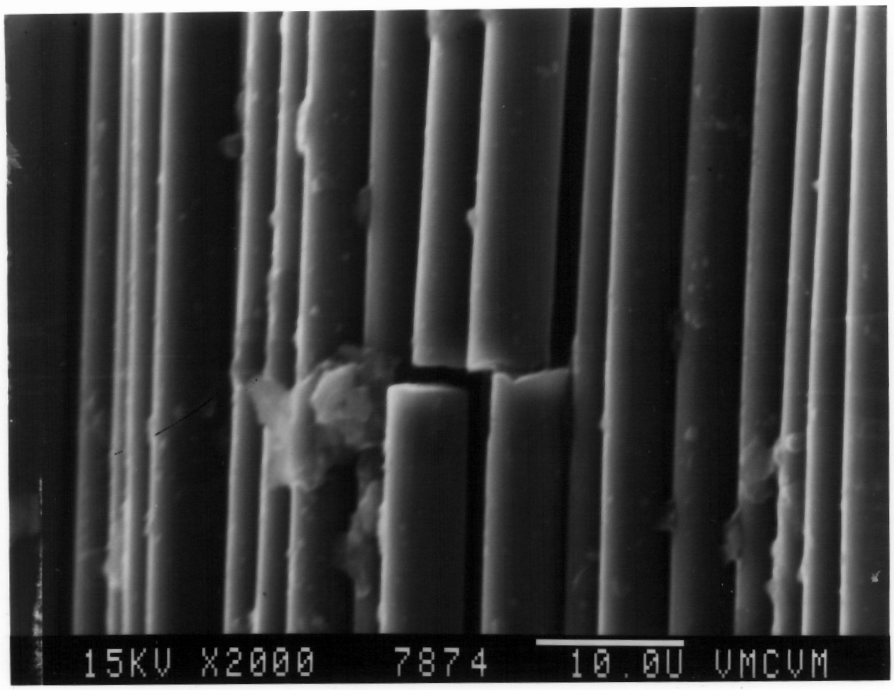

Figure 4. Example of a doublet fiber fracture.

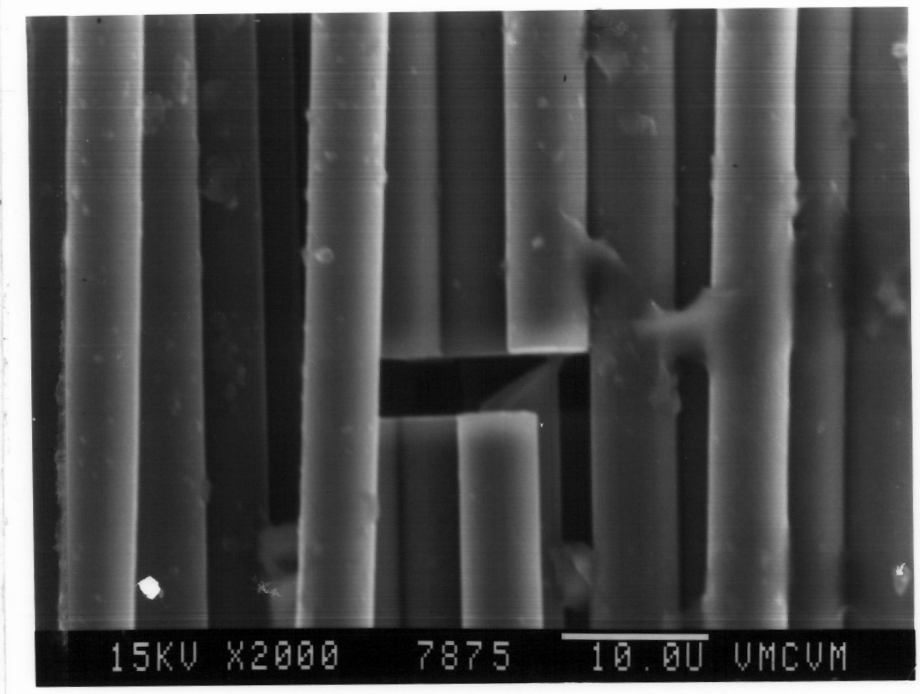

Figure 5. Example of a triplet fiber fracture.

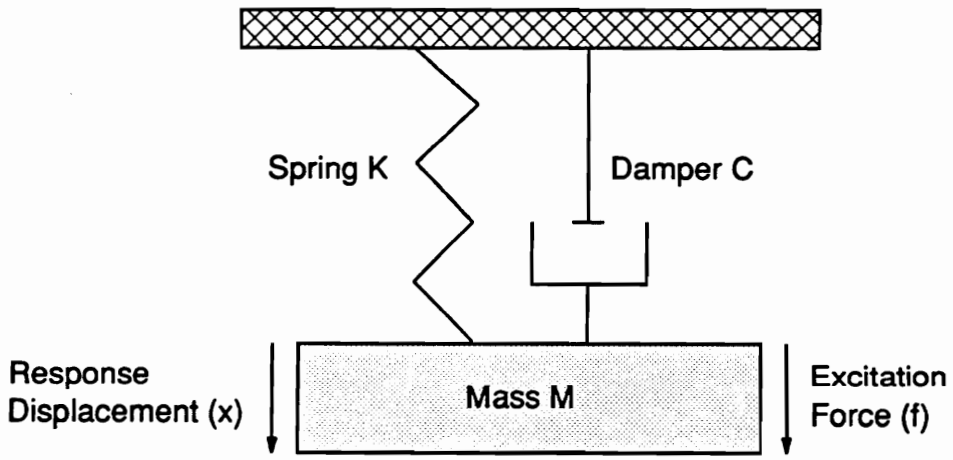

Figure 6. SDOF discrete parameter model.

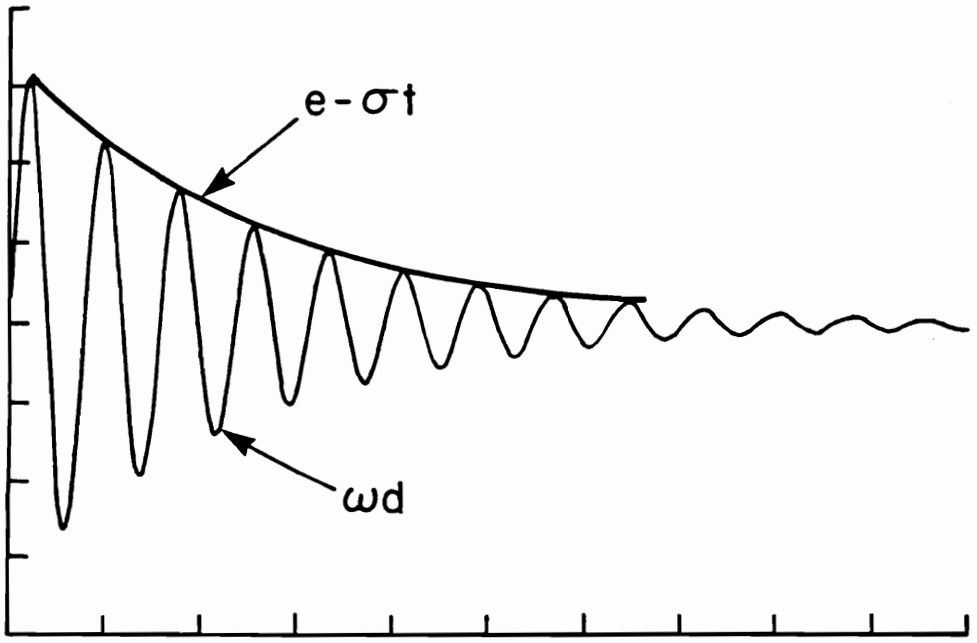

Figure 7. SDOF impulse response/free decay.

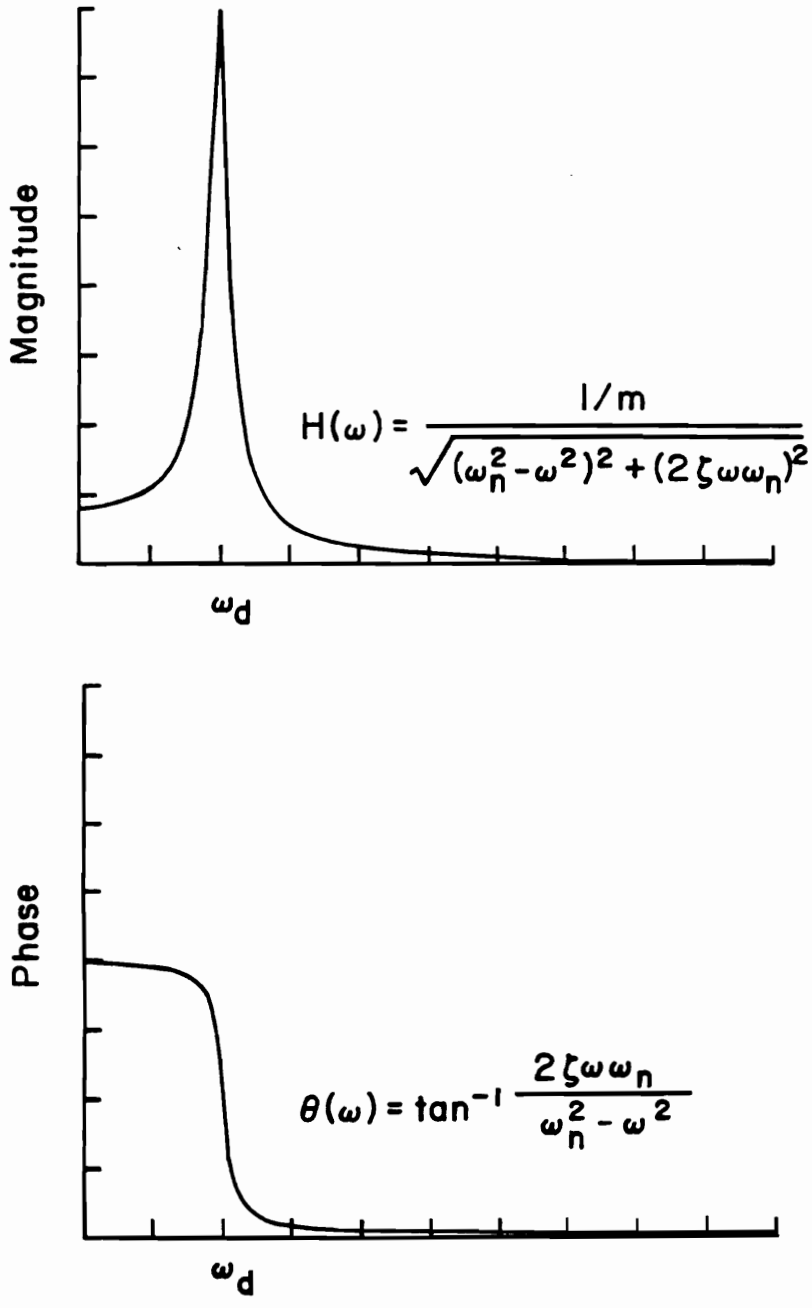

Figure 8. Frequency response — polar coordinates.

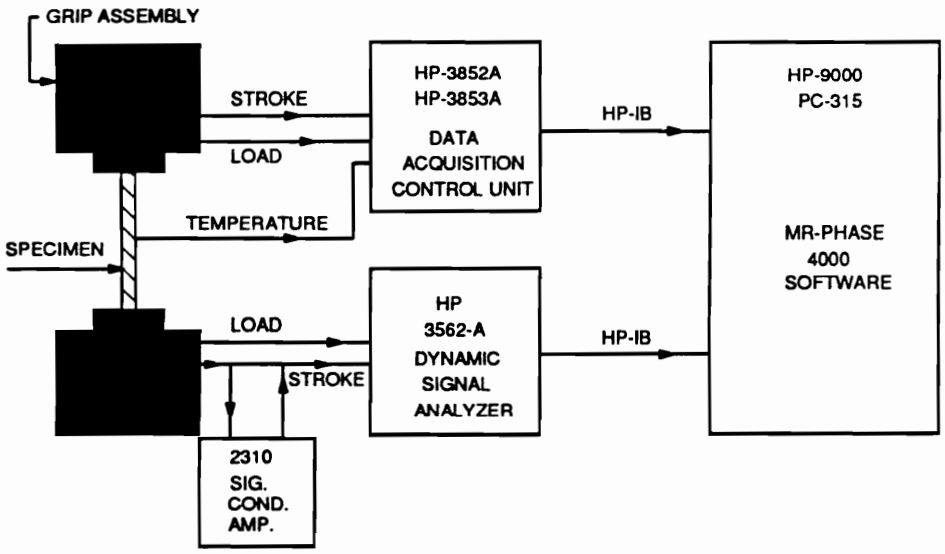

Figure 9. Schematic diagram of the Dynamic Mechanical analysis experimental setup.

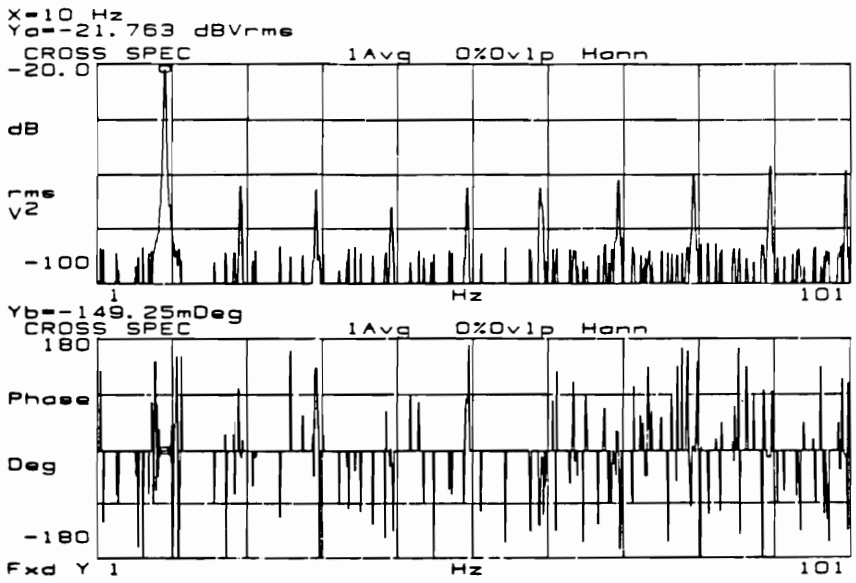

Figure 10. Cross spectrum measurement of an Aluminum specimen: Fatigued at a frequency of 10 Hz, and 40% σ_{yt}

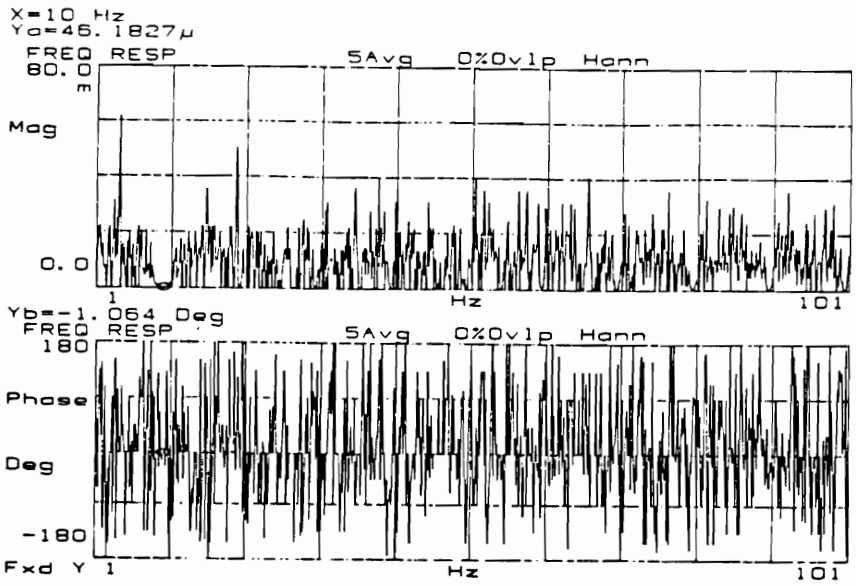

Figure 11. Frequency response measurement of an Aluminum specimen: Fatigued at a frequency of 10 Hz., and 40% σ_{yt}

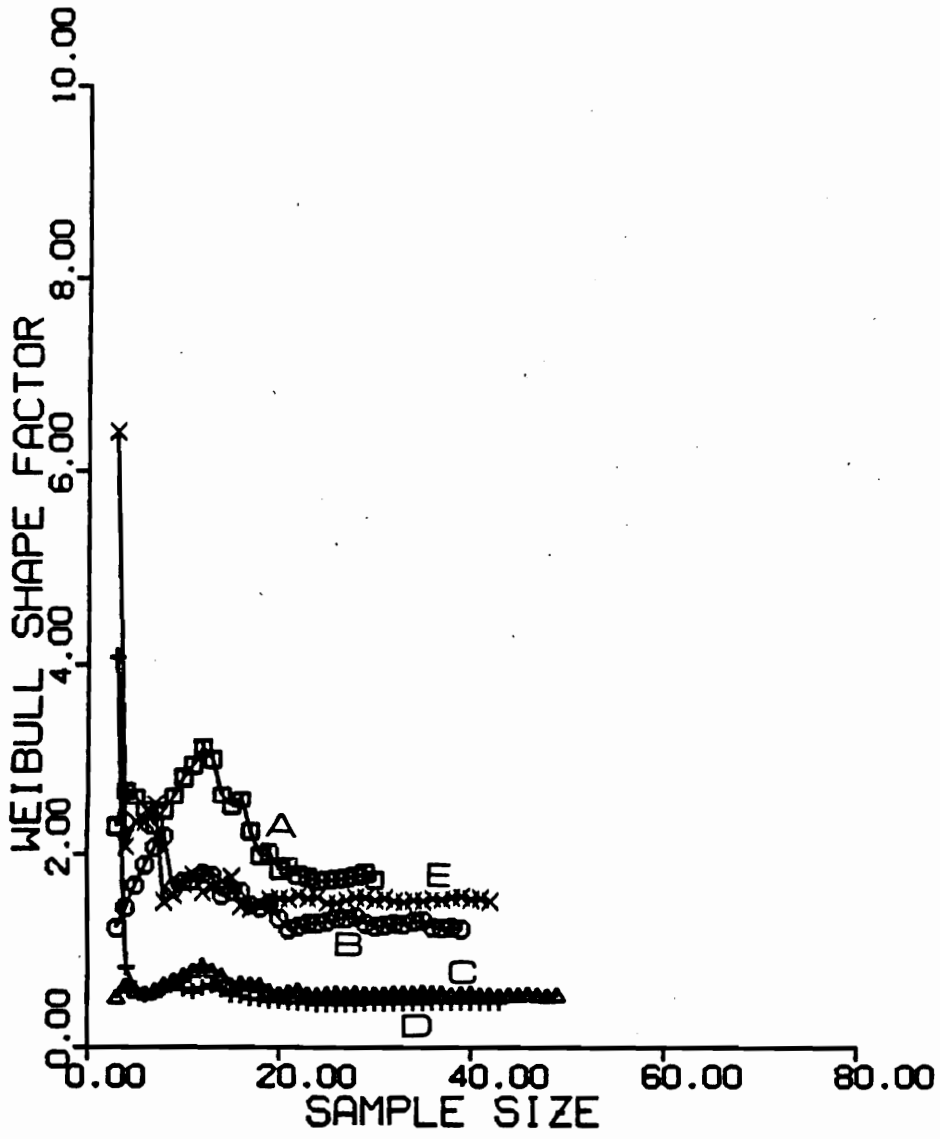

Figure 12. **Weibul shape factor stabilization as a function of sample size at:** A) 60%, B) 65%, C) 70%, D) 75%, and E) 80% σ_u

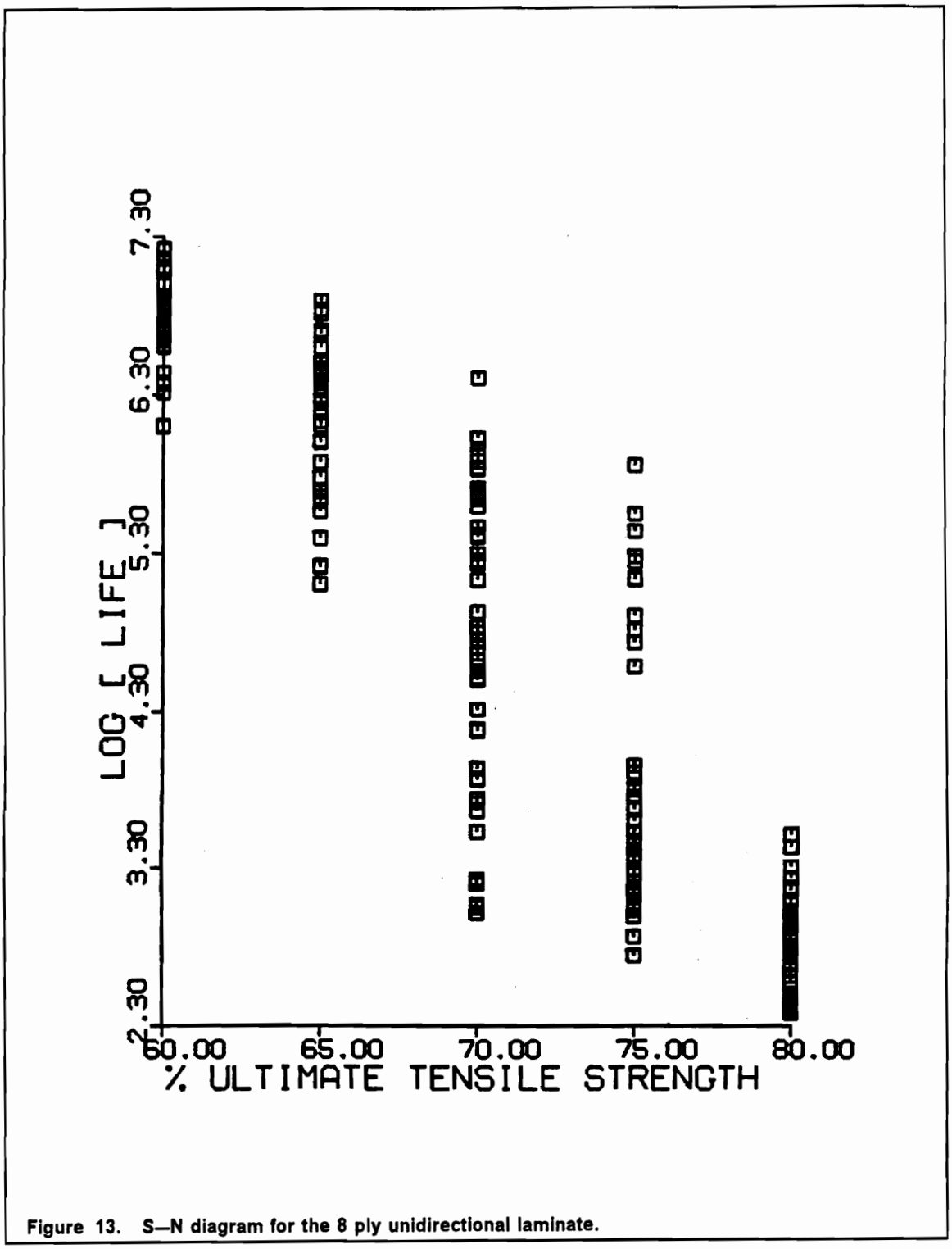

Figure 13. S—N diagram for the 8 ply unidirectional laminate.

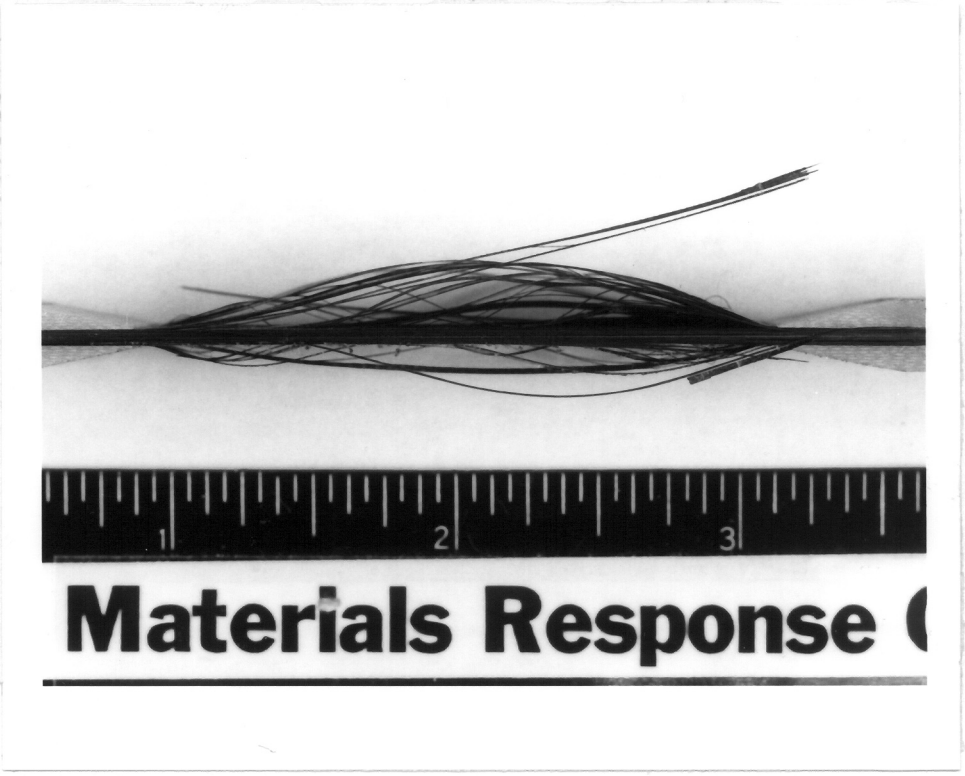

Figure 14. Characteristic surface matrix splittings at approximately 50% of life.

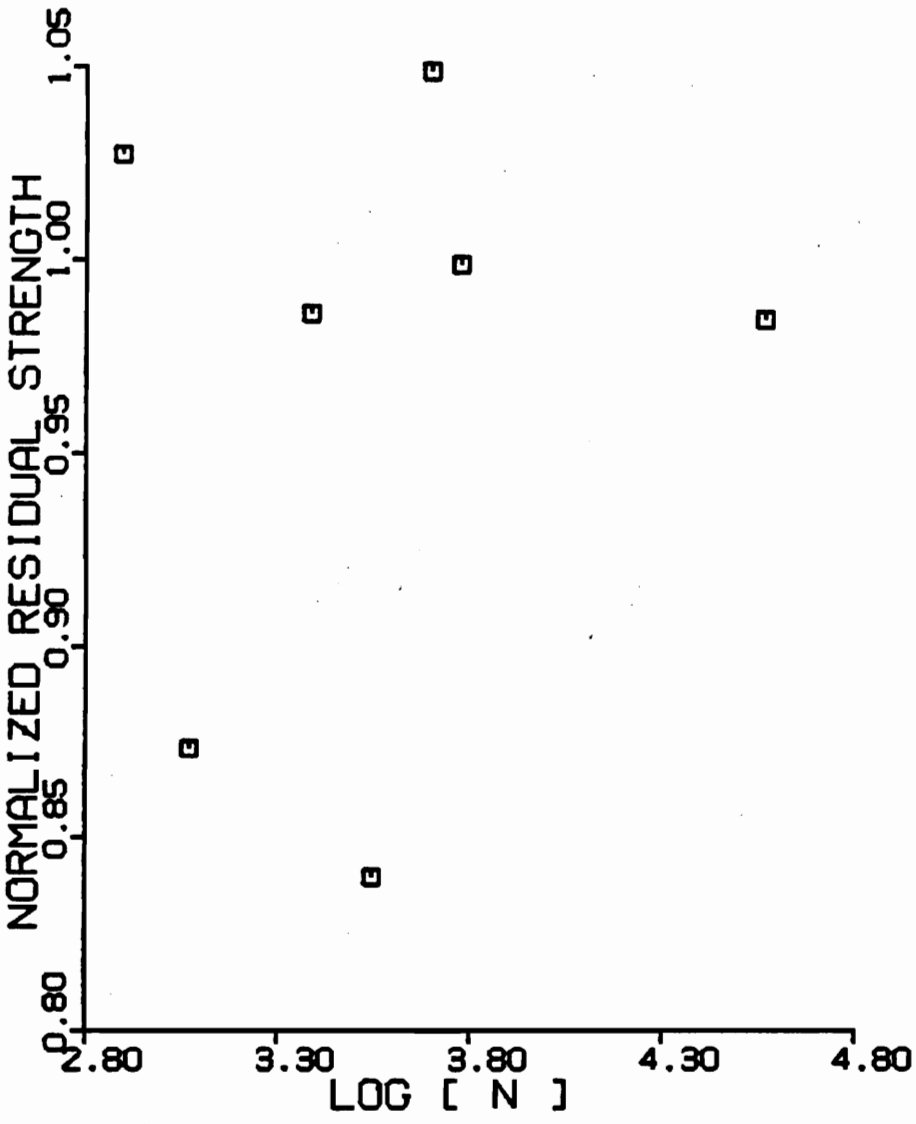

Figure 15. Residual strength as a function of percent of median life.

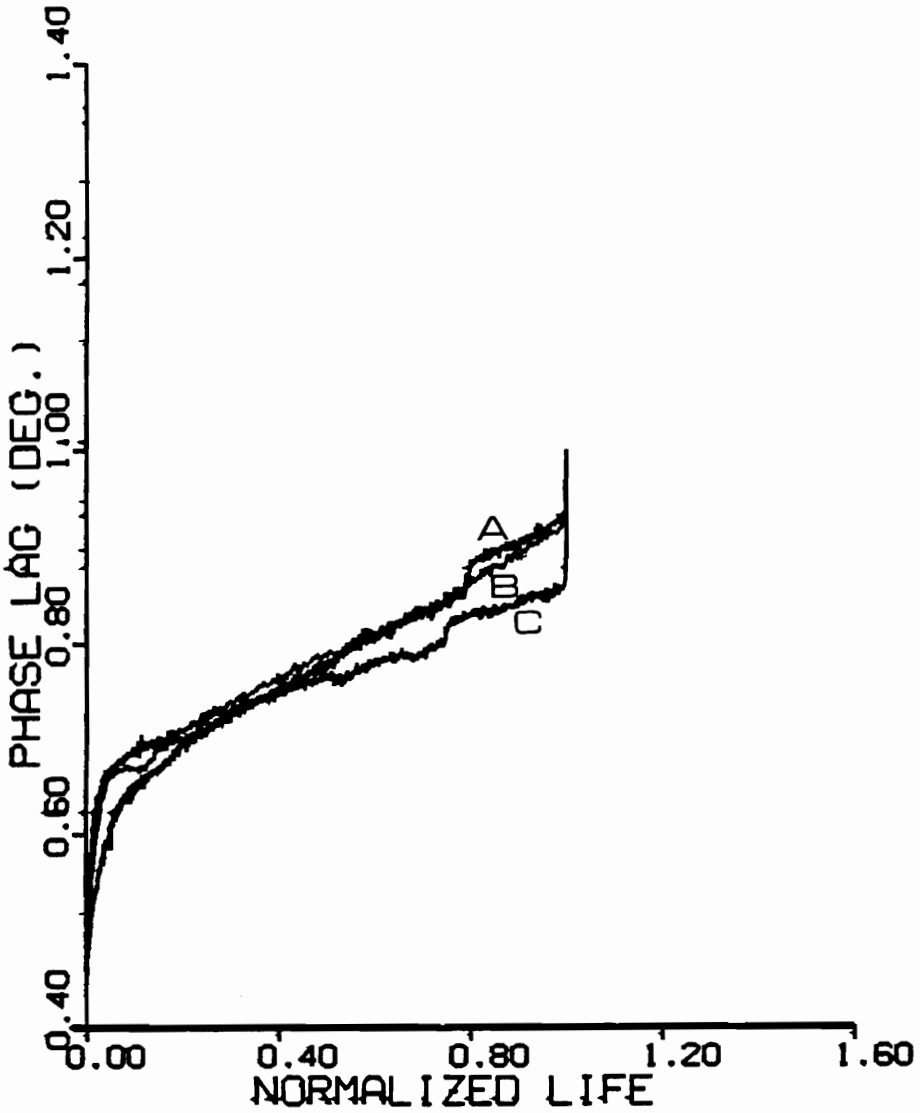

Figure 16. Phase lag response at 65% UTS.: For specimens A) RS-65-E4, B) RS-65-M4, and C) SN-5-47

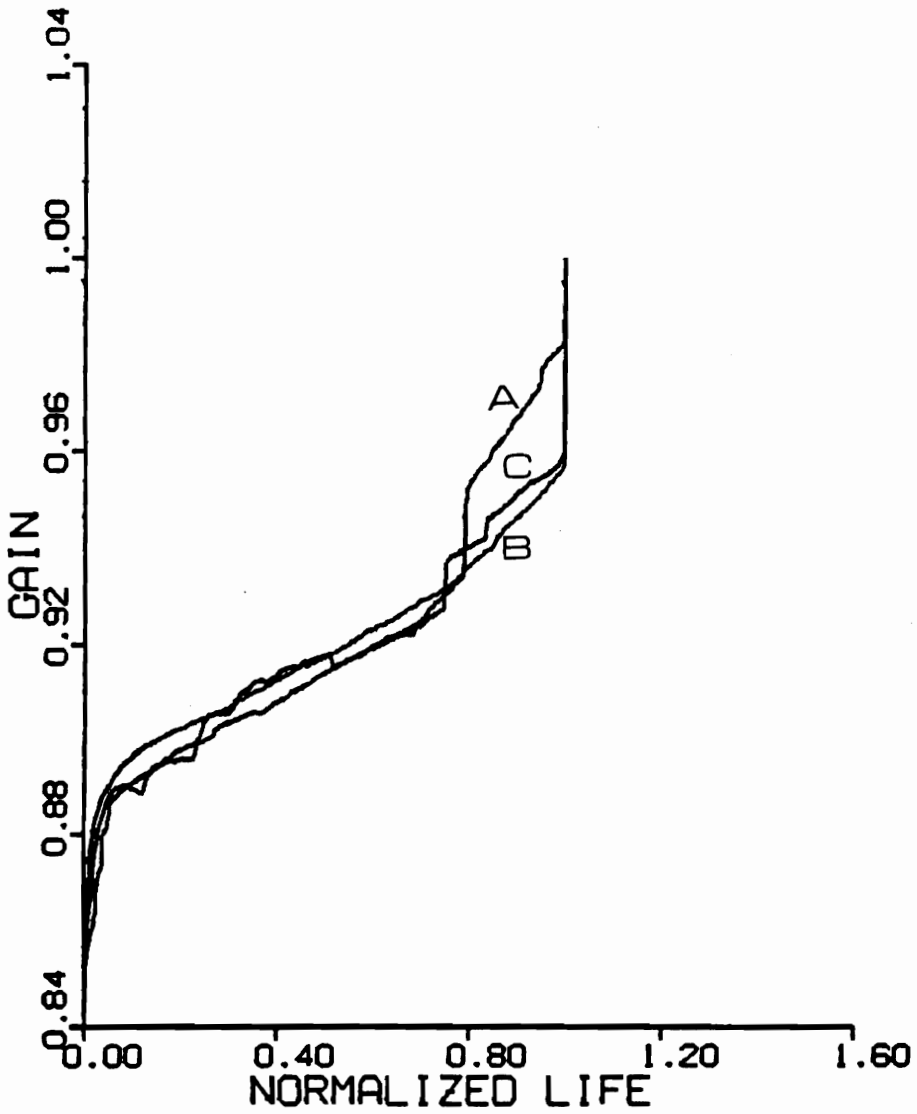

Figure 17. Gain response at 65% UTS.: For specimens A) RS-65-E4, B) RS-65-M4, and C) SN-5-47

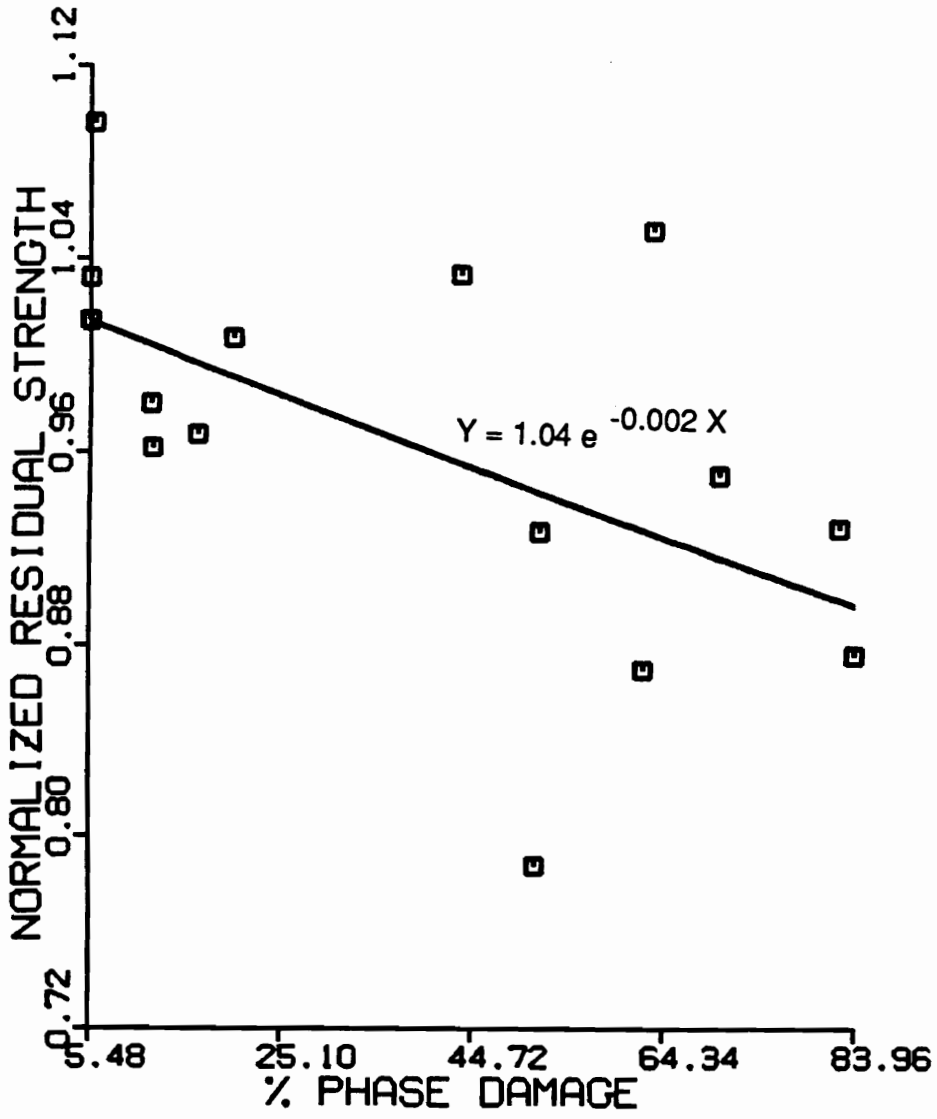

Figure 18. **Residual strength degradation as a function of % phase damage at 65% UTS.:** (Coefficient of determination = 0.27)

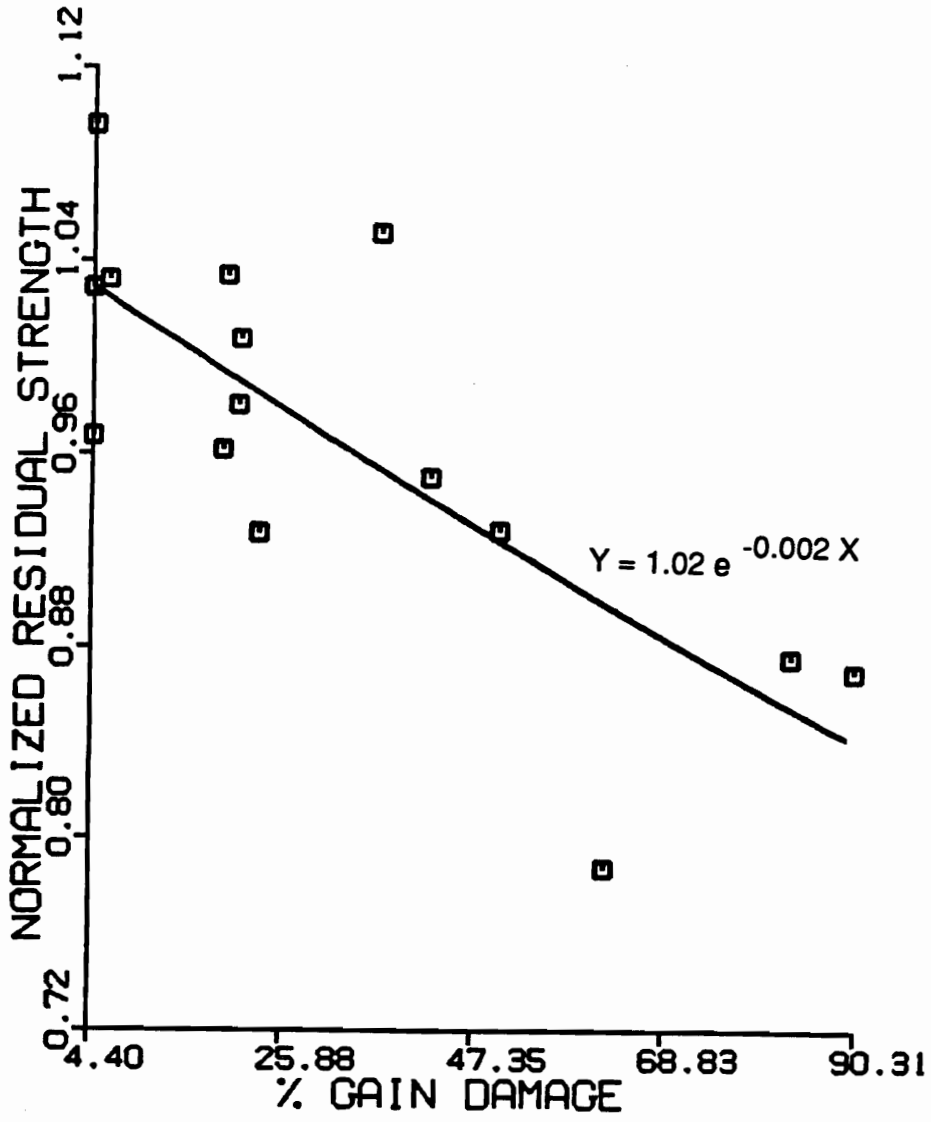

Figure 19. Residual strength degradation as a function of % gain damage at 65% UTS.: (Coefficient of determination = 0.56)

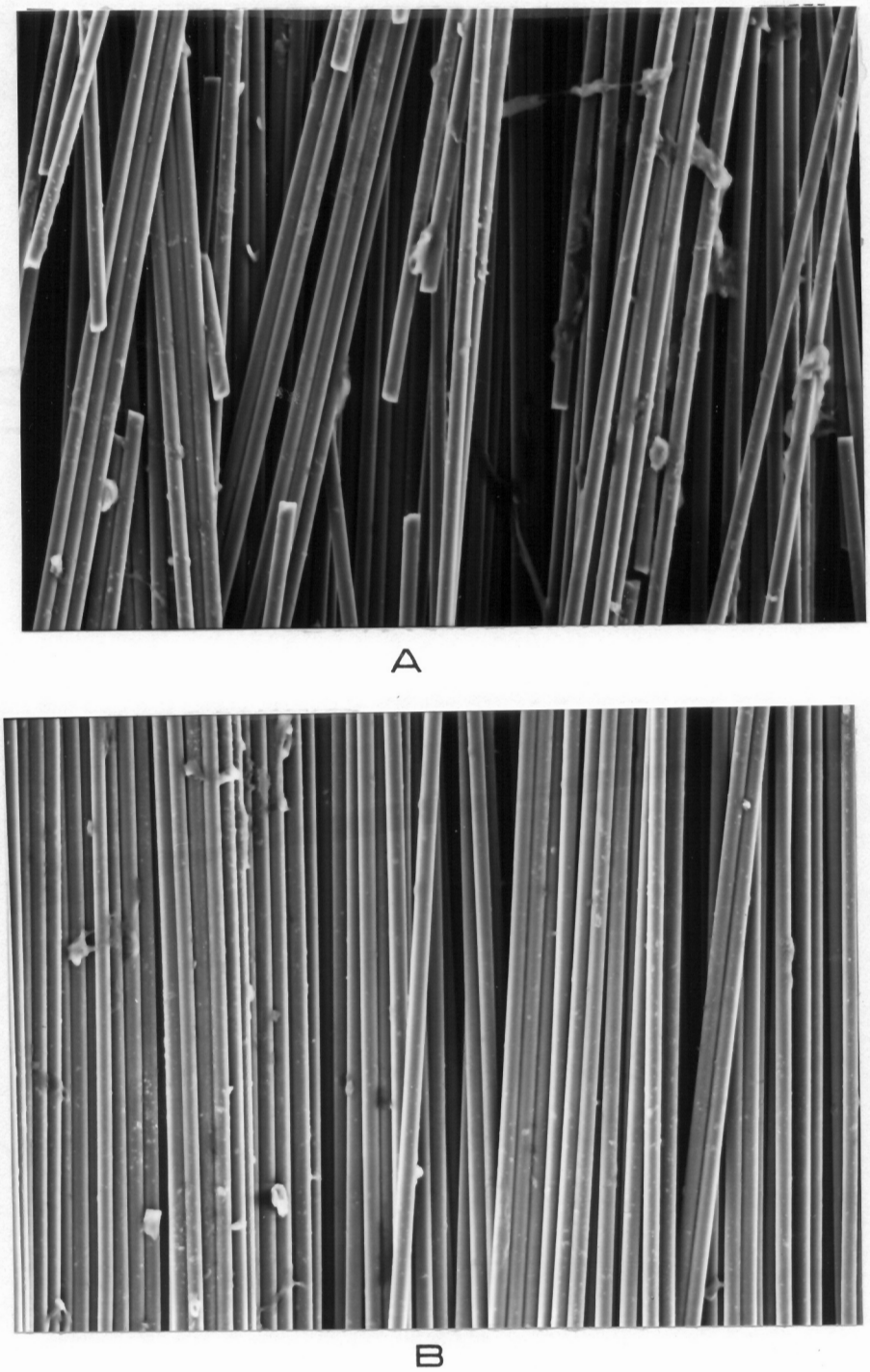

Figure 20. Influence of matrix split on fiber fracture in AS6/F584 laminate: (A) matrix split and (B) neighboring fibers to the matrix split.

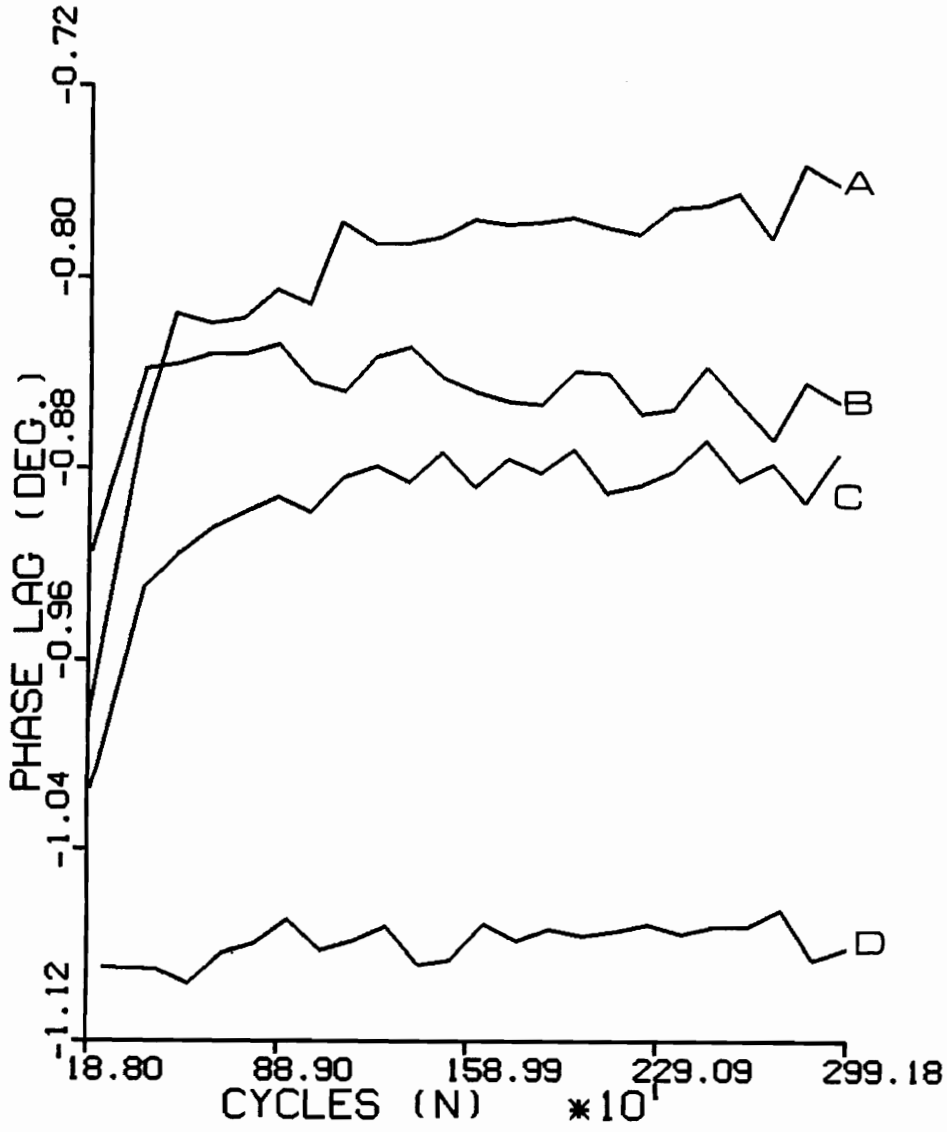

Figure 21. Phase lag response at 50% UTS for 3000 cycles conditioning.: for specimens A) 50-70-28 (life = 70,882 cycles). B) 50-70-29 (life = 45,685 cycles), C) 50-70-33 (life = 23,094 cycles), D) 5F-70-E2 (life = 773 cycles),

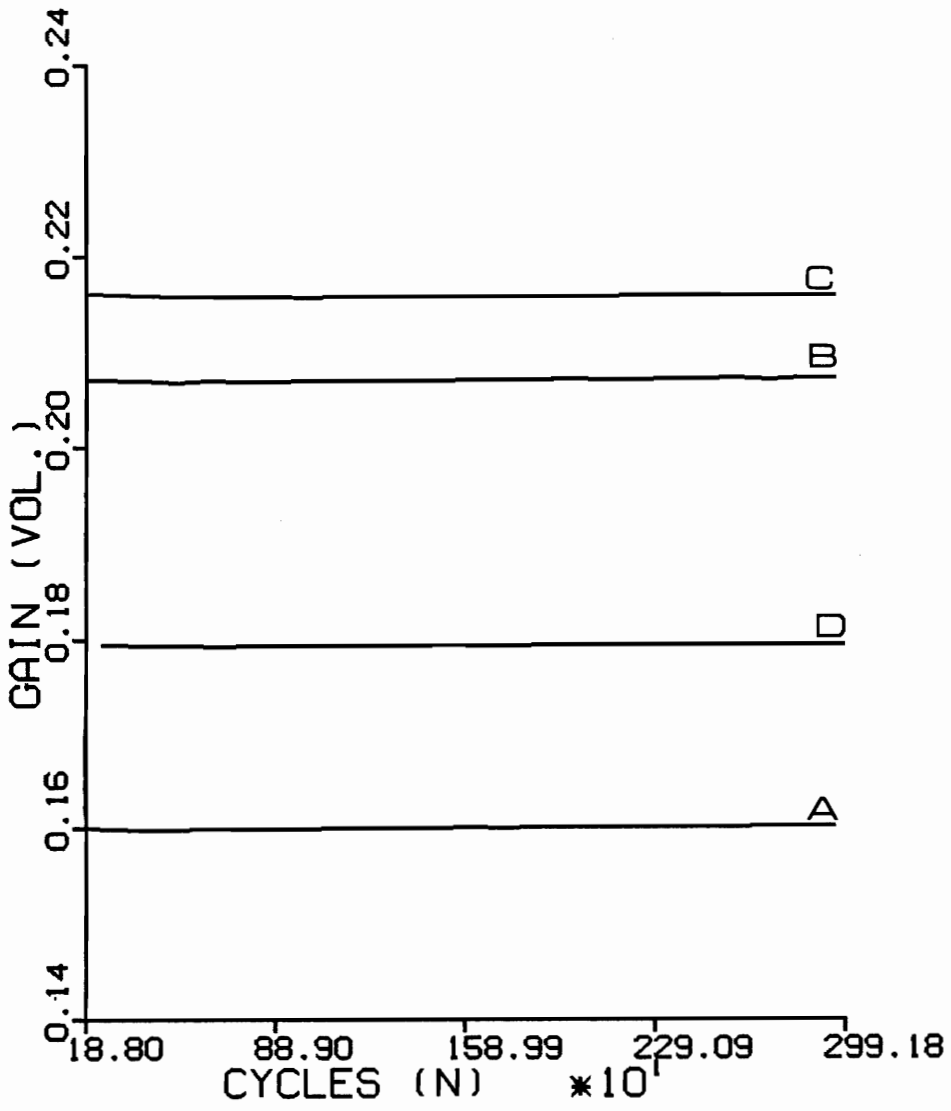

Figure 22. Gain response at 50% UTS for 3000 cycles conditioning.: for specimens A) 50-70-28 (life = 70,882 cycles). B) 50-70-29 (life = 45,685 cycles), C) 50-70-33 (life = 23,094 cycles), D) 5F-70-E2 (life = 773 cycles),

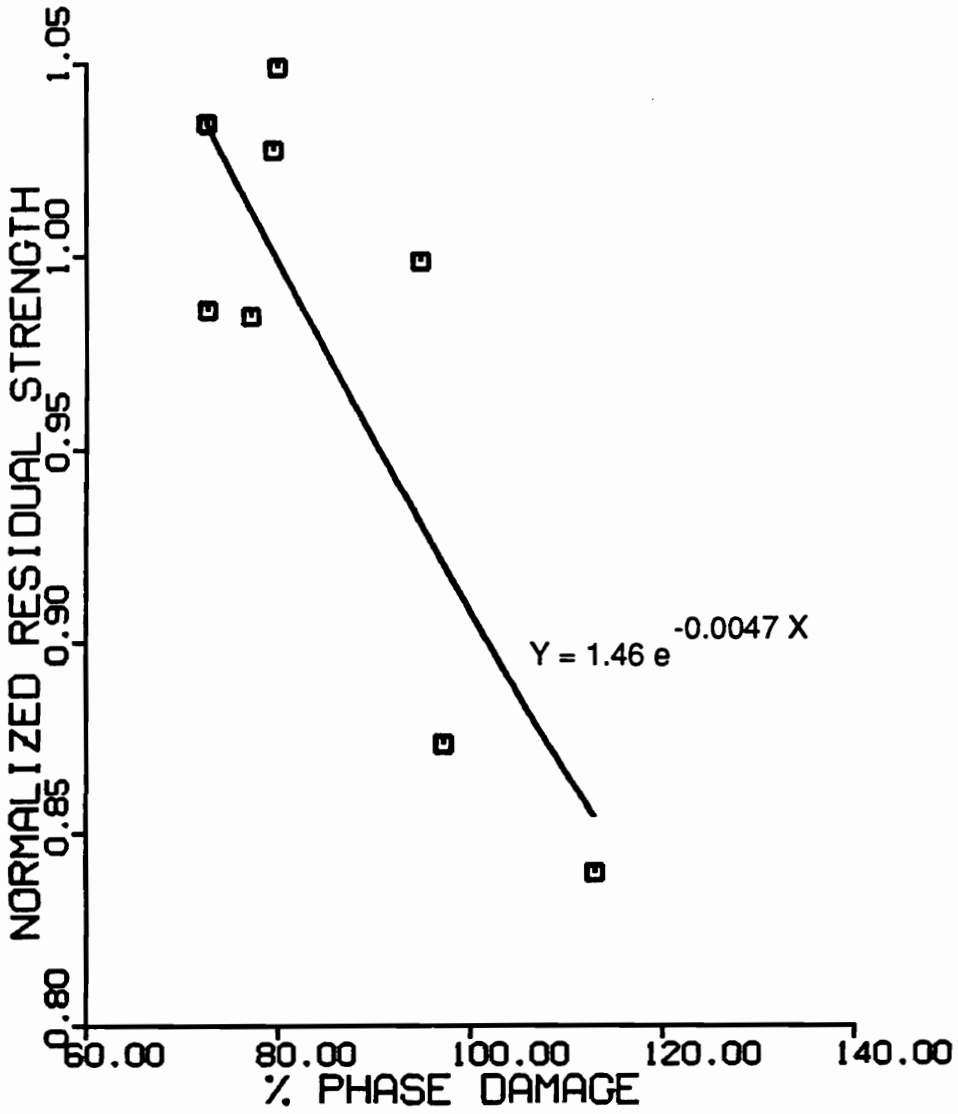

Figure 23. **Residual strength degradation as a function of % phase damage at 70% UTS.:** (Coefficient of determination = 0.67)

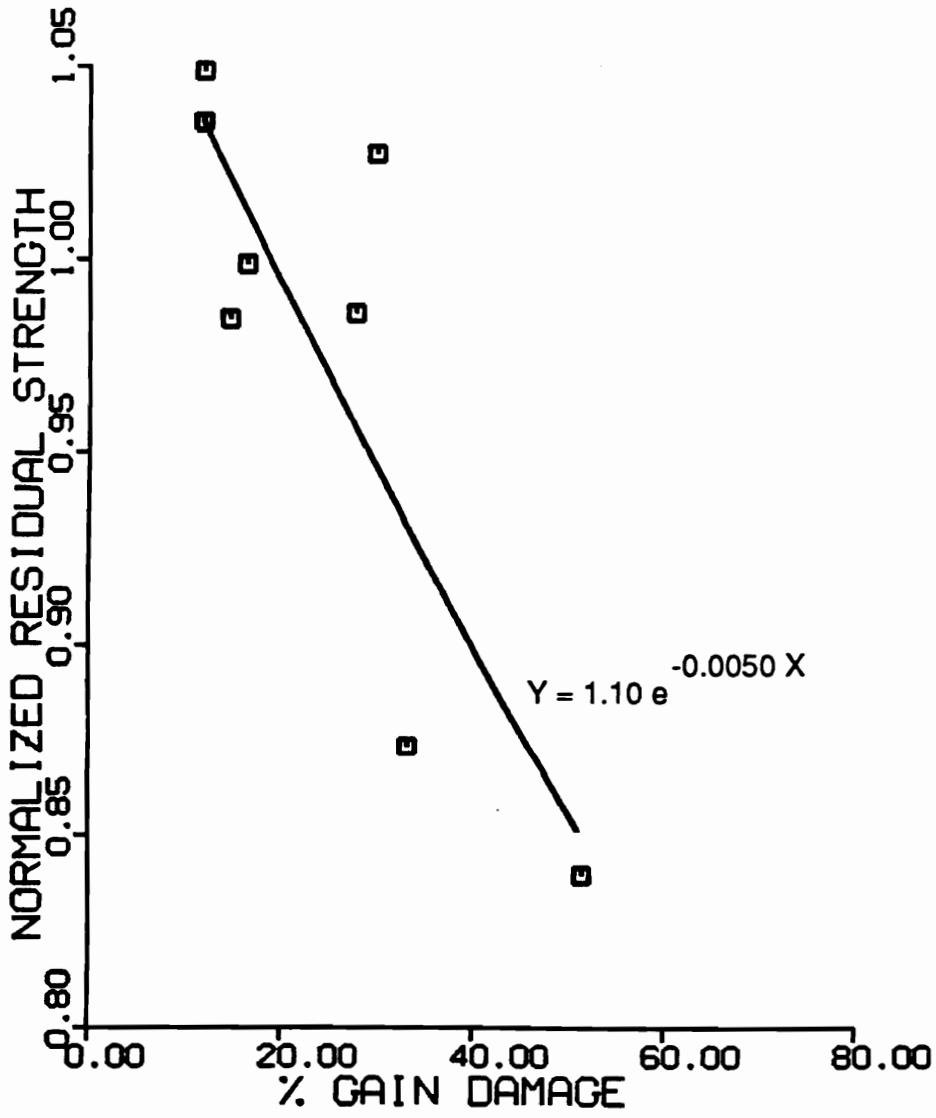

Figure 24. Residual strength degradation as a function of % gain damage at 70% UTS.: (Coefficient of determination = 0.67)

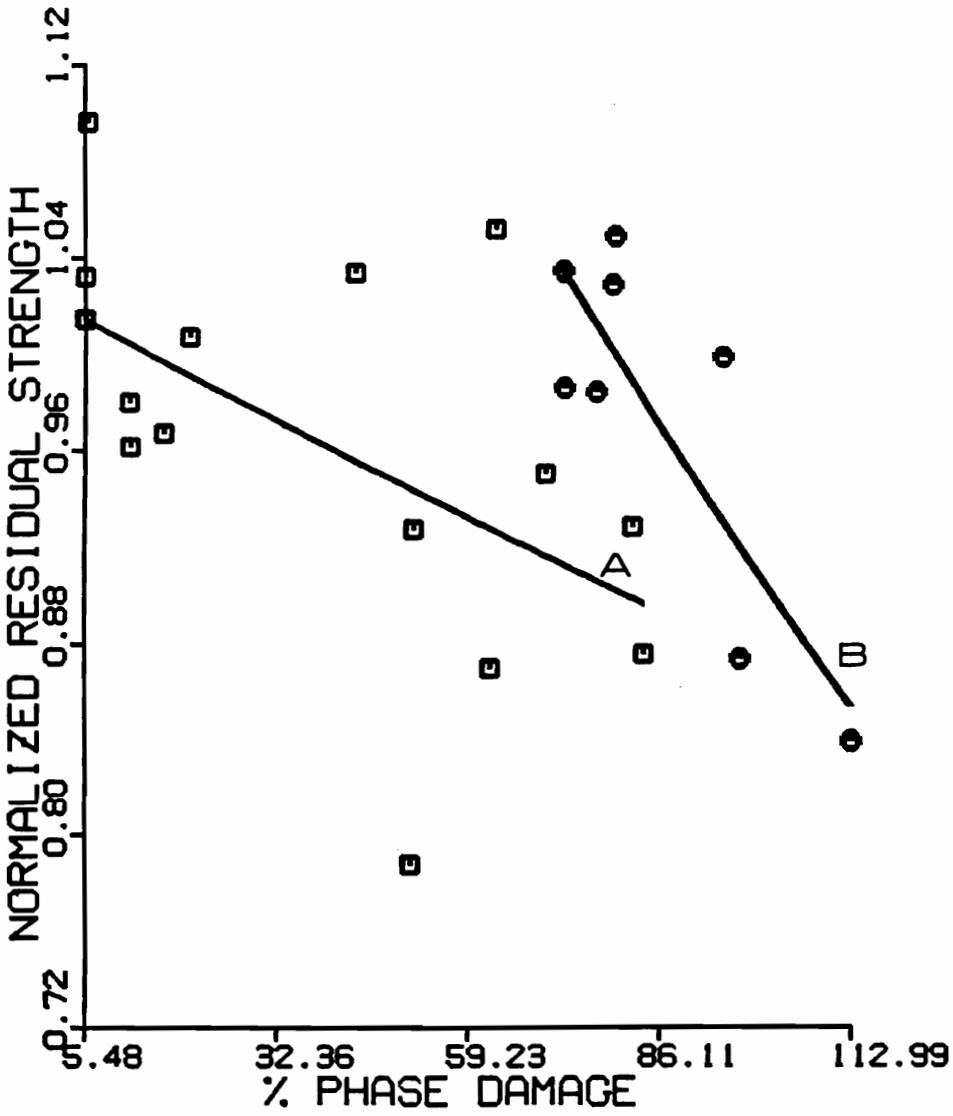

Figure 25. Residual strength degradation as a function of % phase damage: at A) 65% and B) 70% σ_u. (Comparing % of total damage at given load levels)

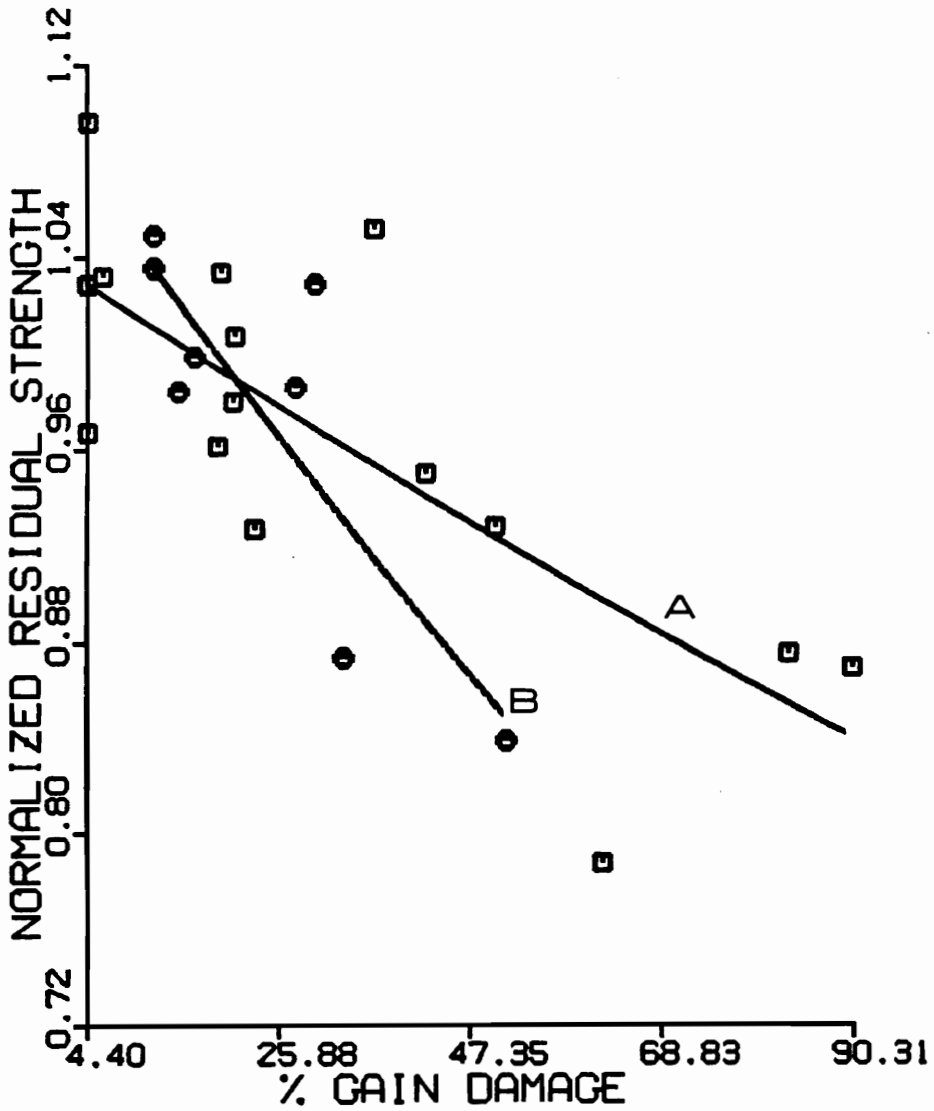

Figure 26. **Residual strength degradation as a function of % gain damage:** at A) 65% and B) 70% σ_u. (Comparing % of total damage at given load levels)

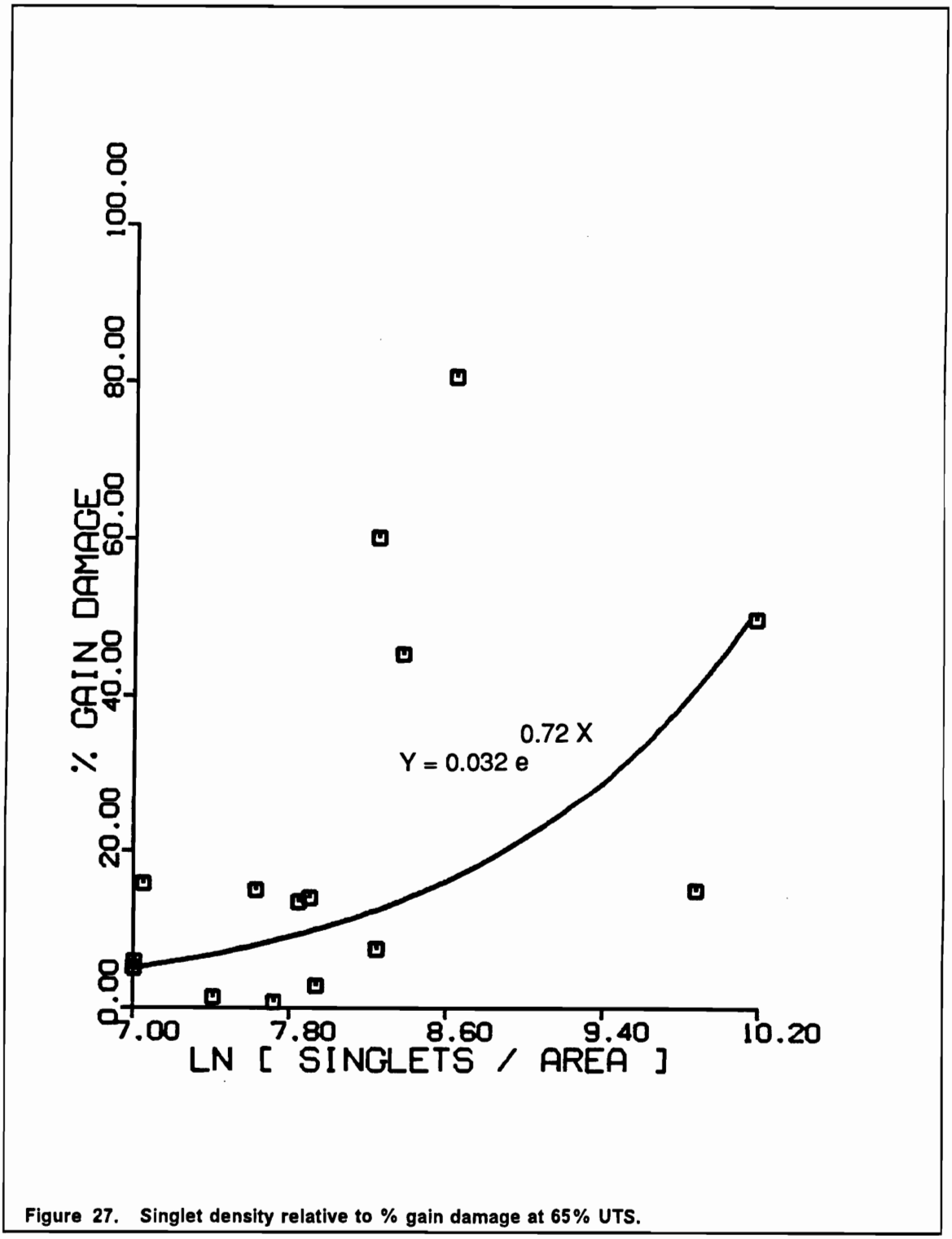

Figure 27. Singlet density relative to % gain damage at 65% UTS.

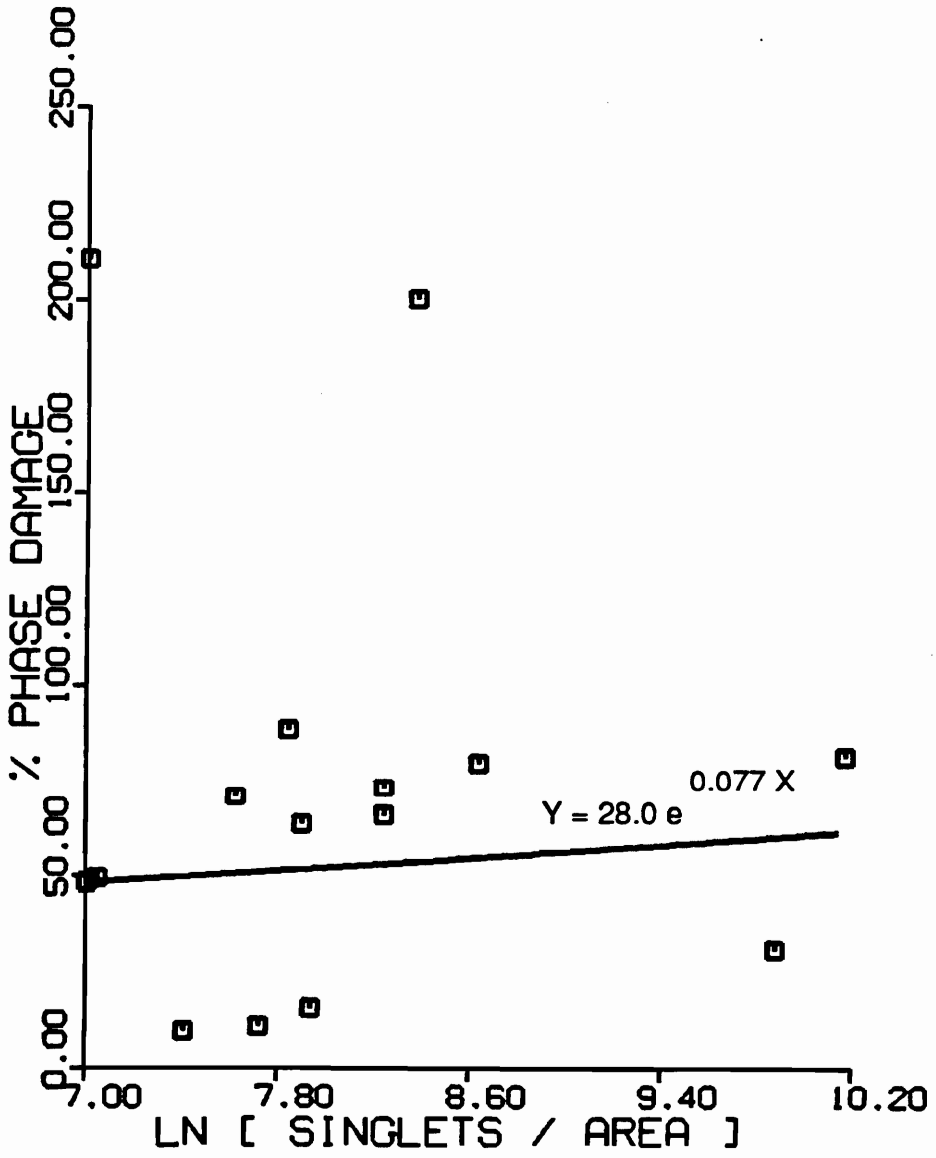

Figure 28. Singlet density relative to % phase damage at 65% UTS.

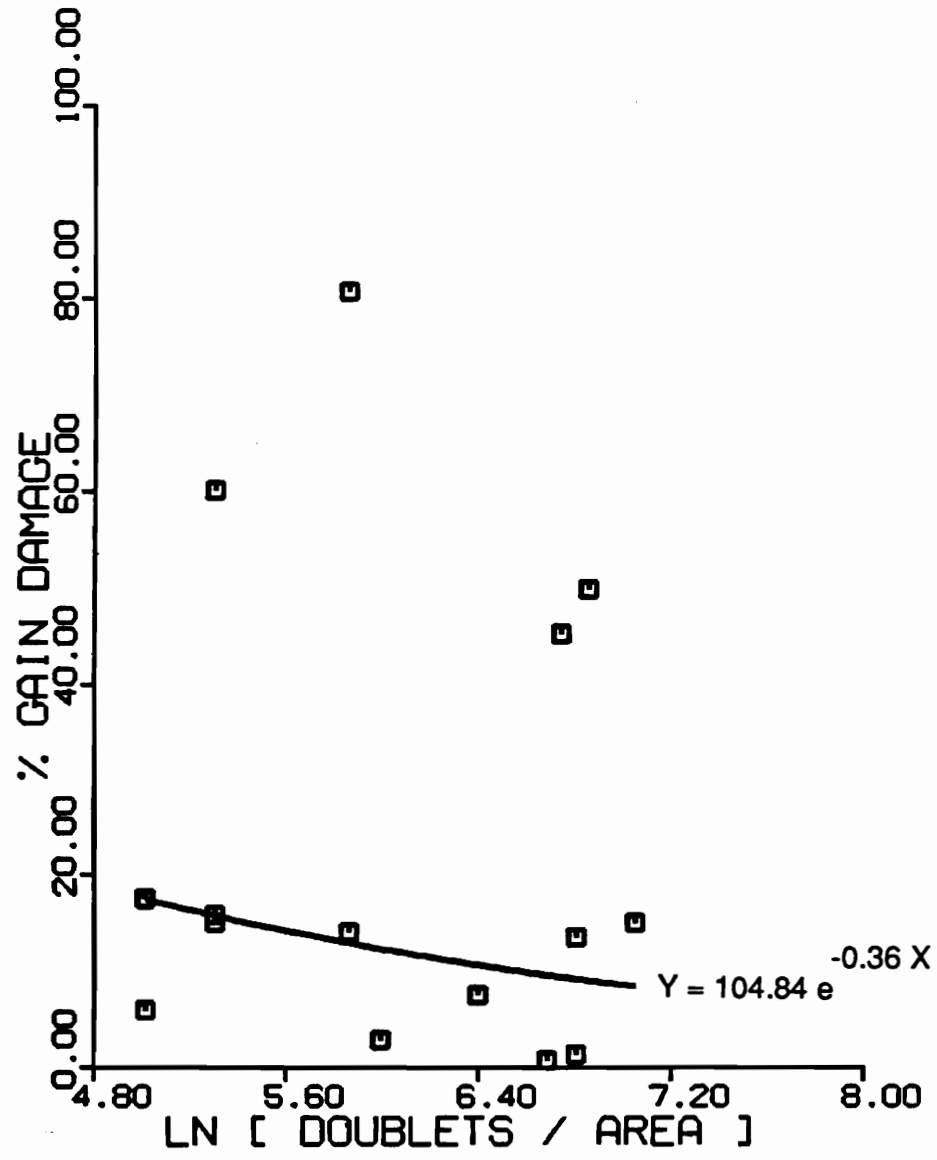

Figure 29. Doublet density relative to % gain damage at 65% UTS.

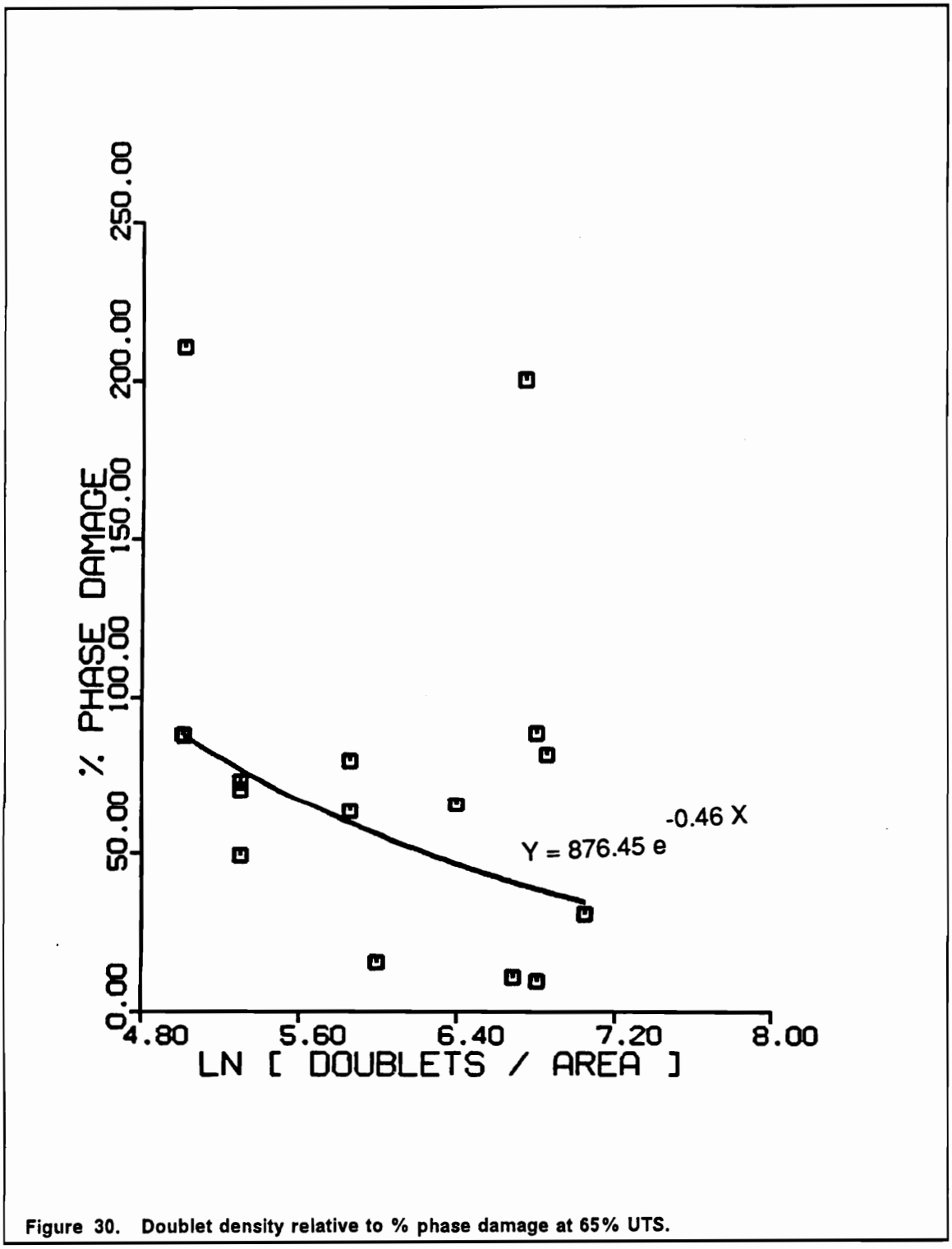

Figure 30. Doublet density relative to % phase damage at 65% UTS.

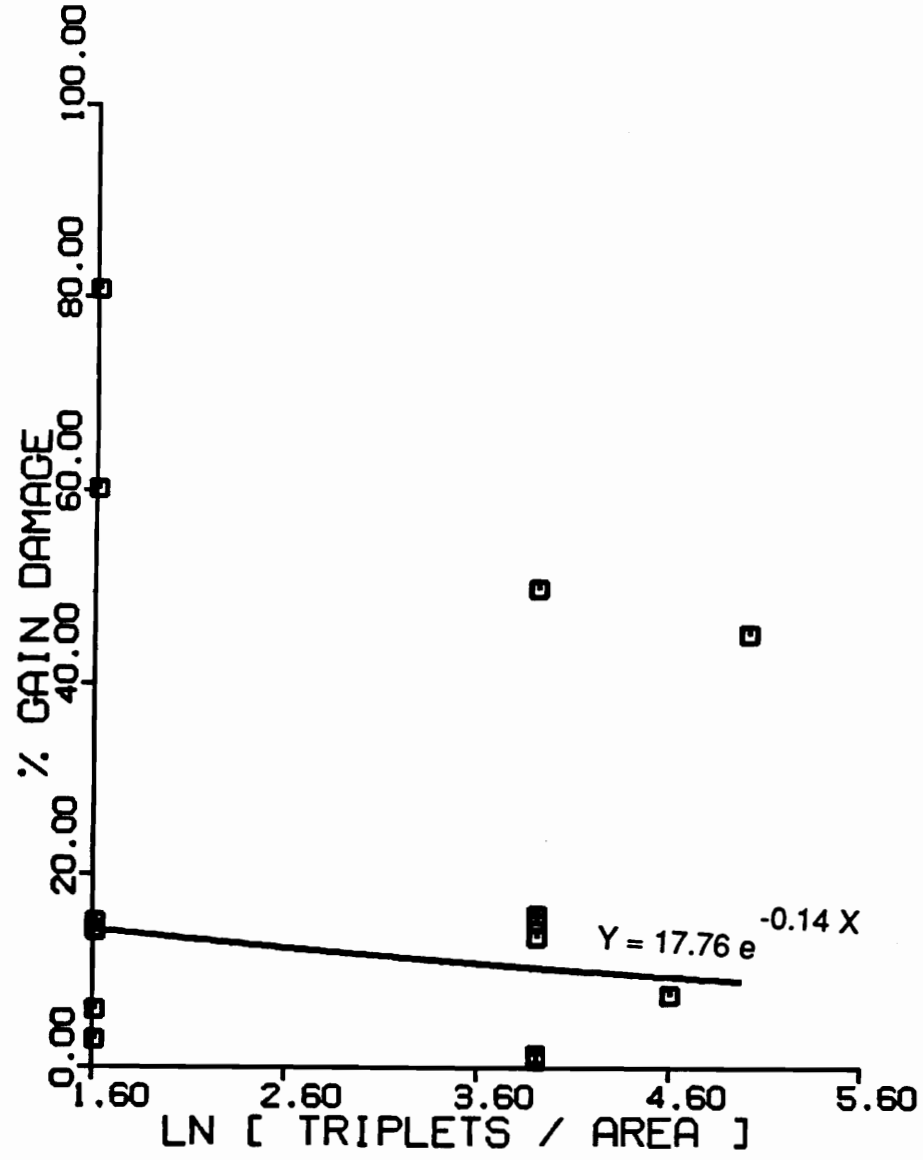

Figure 31. Triplet density relative to % gain damage at 65% UTS.

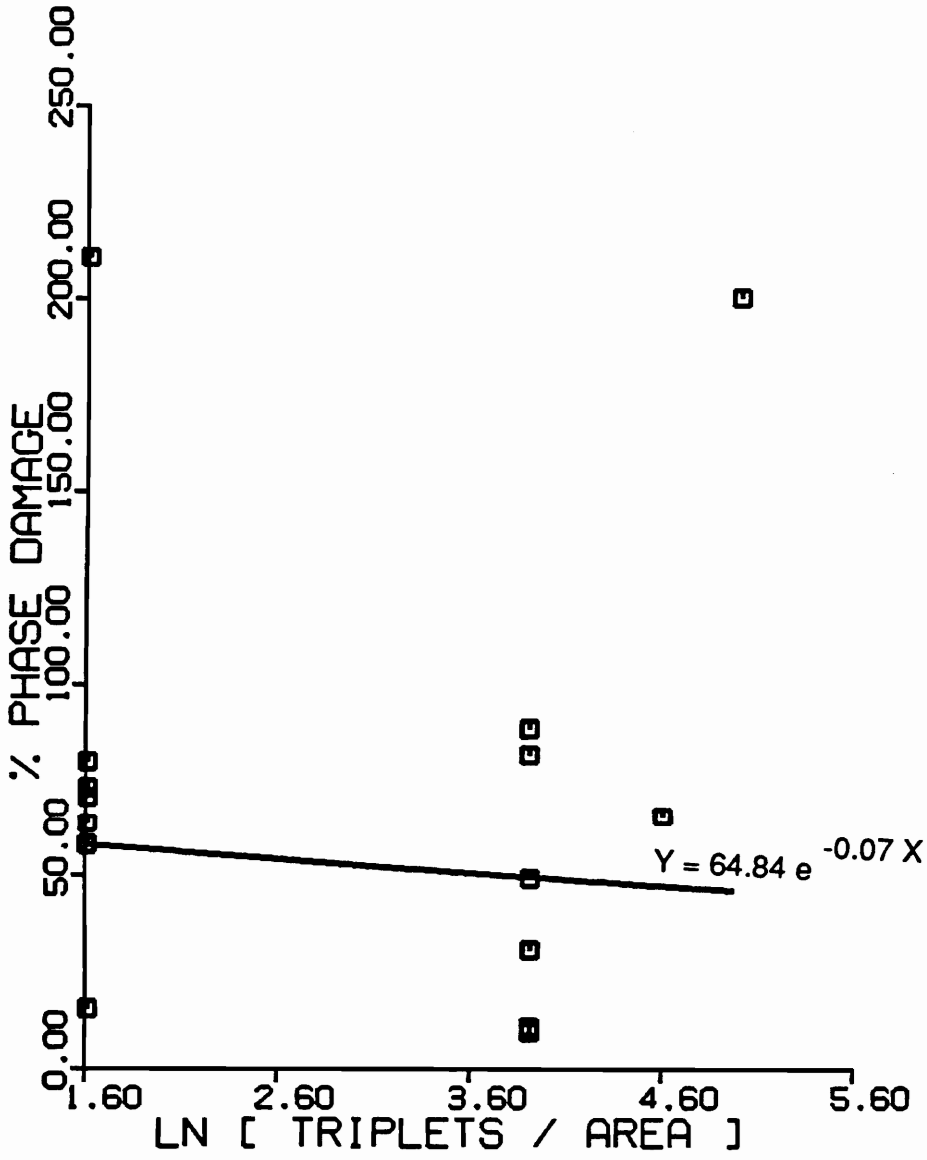

Figure 32. Triplet density relative to % phase damage at 65% UTS.

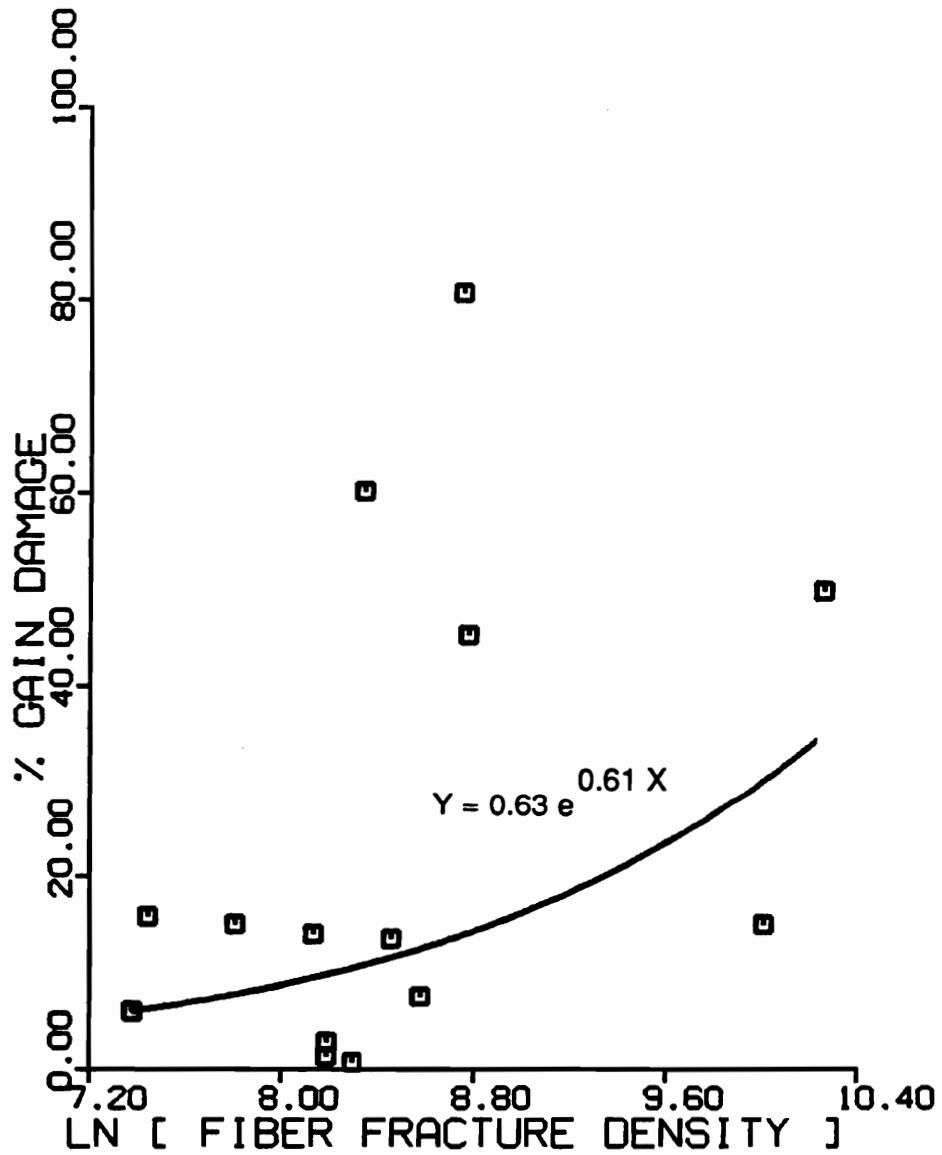

Figure 33. Total Fiber fracture density relative to % gain damage at 65% UTS.

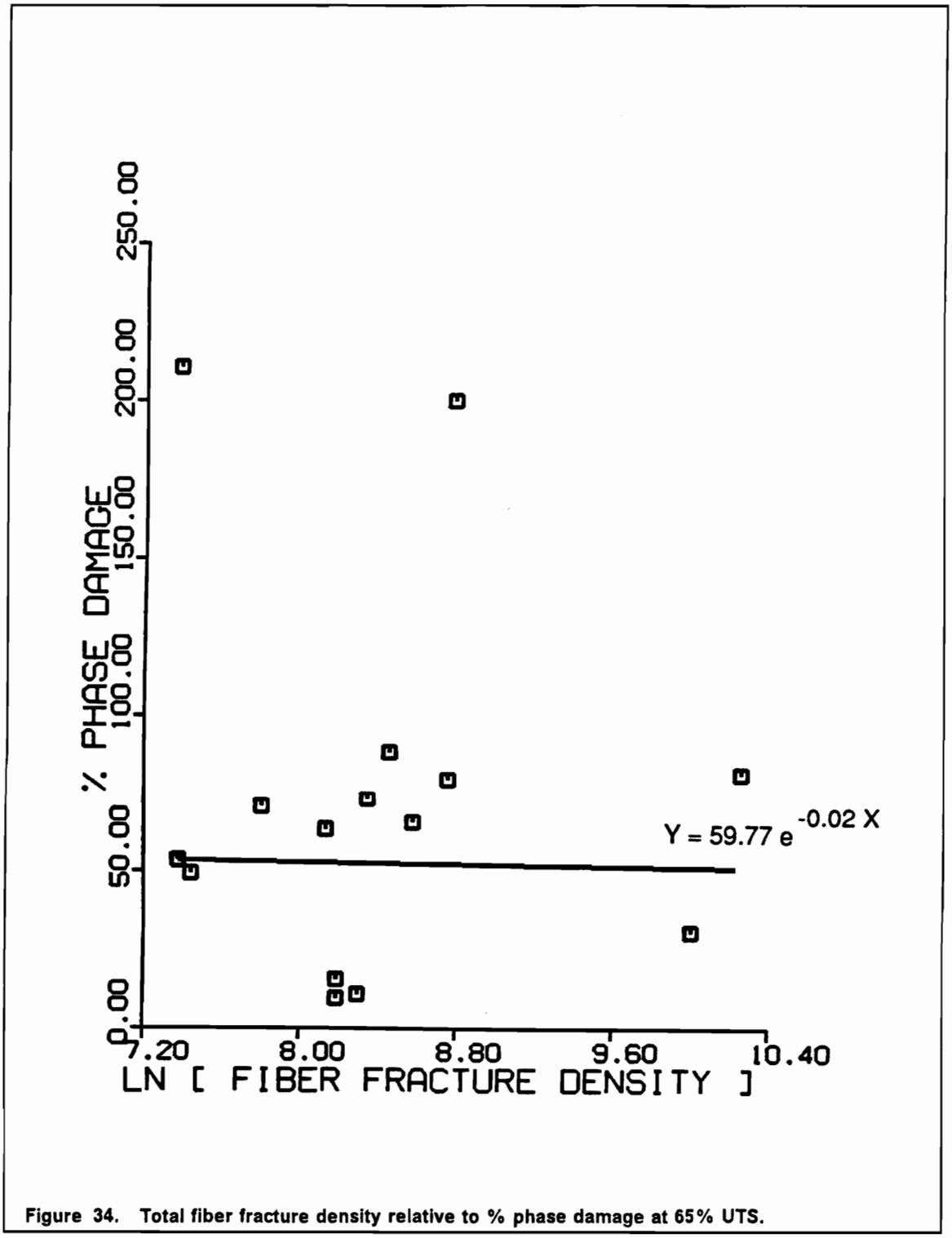

Figure 34. Total fiber fracture density relative to % phase damage at 65% UTS.

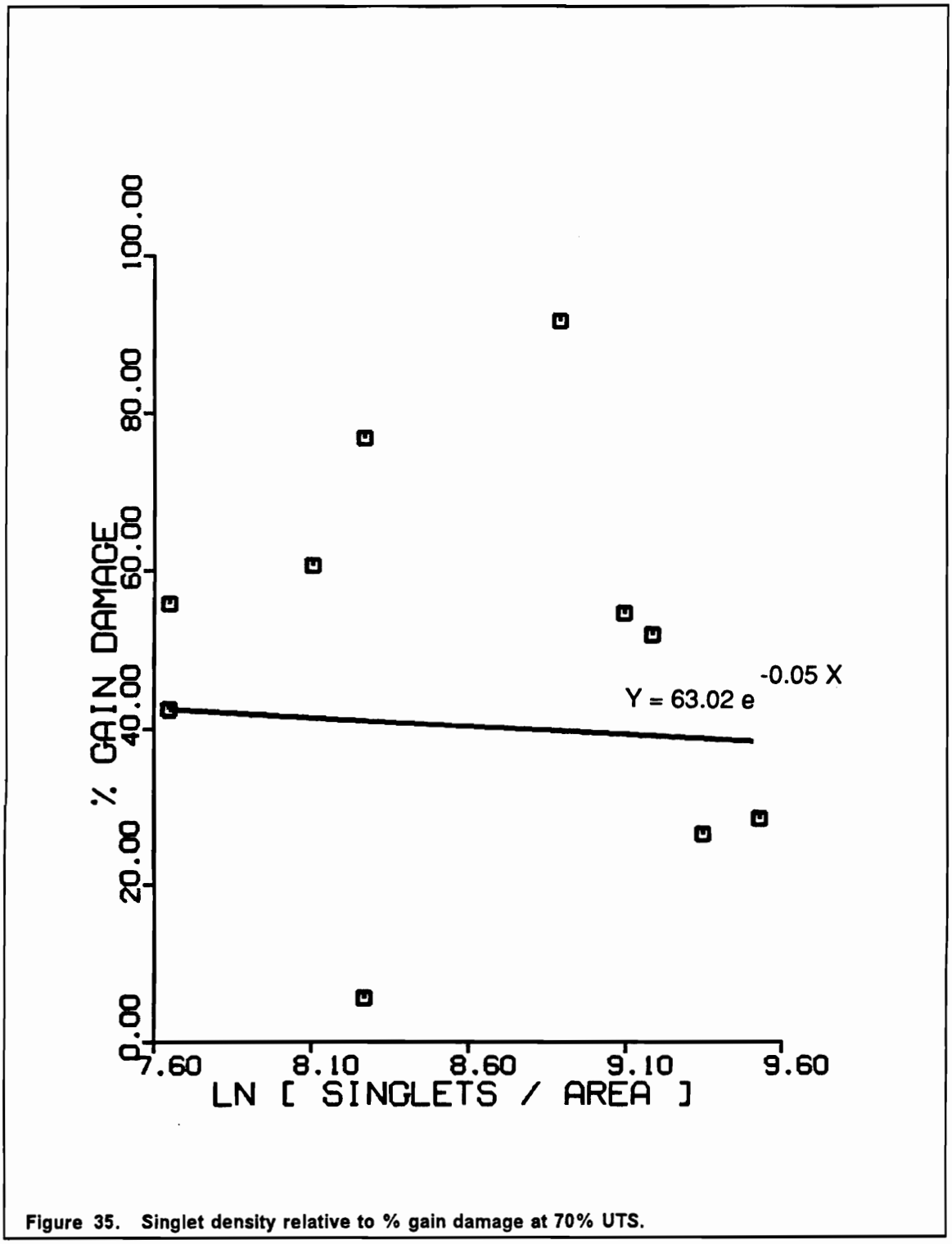

Figure 35. Singlet density relative to % gain damage at 70% UTS.

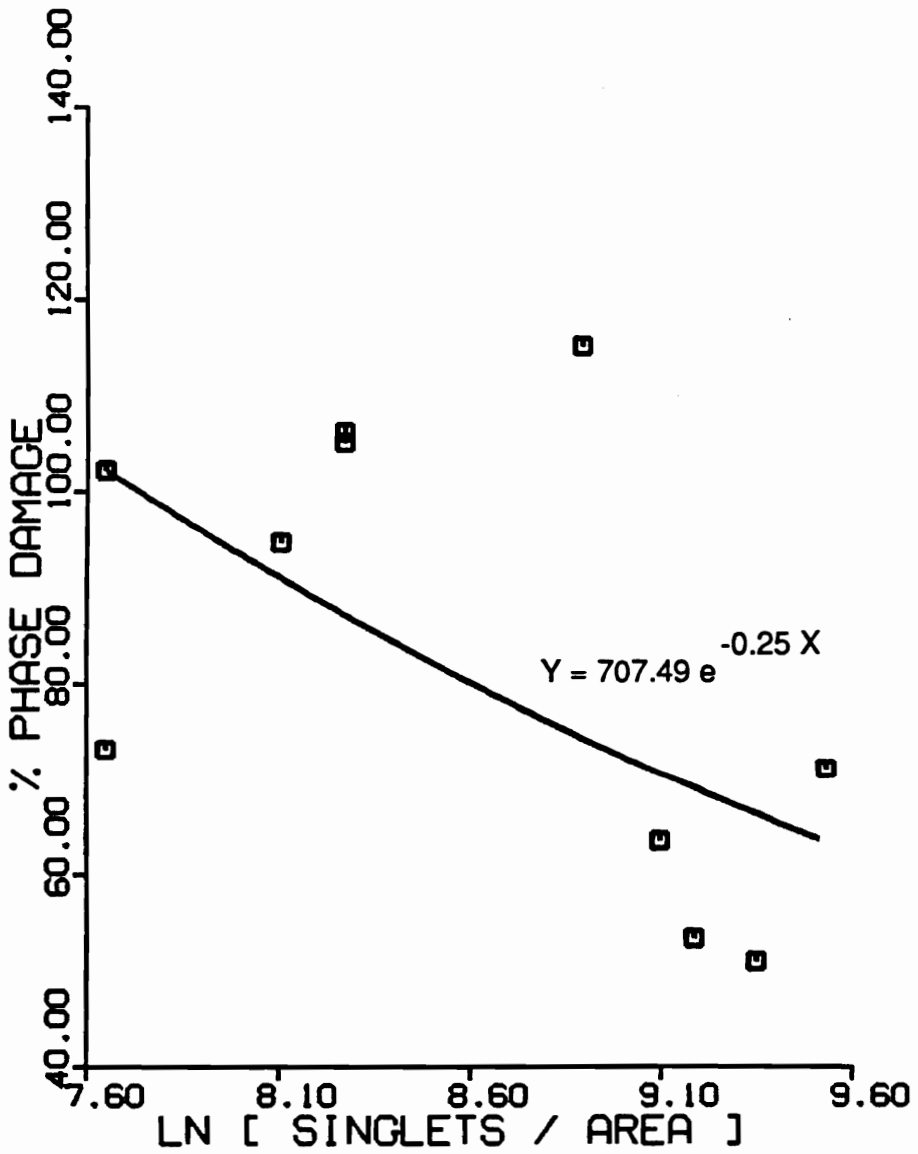

Figure 36. Singlet density relative to % phase damage at 70% UTS.

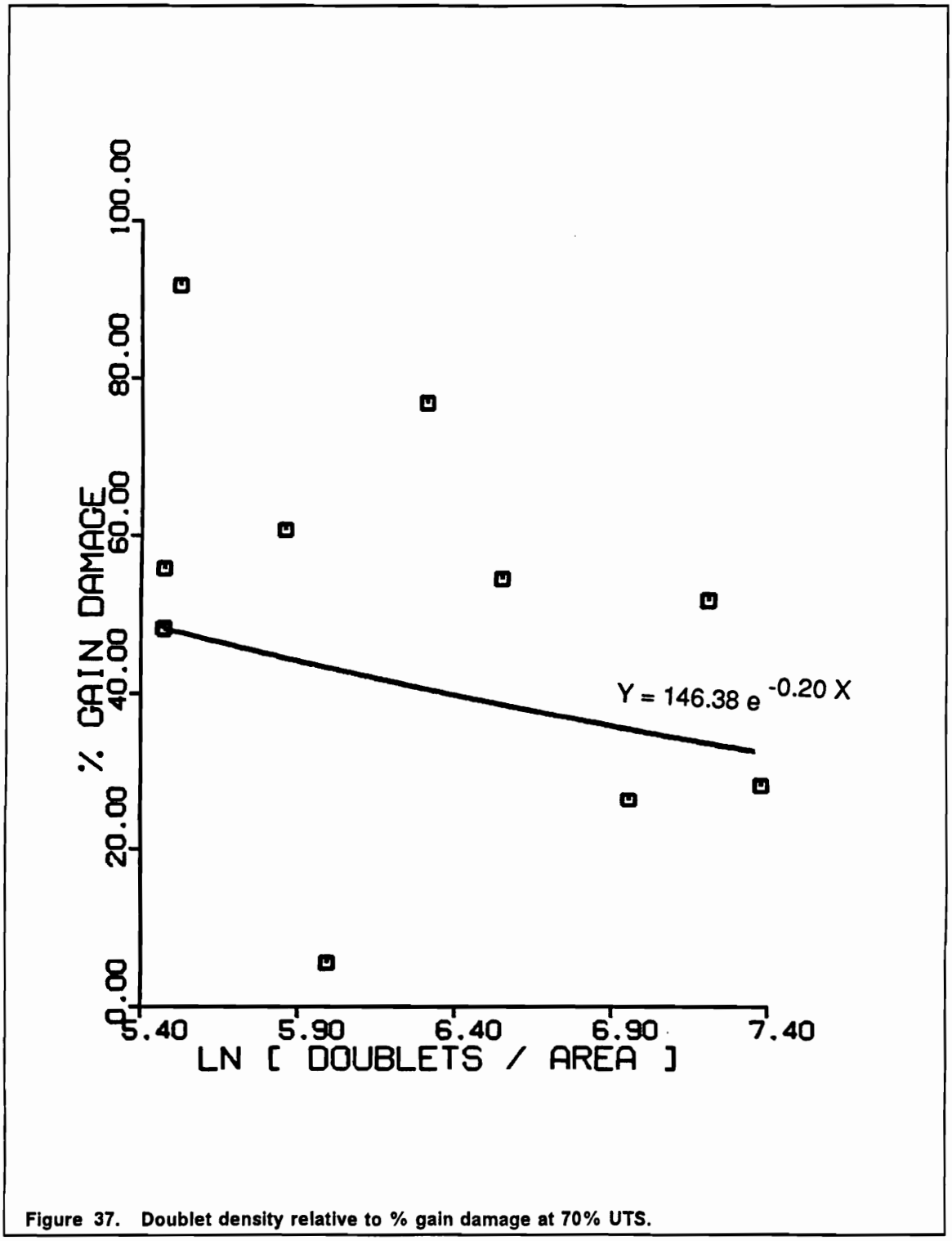

Figure 37. Doublet density relative to % gain damage at 70% UTS.

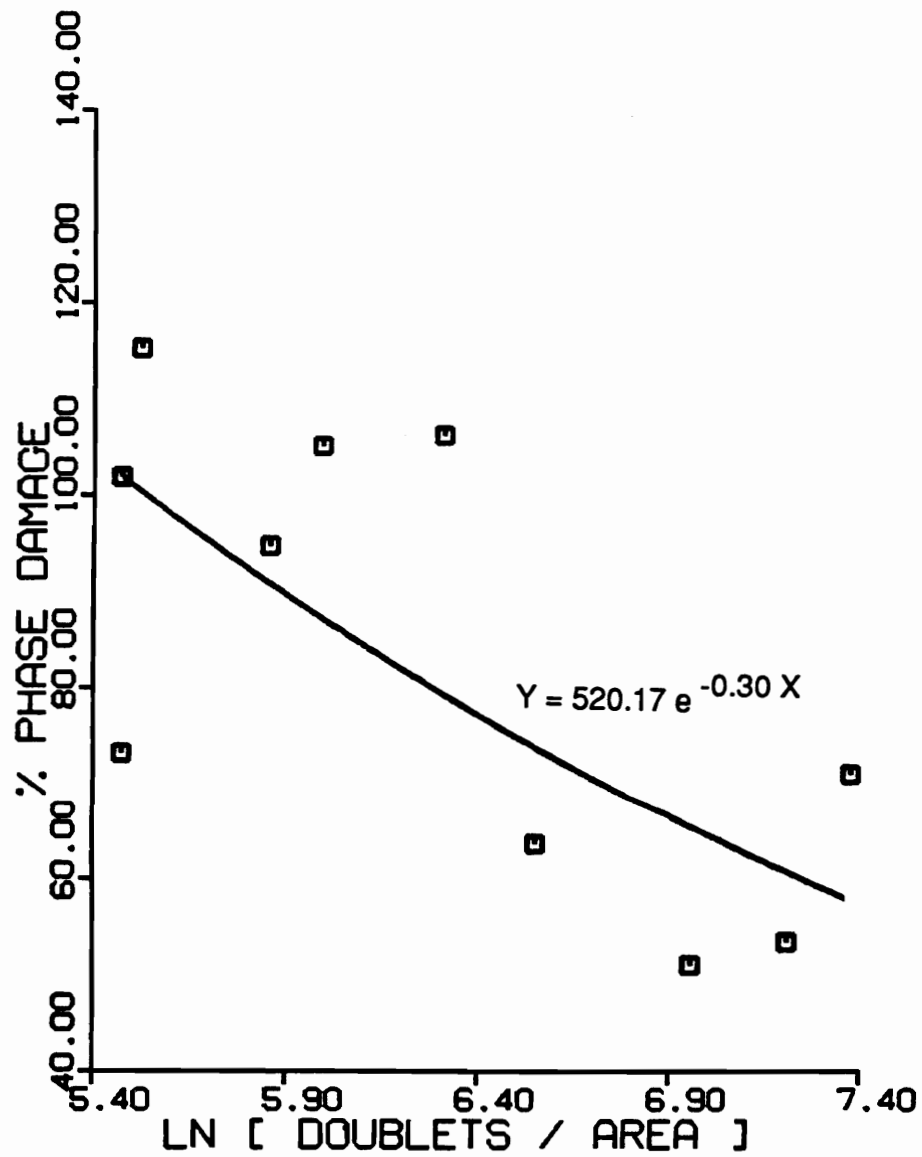

Figure 38. Doublet density relative to % phase damage at 70% UTS.

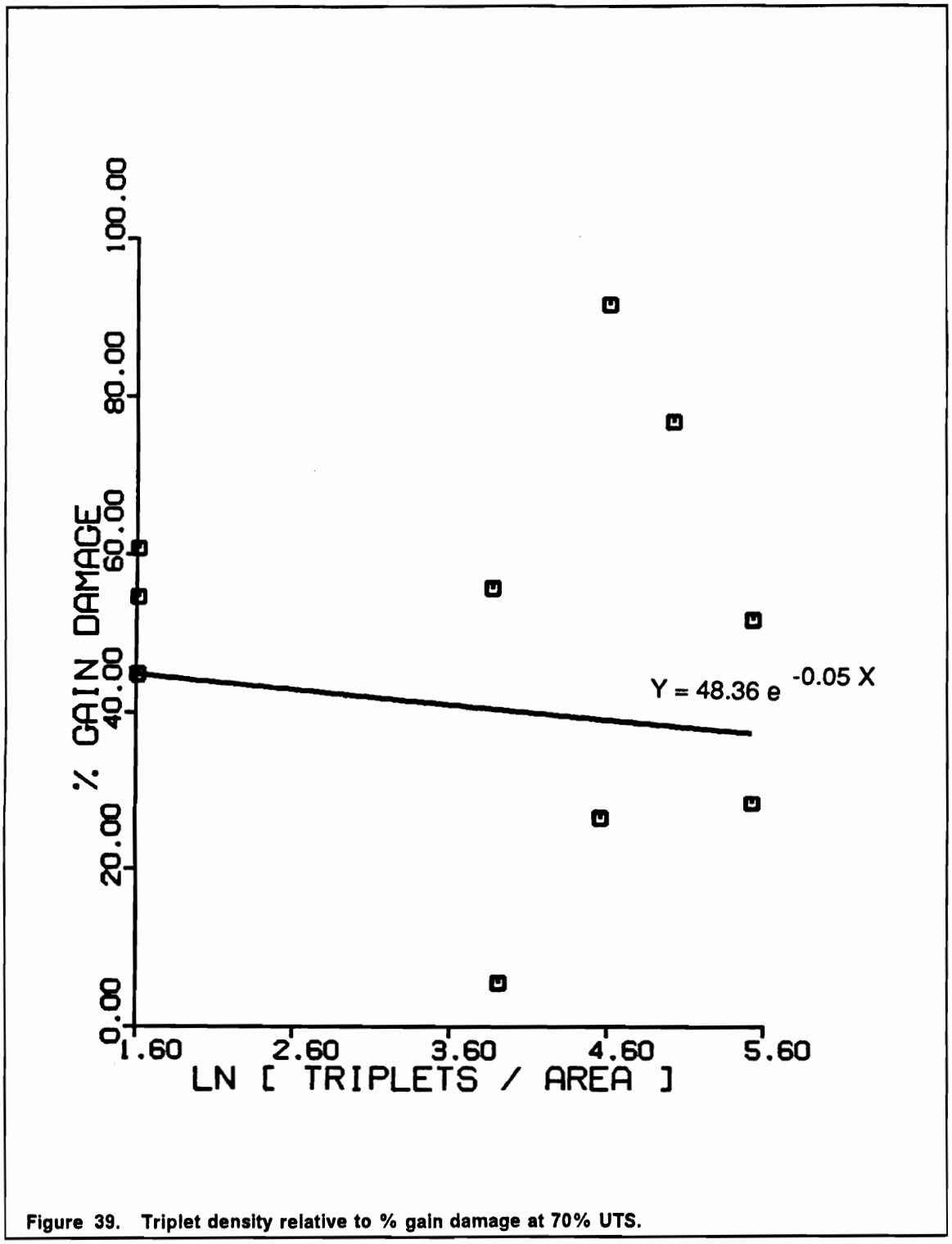

Figure 39. Triplet density relative to % gain damage at 70% UTS.

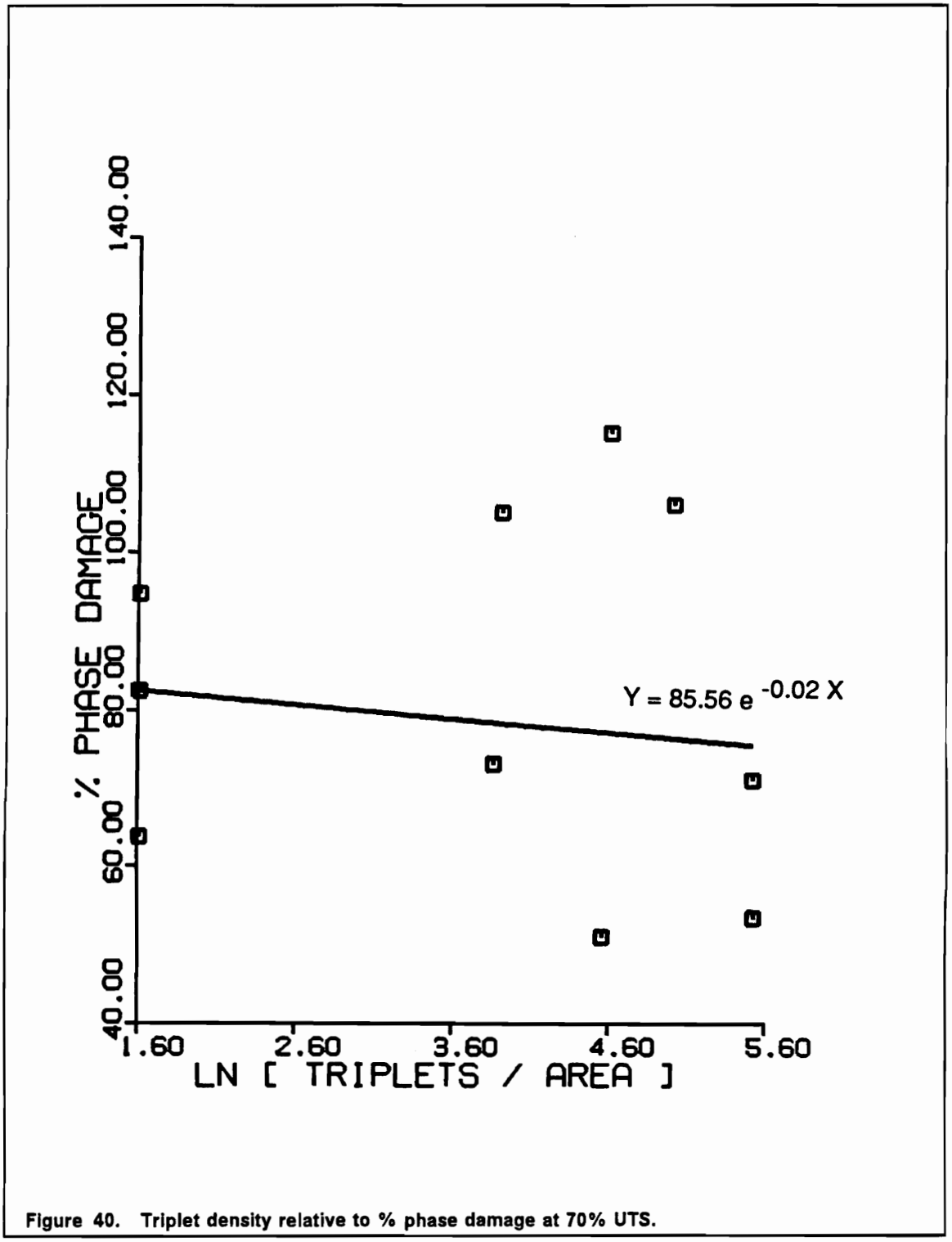

Figure 40. Triplet density relative to % phase damage at 70% UTS.

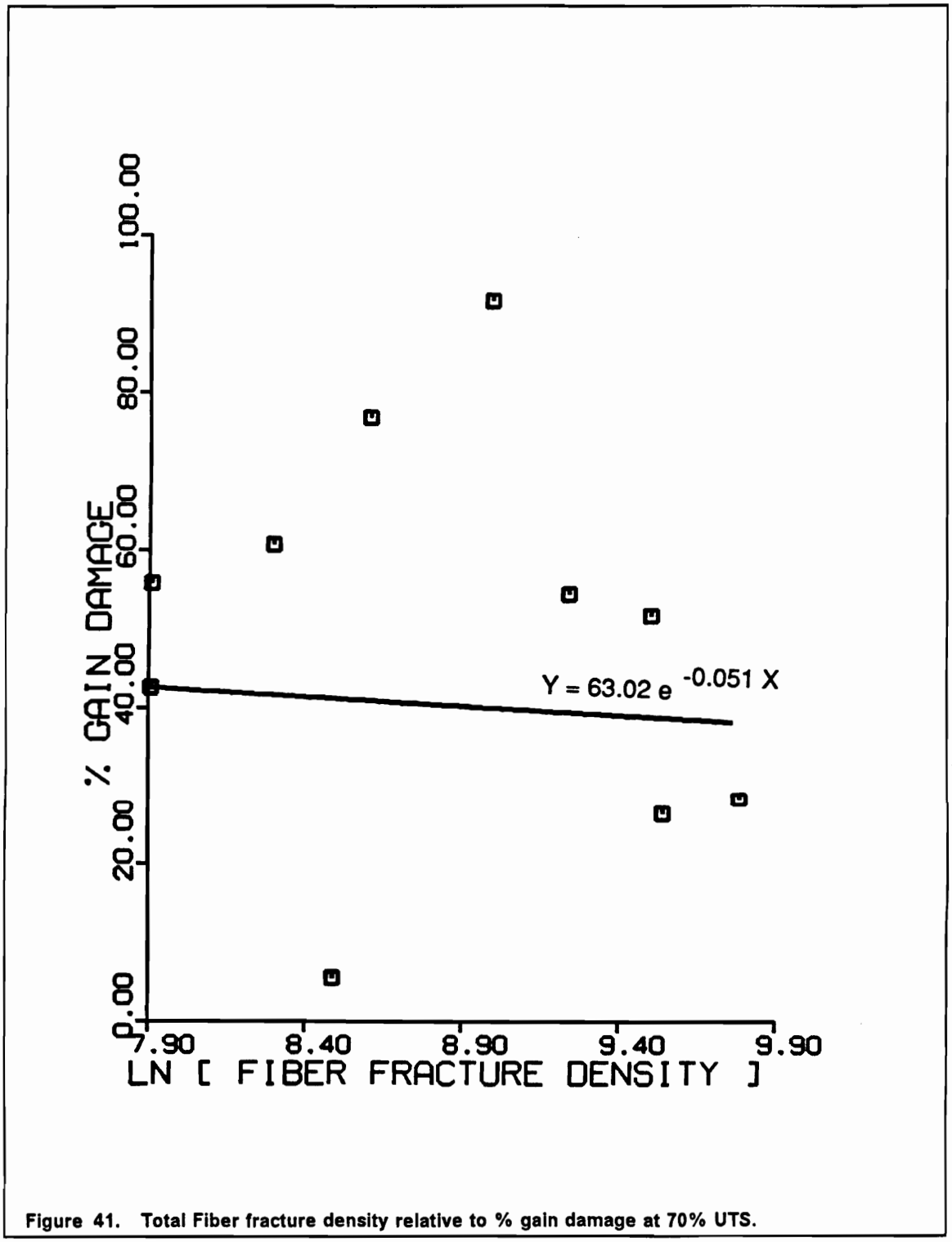

Figure 41. Total Fiber fracture density relative to % gain damage at 70% UTS.

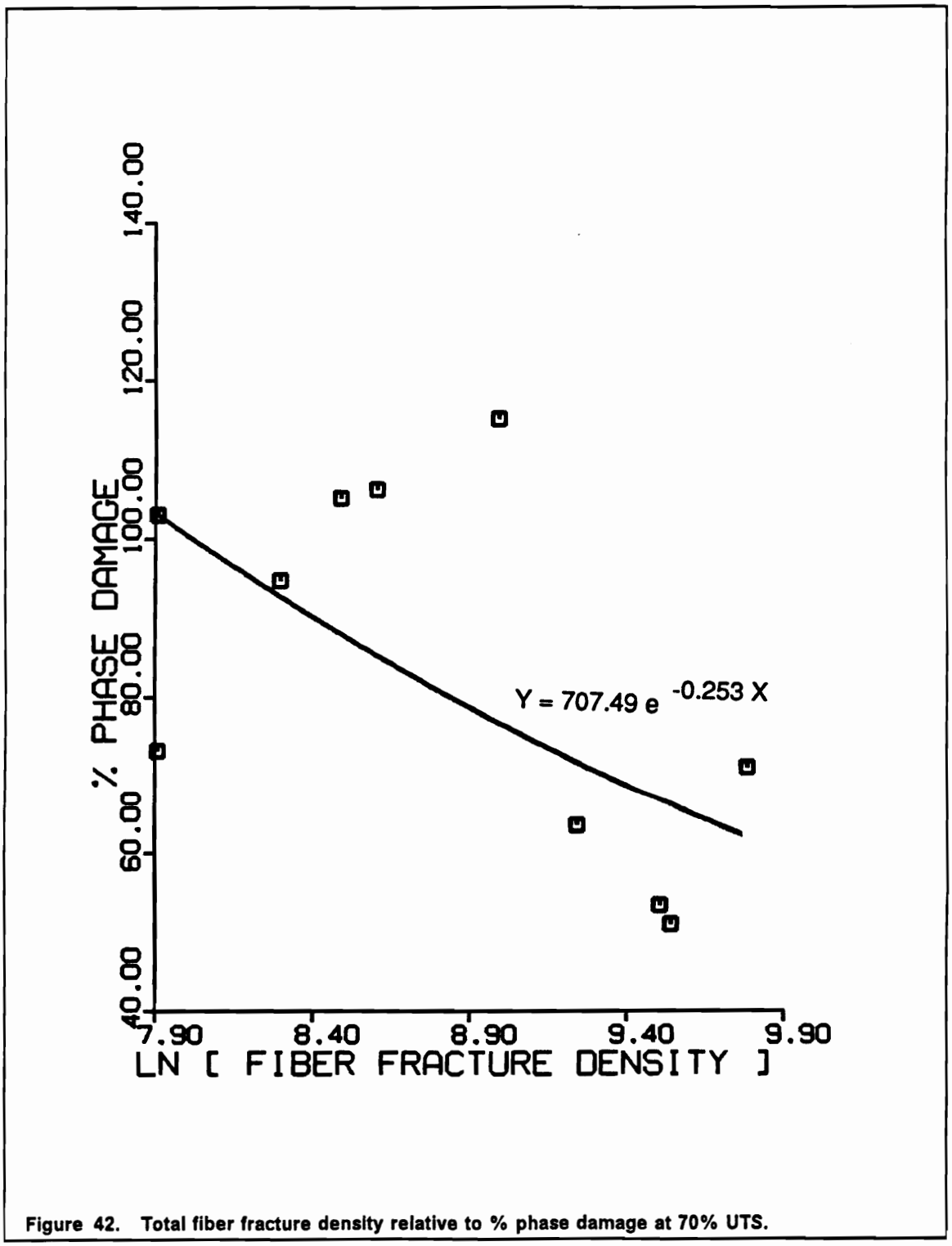

Figure 42. Total fiber fracture density relative to % phase damage at 70% UTS.

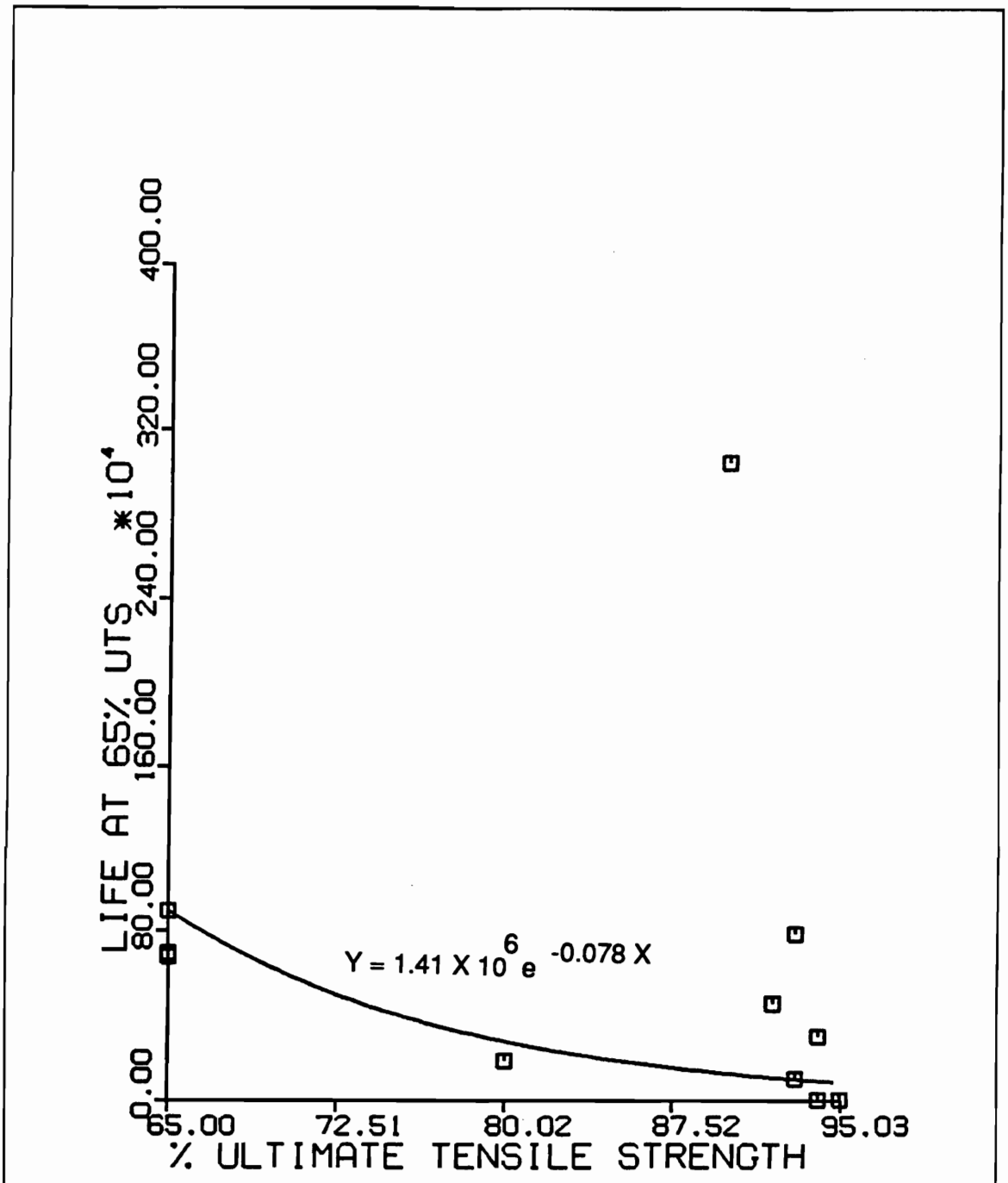

Figure 43. S—N diagram of quasi—statically loaded and fatigued at 65% UTS to failure.

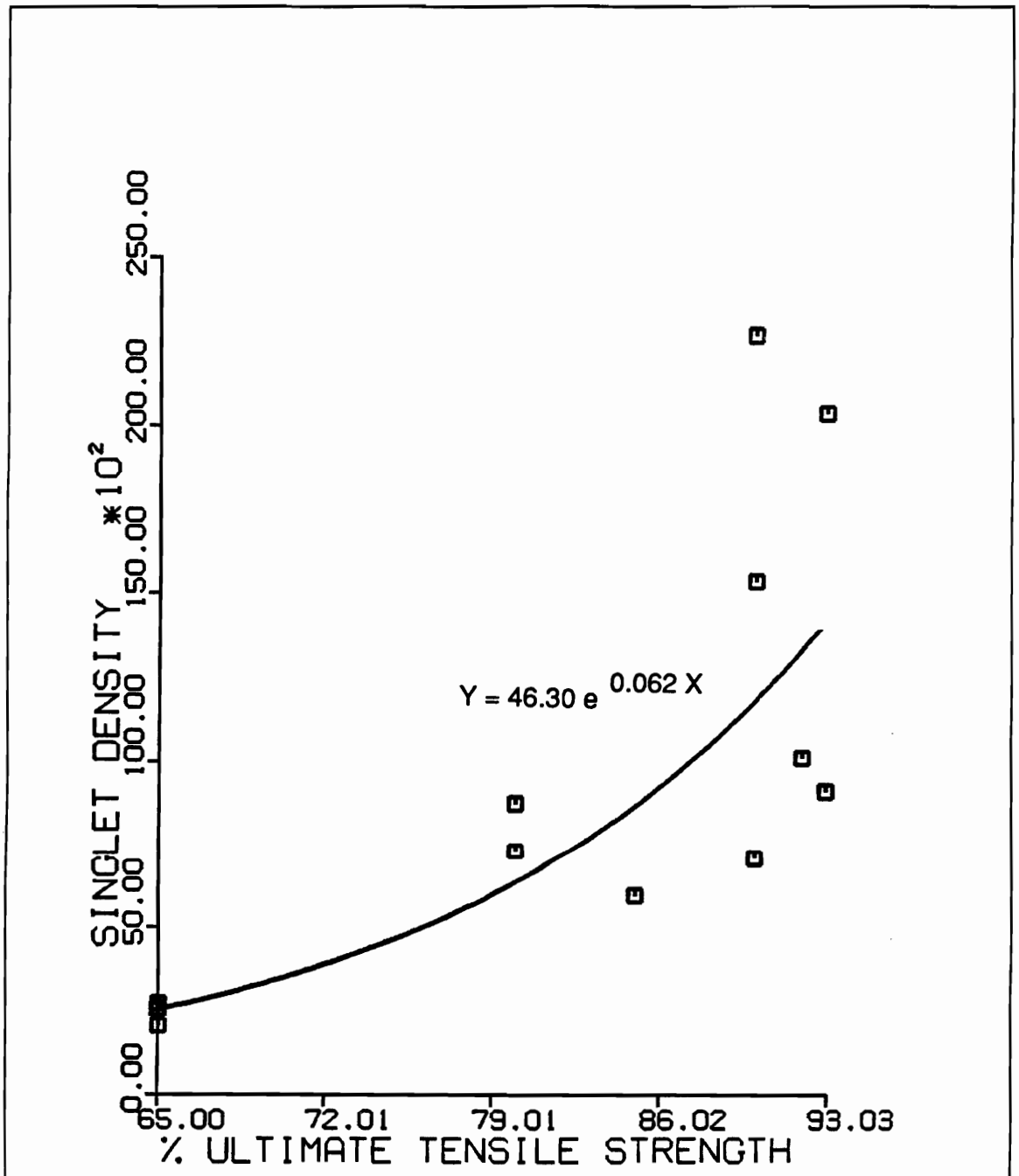

Figure 44. Singlet fiber fracture formation due to the initial high level quasi—static loading.

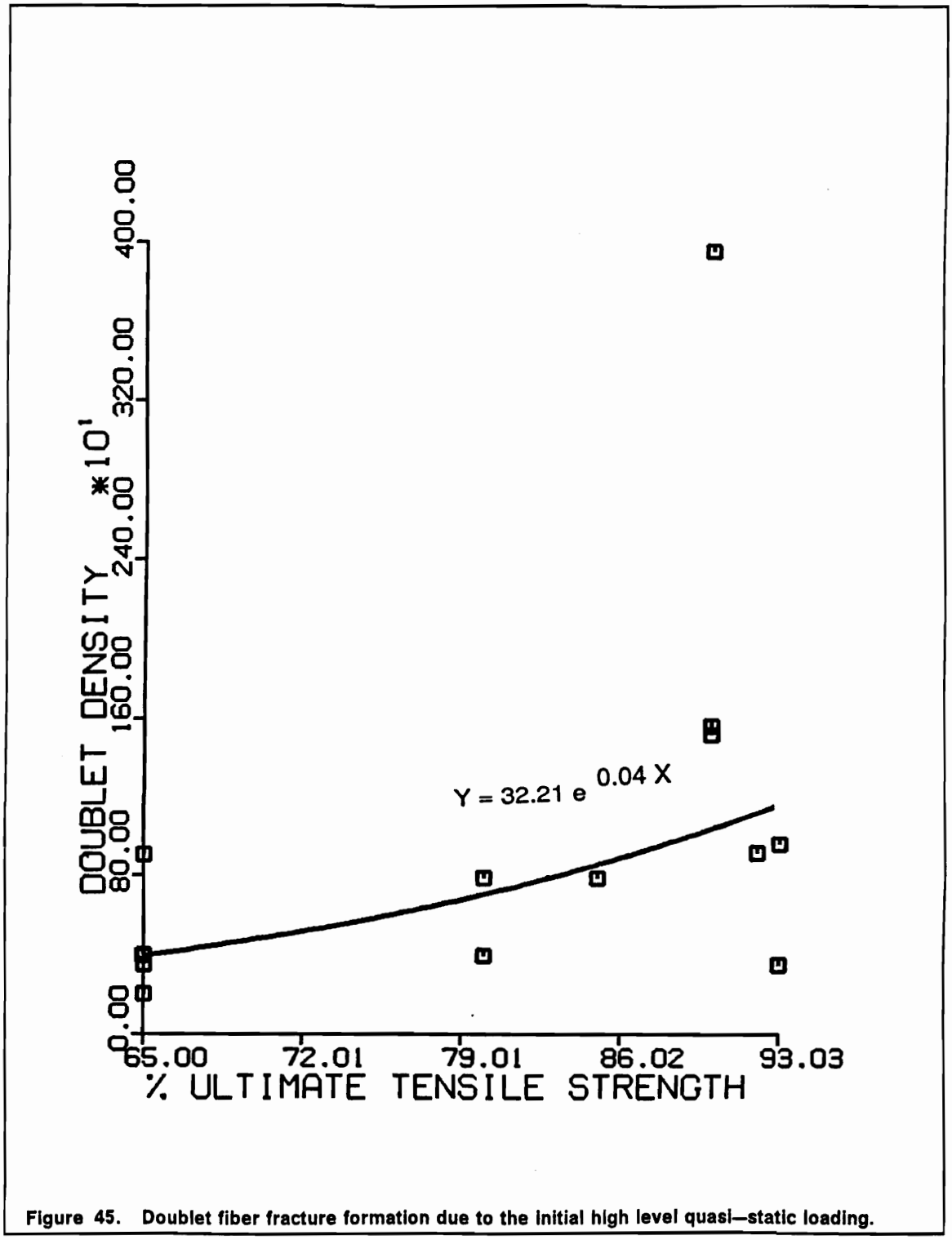

Figure 45. Doublet fiber fracture formation due to the initial high level quasi—static loading.

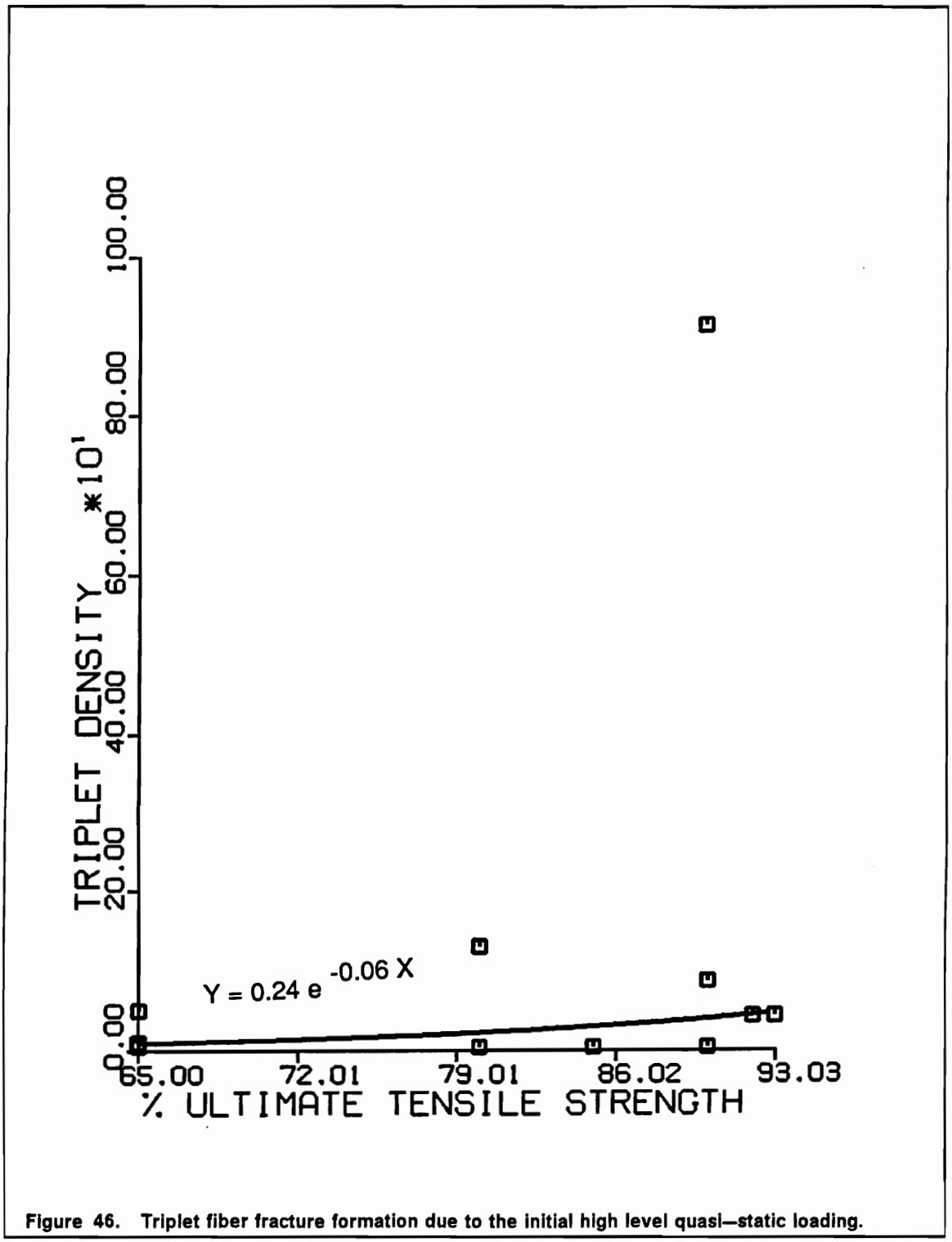

Figure 46. Triplet fiber fracture formation due to the initial high level quasi–static loading.

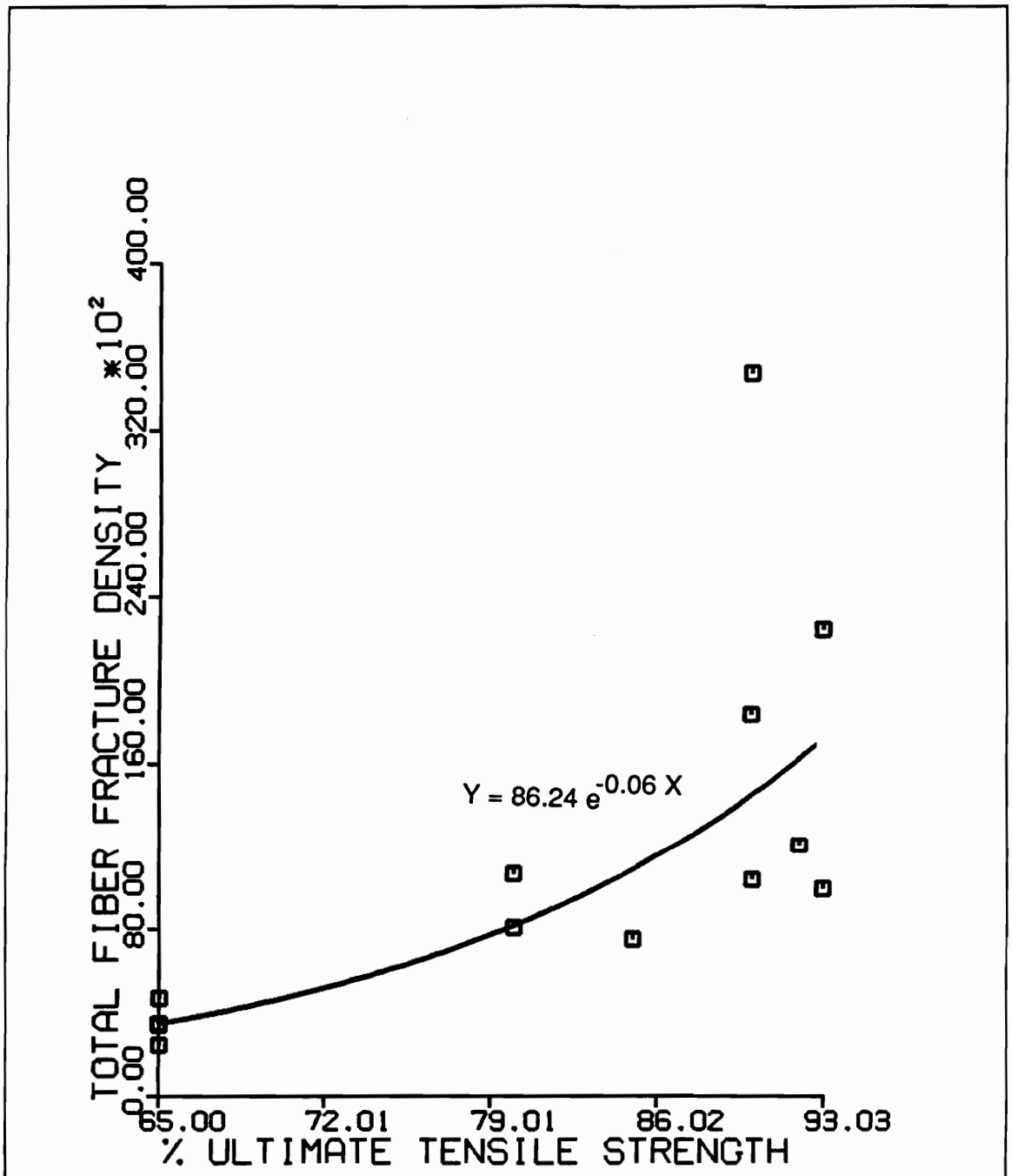

Figure 47. Total number of fractured fibers due to the initial high level quasi—static loading.

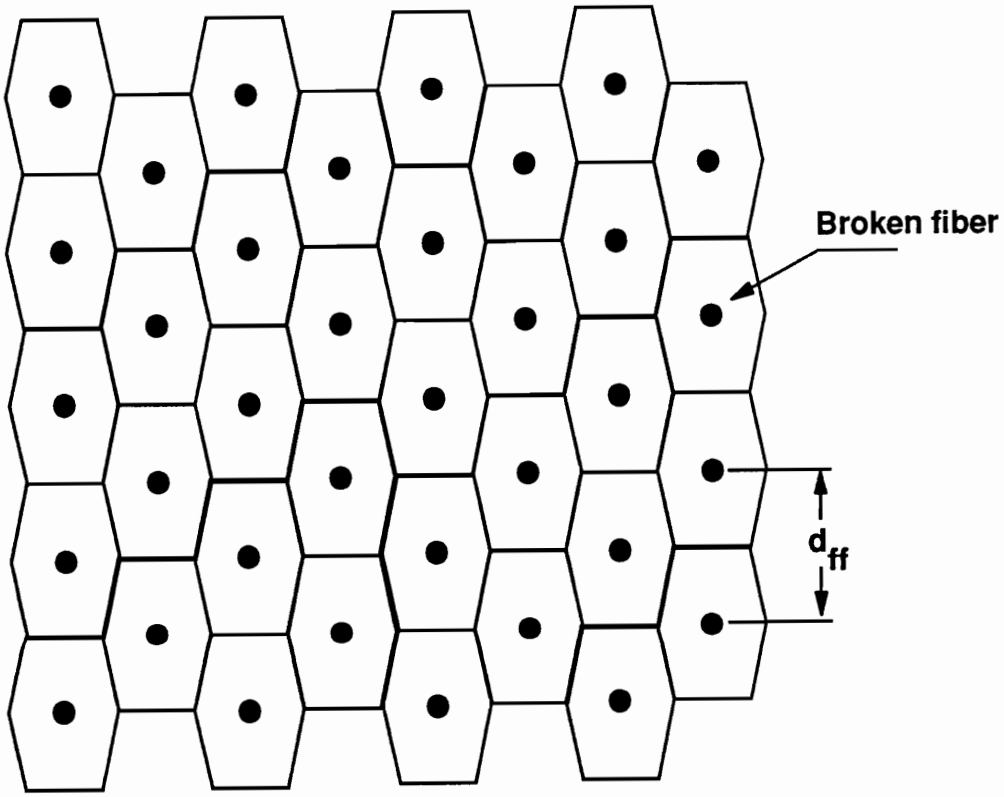

Figure 48. Hexagonal array fiber fracture model.

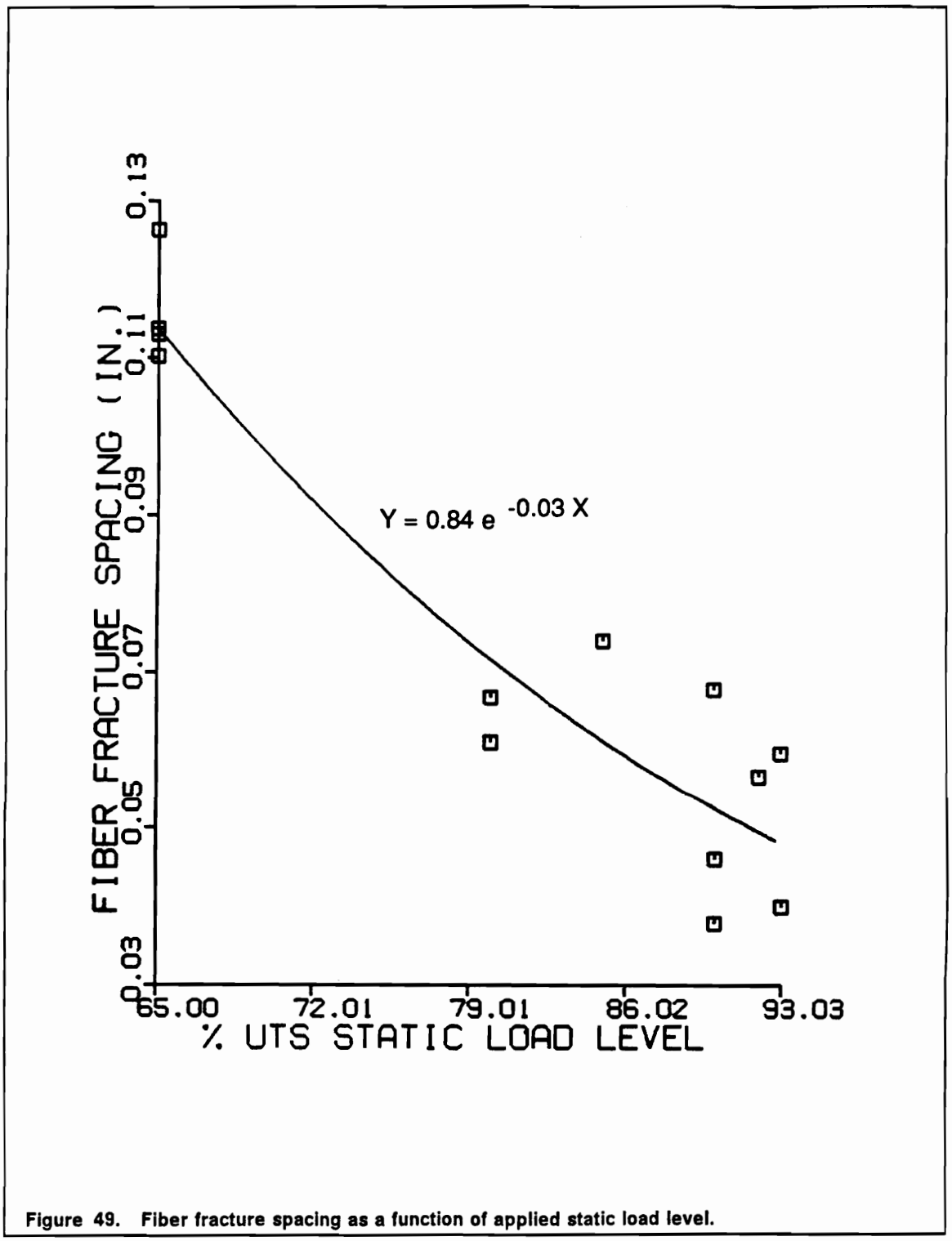

Figure 49. Fiber fracture spacing as a function of applied static load level.

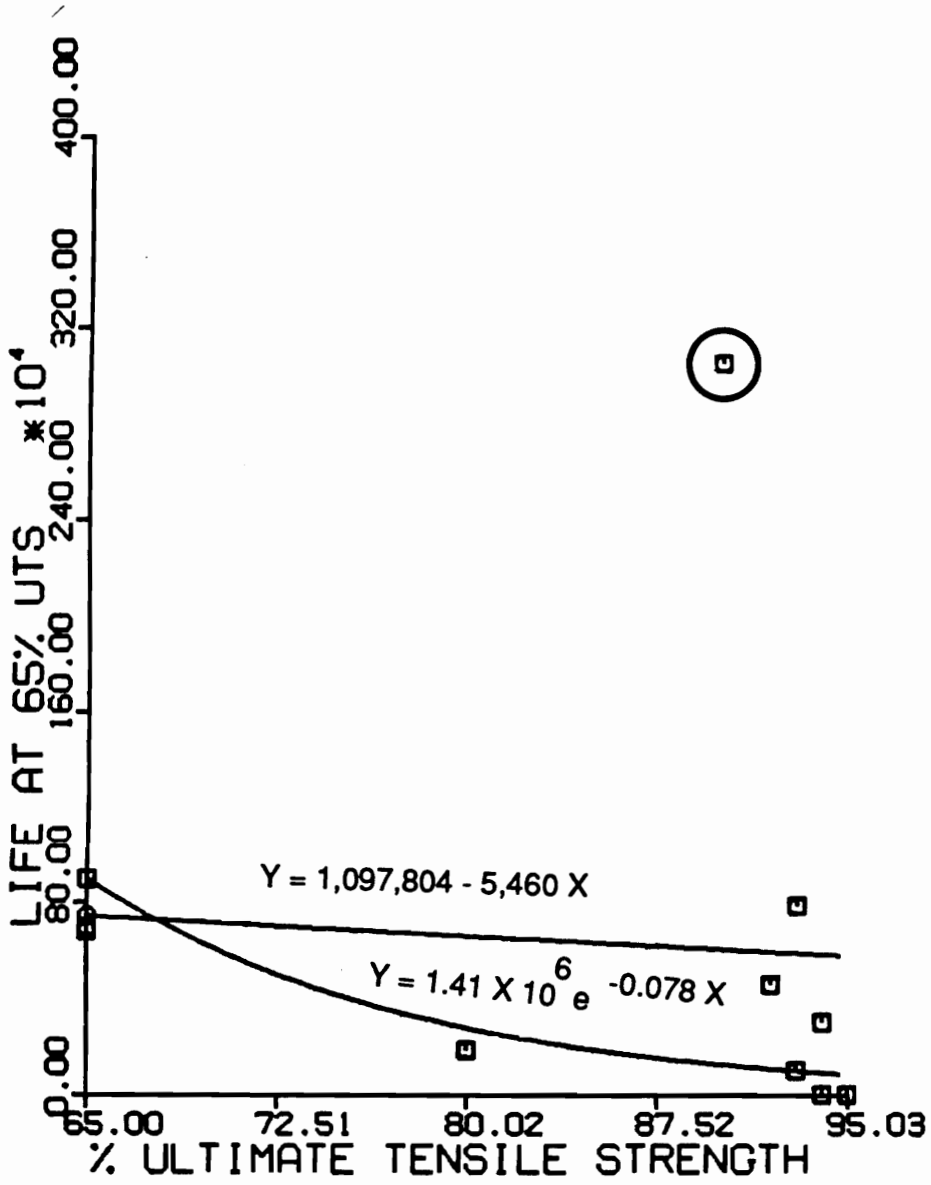

Figure 50. **S—N diagram of quasi—statically loaded and fatigued at 65% UTS to failure.:** A) Linear fit, B) Exponential fit

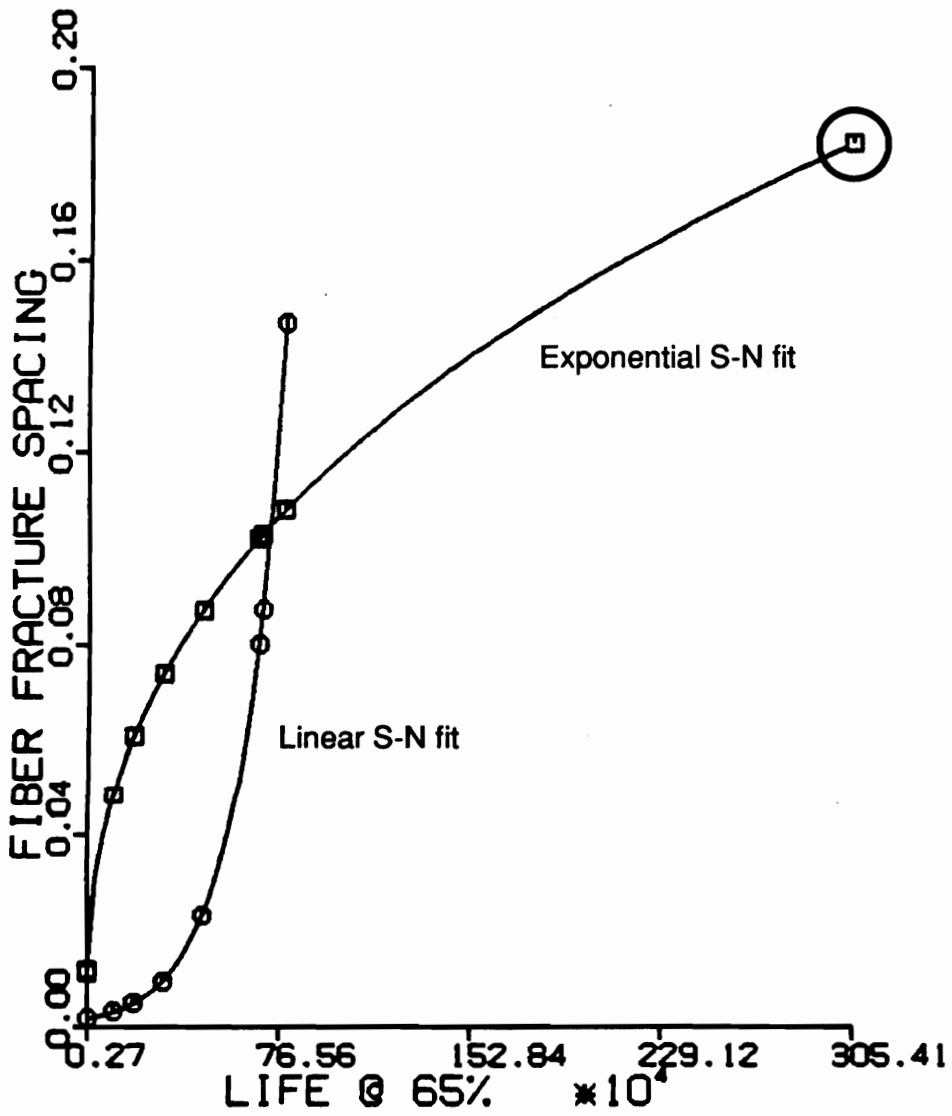

Figure 51. The dependence of fatigue life on fiber fracture spacing. The data points correspond to the actual life data used in fiber fracture spacing calculations.

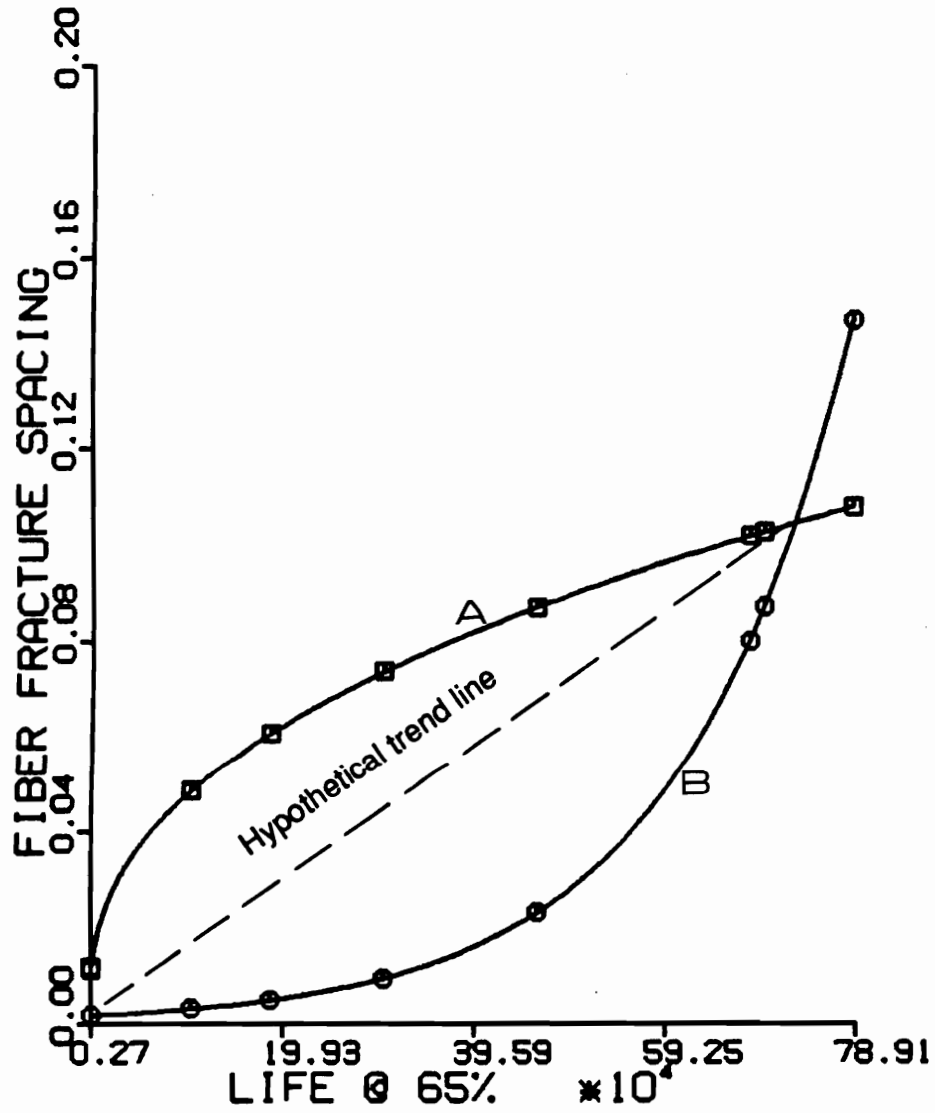

Figure 52. Fiber fracture spacing sensitivity on the S—N diagram's least square fit.: A) Exponential fit, B) Linear fit, C) Assumed general behavior. The data points correspond to the actual life data used in fiber fracture spacing calculations.

Vita

Ahmad Razvan, son of Iraj and Shahrbanou Razvan, was born on May 8, 1962 in Tehran, Iran. He attended Andisheh College Don Bosco in Tehran until 1978 after which he came to the United States and attended Broadmoor Senior High in Baton Rouge, Louisiana. He received his high school diploma in May of 1979 and enrolled in Louisiana State University in Baton Rouge, Louisiana. His major field of study was Mechanical Engineering, and he received his Bachelor of Science degree in May 1983.

In August, 1983, he entered graduate school at Louisiana State University in Baton Rouge and worked as a research assistant for the Mechanical Engineering Department in the area of corrosion science with Dr. A. Raman. He was awarded a Master of Science degree in Mechanical Engineering in December 1985.

Immediately after his graduation, he transferred to Virginia Polytechnic Institute and State University in Blacksburg, Virginia where he started working on his Ph.D. in Engineering Science and Mechanics. He concentrated his studies in the area of composite materials with the Materials Response Group under the supervision of Dr. K.L. Reifsnider. He was awarded the Doctor of Philosophy degree in Engineering Mechanics in May of 1992.

He was a two term president of the Council of International Student Organizations, president of Pars Cultural Society, Board member of the Commission on student affairs, and among many of his activities at Virginia Tech, he was a disk jockey at WUVT, FM 90.7 for classical Persian music as well as jazz. He was also awarded the membership in the Omicron Delta Kappa National Leadership Honor Society for his activities at the university. He is a member of Experimental Mechanics, British Society for Strain Measurement, American Society for Metals, and American Society of Mechanical Engineering.